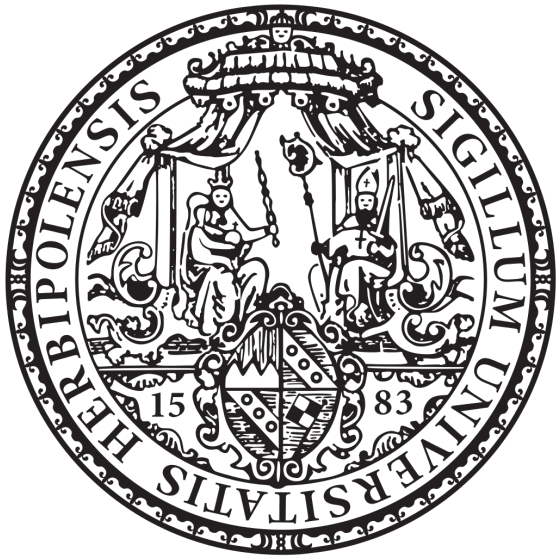

Doctoral thesis for a doctoral degree
at the Graduate School of Life Sciences
Julius-Maximilian-Universität Würzburg

Section Biomedicine

Vascularization Strategies for Full-Thickness Skin Equivalents to Model Melanoma Progression

Vaskularisierungsstrategien für Vollhautäquivalente zur Modellierung der Melanom-Progression

submitted by

Anna Leikeim

born in Lichtenfels

Würzburg 2021

Submitted on: 29.07.2021

Members of the Thesis Committee

Chairperson:	Prof. Dr. Christian Janzen
Primary Supervisor:	Prof. Dr. Heike Walles
Supervisor (Second):	Prof. Dr. Marc Schmidt
Supervisor (Third):	Dr. Florian Groeber-Becker
Supervisor (Fourth):	Dr. Dieter Groneberg
Date of Public Defence:	05.05.2022
Date of Receipt of Certificates:	_____

Abstract

Tissue engineered three-dimensional (3D) skin equivalents have been and still are steadily refined to mimic anatomic and physiological characteristics of human skin. Today, they are employed not only as grafts for patients with severe skin injuries, but also as *in vitro* test systems as alternatives to animal experiments. They can be used for toxicity and efficacy testing in pharmaceutical research as well as to study skin development or pathologies, such as wound healing or skin cancer. Malignant melanoma (MM) is the most dangerous type of skin cancer with rising incidences worldwide. Melanoma skin models can help to elucidate its causes and formation or to develop new treatment strategies. However, most of the current skin models lack a vasculature, limiting their functionality and applicability. MM relies on the vascular system for its own supply and for its dissemination to distant body sites via lymphatic and blood vessels. Thus, to accurately study MM progression, a functional vasculature is indispensable. To date, there are no vascularized skin models to study melanoma metastasis *in vitro*, which is why such studies still rely on animal experimentation.

In the present thesis, two different approaches for the vascularization of skin models are employed with the aim to establish a vascularized 3D *in vitro* full-thickness skin equivalent (FTSE) that can serve as a test system for the investigation of the progression of MM.

Initially, the suitability of the collagen matrix used to build up the dermal equivalent to seed endothelial cells in was investigated. Sprouting assays confirmed the capability of the human dermal microvascular endothelial cells (hdmEC) to sprout even in a high-density collagen hydrogel. Furthermore, the seeding strategy and the supplementation with an additional matrix protein was assessed. Based on these results, hdmEC were incorporated in the dermal part of FTSEs. The optimal seeding density, a spheroid conformation of the cells and the cell culture medium were tested. A high cell density of single hdmEC resulted in the formation of lumen-forming shapes distributed in the dermal part of the model. These capillary-like structures were proven to be of endothelial origin by staining for the endothelial cell marker CD31. The established vascularized FTSE (vFTSE) was characterized histologically after 4 weeks of culture, revealing an architecture similar to

human skin *in vivo* with a stratified epidermis, separated from the dermal equivalent by a basement membrane indicated by collagen type IV. However, this random capillary-like network is not functional as it cannot be perfused.

Therefore, the second vascularization approach focused on the generation of a perfusable tissue construct. A channel was molded within a collagen hydrogel and seeded with hdmEC to mimic a central vessel. It was then connected to an outer fluidic system for perfusion. The generation and the perfusion culture of the collagen hydrogel was enabled by the use of two custom-made, 3D printed bioreactors. They allowed the generation of a high-density collagen hydrogel perfused via the central channel. Histological assessment of the hydrogels revealed the lining of the channel with a monolayer of endothelial cells, expressing the cell specific marker CD31.

For the investigation of MM progression *in vitro*, a 3D melanoma skin equivalent was established. Melanoma cells were incorporated in the epidermal part of FTSEs, representing the native microenvironment of the tumor. Melanoma nests grew at the dermo-epidermal junction within the well stratified epidermis and were characterized by the expression of common melanoma markers. First experiments were conducted showing the feasibility of combining the melanoma model with the vFTSE, resulting in skin models with tumors at the dermo-epidermal junction and lumen-like structures in the dermis.

Taken together, the models presented in this thesis provide further steps towards the refinement of 3D *in vitro* skin models. Melanoma development and progression can be studied within a 3D microenvironment and the combination of the melanoma models with the vFTSEs enables further investigation of the interaction of the tumor cells with the vasculature.

Zusammenfassung

Mithilfe des Tissue Engineerings hergestellte dreidimensionale (3D) Hautäquivalente wurden und werden stetig verfeinert, um die anatomischen und physiologischen Eigenschaften der menschlichen Haut nachzuahmen. Heute werden sie nicht nur als Implantate für Patienten mit schweren Hautverletzungen eingesetzt, sondern auch als *in vitro*-Testsysteme als Alternative zu Tierversuchen. Sie können sowohl für Toxizitäts- und Wirksamkeitstests in der pharmazeutischen Forschung als auch zur Untersuchung der Entwicklung der Haut oder von pathologischen Zuständen, wie Wundheilung oder Hautkrebs, verwendet werden. Das maligne Melanom (MM) ist die gefährlichste Form von Hautkrebs mit weltweit steigender Inzidenz. Melanom-Hautmodelle können helfen, seine Ursachen und Entstehung aufzuklären oder neue Behandlungsstrategien zu entwickeln. Den meisten bisherigen Hautmodellen fehlt jedoch ein Gefäßsystem, was ihre Funktionalität und Anwendbarkeit einschränkt. Das MM ist auf das Gefäßsystem angewiesen, sowohl für die eigene Versorgung als auch für die Ausbreitung über Lymph- und Blutgefäße zu entfernten Körperstellen. Um die Entwicklung des MM genau zu studieren, ist daher eine funktionelles Gefäßsystem unabdingbar. Bislang gibt es keine vaskularisierten Hautmodelle, um die Melanommetastasierung *in vitro* zu untersuchen, weshalb solche Studien immer noch auf Tierversuche angewiesen sind.

In der vorliegenden Arbeit werden zwei unterschiedliche Ansätze zur Vaskularisierung von Hautmodellen mit dem Ziel verfolgt, ein vaskularisiertes 3D *in vitro* Vollhautmodell (full-thickness skin equivalent, FTSE) zu etablieren, das als Testsystem zur Untersuchung der Entwicklung des MM dienen kann.

Zunächst wurde die Eignung der Kollagenmatrix, die zum Aufbau des Hautäquivalents verwendet wurde, untersucht, um Endothelzellen darin auszusäen. Sprouting-Assays zeigten, dass die humanen dermalen mikrovaskulären Endothelzellen (hdmEC) auch in einem Kollagen-Hydrogel mit hoher Dichte aussprossen können. Weiterhin wurde die Aussaatstrategie und die Supplementierung mit einem zusätzlichen Matrixprotein untersucht. Basierend auf diesen Ergebnissen wurden hdmEC in den dermalen Teil von FTSEs integriert. Die optimale Aussaatdichte, eine sphäroidale Konformation der Zellen und das Zellkulturmedium wurden getestet. Eine hohe Zelldichte einzelner hdmEC führte

zur Bildung von lumenbildenden Formen, die im dermalen Teil des Modells verteilt waren. Diese kapillarähnlichen Strukturen wurden durch Färbung für den Endothelzellmarker CD31 als endothelialen Ursprungs nachgewiesen. Das etablierte vaskularisierte FTSE (vFTSE) wurde nach 4 Wochen Kultur histologisch charakterisiert und zeigte eine der menschlichen Haut *in vivo* ähnliche Architektur mit einer geschichteten Epidermis, die vom dermalen Äquivalent durch eine Basalmembran, gezeigt durch Kollagen Typ IV, getrennt ist. Dieses zufällige kapillarartige Netzwerk ist jedoch nicht funktional, da es nicht durchblutet werden kann.

Daher konzentrierte sich der zweite Vaskularisierungsansatz auf die Erzeugung eines perfundierbaren Gewebekonstrukts. Ein Kanal wurde in einem Kollagenhydrogel geformt und mit hdmEC besiedelt, um ein zentrales Gefäß zu imitieren. Dieser wurde dann mit einem äußeren Flüssigkeitssystem zur Perfusion verbunden. Die Erzeugung und die Perfusionskultur des Kollagenhydrogels wurde durch die Verwendung von zwei speziell angefertigten, 3D-gedruckten Bioreaktoren ermöglicht. Sie erlaubten die Erzeugung eines Kollagenhydrogels mit hoher Dichte, das über den zentralen Kanal perfundiert wurde. Die histologische Beurteilung der Hydrogele zeigte die Auskleidung des Kanals mit einer Einzelschicht von Endothelzellen, die den zellspezifischen Marker CD31 exprimieren.

Für die Untersuchung der MM-Progression *in vitro* wurde ein 3D-Melanom-Hautäquivalent hergestellt. Melanomzellen wurden in den epidermalen Teil von FTSEs integriert, was die native Mikroumgebung des Tumors darstellt. Die Melanomnester wuchsen an der dermo-epidermalen Grenzfläche innerhalb der gut stratifizierten Epidermis und wurden durch die Expression gängiger Melanommarker charakterisiert. Erste Experimente wurden durchgeführt, die die Machbarkeit der Kombination des Melanom-Modells mit dem vFTSE zeigten, was zu Hautmodellen mit Tumoren an der dermo-epidermalen Grenzfläche und lumenartigen Strukturen in der Dermis führte.

Alles in allem bieten die in dieser Arbeit vorgestellten Modelle weitere Schritte zur Verfeinerung von 3D *in vitro*-Hautmodellen. Die Melanomentwicklung und -progression kann innerhalb einer 3D-Mikroumgebung untersucht werden und die Kombination der Melanommodelle mit den vFTSEs ermöglicht eine weitere Untersuchung der Interaktion der Tumorzellen mit dem Gefäßsystem.

Table of Contents

List of Abbreviations

2D ..... two-dimensional
3D ..... three-dimensional
PBS^- ..... phosphate buffered saline without $MgCl_2$ and $NaCl_2$
PBS^+ ..... phosphate buffered saline with $MgCl_2$ and $NaCl_2$
ATP ..... adenosine triphosphate
bFGF ..... basic fibroblast growth factor
BRAF ..... v-raf murine sarcoma viral oncogene homolog B
CD ..... cluster of differentiation
CK10 ..... cytokeratin 10
CK14 ..... cytokeratin 14
DAB ..... 3,3'-diaminobenzidine
DAPI ..... 4',6-diamidino-2-phenylindole
DMEM ..... Dulbecco's Modified Eagle's Medium
DMSO ..... dimethyl sulfoxide
ECM ..... extracellular matrix
EDTA ..... ethylenediaminetetraacetate
EU ..... European Union
FCS ..... fetal calf serum
FFF ..... fused filament fabrication
FTSE ..... full-thickness skin equivalent
g ..... g-force, gravitational force equivalent
GNS ..... gel neutralisation solution
hdF ..... human dermal fibroblasts
hdmEC ..... human dermal microvascular endothelial cells
HE ..... hematoxylin and eosin
heK ..... human epidermal keratinocytes
HEPES ..... 4-(2-hydroxyethyl)-1-piperazineethanesulfonic acid
HRP ..... horseradish peroxidase
HUVEC ..... human umbilical vein endothelial cells

MACS ..... magnetic-activated cell sorting
MAPK ..... mitogen-activated protein kinase
mFTSE ..... melanoma full-thickness skin equivalent
MHC ..... major histocompatibility complex
MM ..... malignant melanoma
MTT ..... 3-(4,5-dimethylthiazol-2-yl)-2,5-diphenyltetrazolium bromide
NRAS ..... neuroblastoma RAS viral oncogene homolog
PCL ..... polycaprolactone
PECAM-1 ..... platelet endothelial cell adhesion molecule
PLGA ..... poly(lactic-co-glycolic acid)
RHE ..... reconstructed human epidermis
SD ..... standard deviation
TGFβ ..... transforming growth factor β
VEGF ..... vascular endothelial growth factor
vmFTSE ..... vascularized melanoma full-thickness skin equivalent

List of Figures

List of Tables

1 Introduction

1.1 Tissue Engineering of skin

Investigated and applied much earlier, the term "tissue engineering" was defined in 1993 by Langer and Vacanti as "an interdisciplinary field that applies the principles of engineering and the life sciences toward the development of biological substitutes that restore, maintain, or improve function" [1]. Cell biology, engineering, material science and medicine are combined with the intention to create new, physiologic and functional tissue [2]. Thus, tissue engineered constructs aim to recreate a certain organ or tissue *in vitro*.

The principle of tissue engineering appears to be easy: Cells isolated from human donor tissue are expanded in cell culture and afterwards seeded onto scaffolds, that can be of artificial or natural origin. The scaffold serves as surface for the cells to adhere and proliferate on, it provides structural stability and spatial organisation for the cells and mimics the natural environment of the tissue. The combination of cells, scaffold and chemical and physical signals contributes to the maturation of the engineered tissue *in vitro* [3].

First intended to replace damaged tissues *in vivo* as implants, tissue engineered constructs are nowadays widely used in research to study the pathology of diseases, find new therapeutic strategies or test the toxicity of distinct substances. Here, tissue engineered models help to increase the precision and predictive power of study results as they provide a human test system and contribute to the reduction of animal experimentation [4, 5]. This is in accordance with the globally accepted 3R principle published in 1959 by Russell and Burch. These guiding principles for more ethical use of animals in science demanded the replacement, reduction and refinement of animal experimentation [6, 7]. In 2010, the 3R principle was legally recognised in the European Directive 2010/63/EU on the protection of animals used for scientific purposes [8].

Considered relatively simple in its anatomical organisation, skin was the first tissue engineered organ, that went from bench to bedside [9, 10]. Nowadays, there are several commercially available skin grafts to treat patients with severe skin wounds [9, 11–14].

Furthermore, tissue engineered skin models have gained more and more attention in recent years as *in vitro* test systems in chemical, pharmaceutical and cosmetic industry [13,15–18]. They strive to encompass high-throughput and high standardizability, are cost-efficient, adaptable to different scientific questions, their results are more reliable due to their human origin and they can contribute to reduce animal experimentation [13, 16, 18].

1.1.1 Anatomy and function of the skin

The skin is the outermost barrier of the body, shielding it from physical, chemical and biological influences. Besides this mechanical protection, it prevents excessive water loss and plays a vital role in thermoregulation and immunosurveillance [19–21]. The skin is organised in three layers, which are from top to bottom the epidermis, the dermis and the subcutis or hypodermis (see figure 1.1) [22, 23]. The shape of the skin is not homogenous all over the body but varies regionally concerning its thickness, the frequency of skin appendages or the distribution of melanocytes [22].

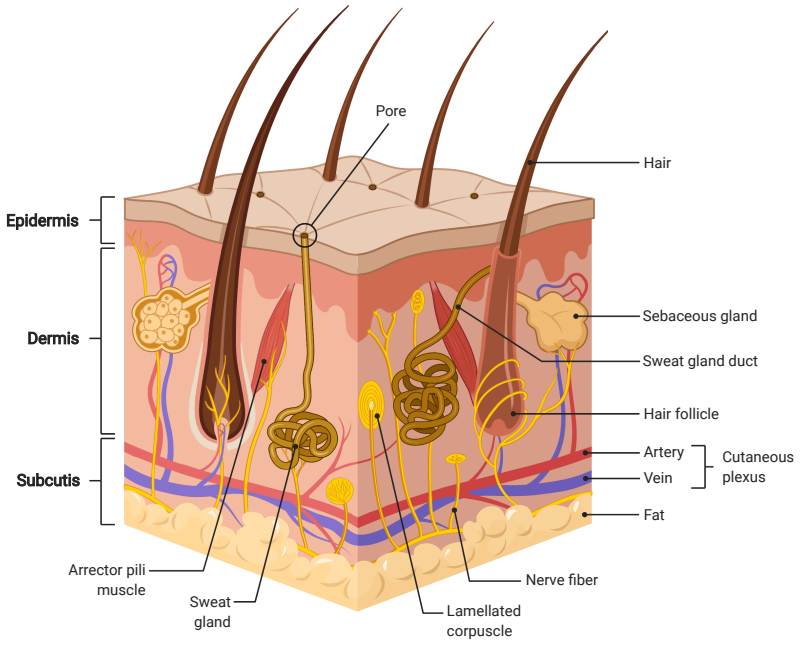

Figure 1.1: Anatomy of human skin. Human skin is organised in the three layers epidermis, dermis and subcutis. Furthermore, it possesses skin appendages, nerves and vasculature. Illustration adapted from "Anatomy of the Skin", by BioRender.com (2021). Retrieved from https://app.biorender.com/biorender-templates.

The epidermis

The epidermis is a stratified epithelium, that renews itself continuously [24] with a varying thickness of 0.1 to 1.5 mm [20, 22]. The predominant cell type are keratinocytes, which make up 90-95 % of all cells and are characterised by high content of structural proteins [22, 24]. They undergo a differentiation process to form the different layers of the epidermis (see figure 1.2). At the dermo-epidermal junction, undifferentiated keratinocytes form the basal layer as a palisade-like structure on the basement membrane. To this they are anchored via hemidesmosomes, whereas they are connected to neighbouring cells via gap and adherens junctions and predominantly via desmosomes, abundant in all viable cell layers [21, 22]. Within the basal layer, epidermal stem cells are mitotically active and divide to form the suprabasal layers *stratum spinosum* and *stratum granulosum*. Thus, keratinocytes originating from the basal layer migrate outwards towards the skin surface. On their way, they enter a differentiation process called keratinisation. Thereby, their morphology changes to a more flattened shape and a bigger size, their lipid and protein

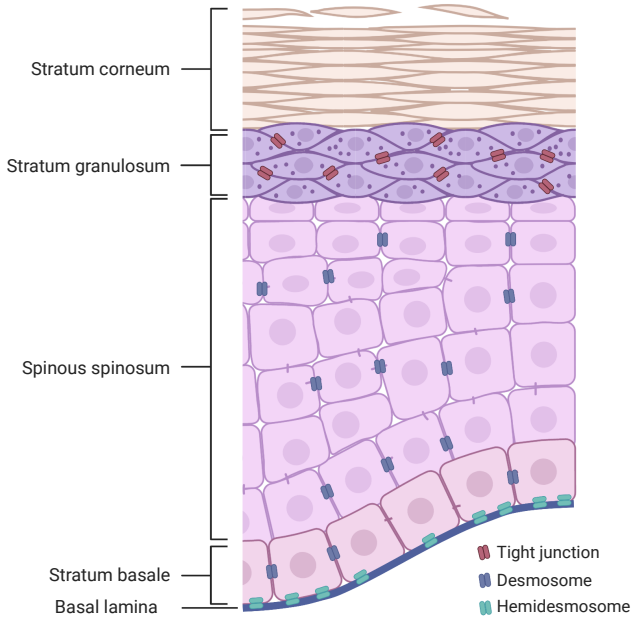

Figure 1.2: Structure of the epidermis. The epidermis shows a multilayered architecture with the *stratum basale*, the *stratum spinosum*, the *stratum granulosum* and the *stratum corneum*. Illustration adapted from "Desmosomal Protein Distribution in the Epidermis", by BioRender.com (2021). Retrieved from https://app.biorender.com/biorender-templates.

content changes and they start to dehydrate [24, 25]. In the outermost layer, the *stratum corneum*, the highly flattened cells are devoid of the nucleus and cell organelles but contain a large amount of filamentous keratins. Embedded in a lipid matrix, these corneocytes contribute to a large extent to the epidermal barrier function [25]. The second major barrier structure in the epidermis are tight junctions between adjacent keratinocytes within the *stratum granulosum* [21]. 24 to 30 days after their origin in the *stratum basale*, the terminally differentiated cells eventually shed from the skin surface [22–24].

Melanocytes reside between the keratinocytes in the basal layer with one melanocyte and around 36 associated keratinocytes forming an epidermal melanin unit. The produced pigment melanin is stored in melanosomes, which are transferred to adjacent keratinocytes where they form a cap over the nucleus to protect it from dangerous ultraviolet radiation. Other non-keratinocytes in the epidermis are antigen-presenting Langerhans cells as part of the immune system and Merkel cells as mechanoreceptors [22, 23].

The dermis

Directly underneath the epidermis is the dermis. The dermo-epidermal junction separates but also tightly connects the two skin layers. The dermo-epidermal junction is a complex basement membrane synthesized by basal keratinocytes and dermal fibroblasts. Major components of the dermo-epidermal junction are laminin-5 [24], collagen type IV [20, 23] and collagen type VII [22], furthermore nidogen and the proteoglycan perlecan [26]. The dermo-epidermal junction controls as semipermeable barrier the exchange of substances and cells between the skin layers and is important for the adhesion and polarity of the basal keratinocytes [20, 22].

The dermis underneath serves as scaffold of the skin, supporting and feeding the epidermis. It is a compressible and elastic connective tissue responsible for the pliability and the tensile strength of the skin [22,24]. The major cell type in the dermis are fibroblasts which are embedded in an extracellular matrix (ECM). The dermal ECM consists of collagen and elastic fibres which provide stability and elasticity. The great majority of dermal fibres are made of collagen type I and III, arranged in bundles [22, 24]. Filling the space between fibres and cells, glycoproteins, glycosaminoglycans and proteoglycans such as hyaluronic acid, fibronectin, decorin and chondroitin-4-sulphate are components of the ECM, being important due to their water binding properties [22–24]. The fibroblasts constantly degrade and synthesise the fibrous and non-fibrous components of the ECM, thereby migrating through and remodelling the dermis [24]. Moreover, cells of the immune system such as monocytes, macrophages, mast cells and dendrocytes reside in

the dermis, contributing to the immune response of the skin [22, 24]. Furthermore, the dermis contains nerves, blood and lymph vessels and encompasses the skin appendages such as hair follicles and glands developmentally originating from the epidermis [22, 23].

The dermis is structurally separated in two layers, distinguishable by the density and arrangement of the cell and fibre components as well as the distribution pattern of nerves and vasculature [24]. The uppermost part of the dermis, directly underneath the epidermis, is the papillary dermis named for its extensions called dermal papillae protruding in the epidermis. By this intertwining of epidermis and dermis, the surface of the dermo-epidermal junction increases allowing for a better adhesion between these two skin layers [22]. The papillary dermis is characterised by loosely arranged small collagen fibre bundles and thin elastic fibres [22]. Due to this properties, it helps the skin to accommodate to mechanical stress [24]. Blood vessels within the papillary dermis form the superficial horizontal plexus that provides a vascular loop to every papilla, nourishing the vessel-free epidermis [22, 24]. The reticular dermis is the lower layer and major part of the dermis. In contrast to the papillary dermis, the reticular dermis consists of denser and larger collagen bundles and a thicker elastic network [22, 24]. The two fibre systems are highly integrated, providing the tensile strength of the skin [23, 24]. The reticular dermis contains the deep horizontal plexus of vessels, connected to the superficial plexus via vessels traversing the dermis vertically. It provides nutritional arteries to hair follicles and sweat glands [22].

The subcutis

The subcutis or hypodermis as lowest skin layer is an adipose-rich, loose connective tissue. It serves as energy reservoir, cushions and protects the underlying tissue and has importance in thermal isolation of the body. Mesenchymally derived adipocytes are the the primary cell type here, organised into lobules which are separated by septa of connective tissue [23, 24]. Within these septa, nerves, blood and lymph vessels run, supplying the tissue and branching in the dermis [24]. Furthermore, the deepest parts of hair follicles and sweat glands protrude from the dermis into the subcutis [22].

Vasculature in the skin

In general, the vascular network branches in a hierarchical fashion. Coming from the heart, large arteries carrying oxygenated blood branch into smaller arterioles and finally into capillaries (see figure 1.3). Capillaries are the smallest blood vessels with an average lumen diameter of 5-10 µm. The high surface-to-volume ratio facilitates the exchange

of gas, nutrients and waste products taking place in the capillary network to keep the cells alive and maintain homeostasis within the tissue. The capillaries then reassemble to venules to transport oxygen-depleted blood via veins back to the heart [23, 27, 28].

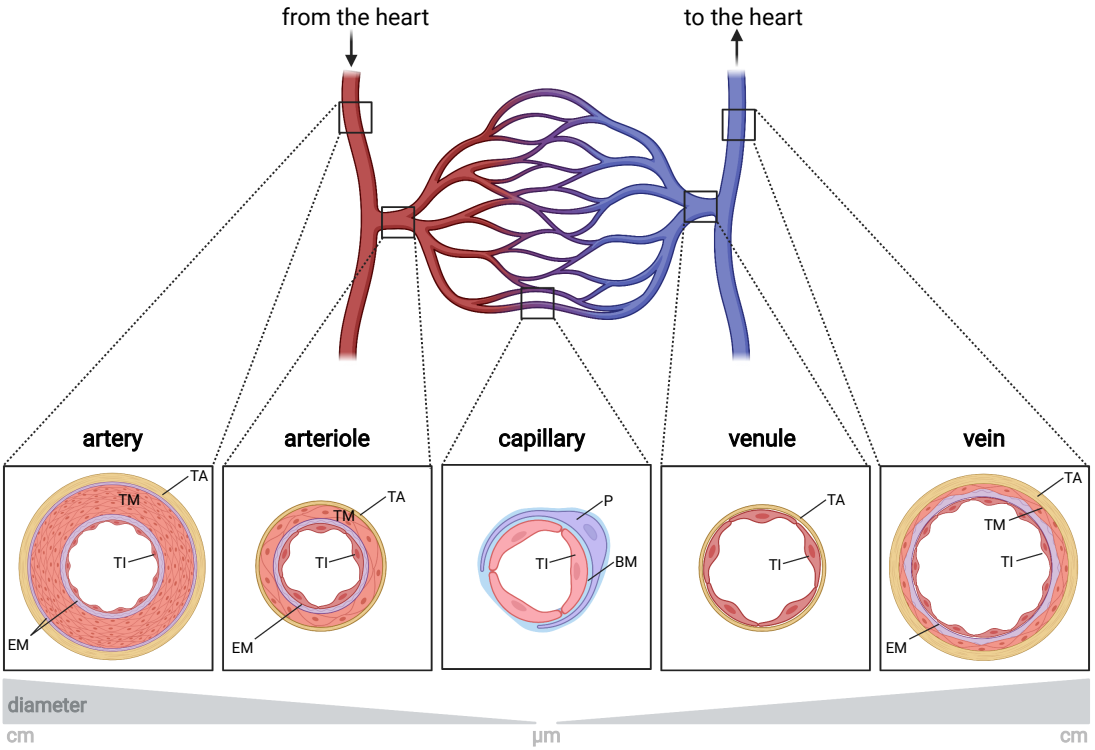

Figure 1.3: Hierarchy and structure of blood vessels. Blood vessels are organised in a hierarchical circuit of arteries and arterioles (red) coming from the heart, connecting capillaries, and venules and veins (blue) transporting blood back to the heart. The *tunica intima* (TI), composed of endothelial cells on a basement membrane, is the innermost layer of all vessel types. The middle layer, the *tunica media* (TM), is the muscular layer, most pronounced in arteries and arterioles and to a lesser extend in veins. Also elastic membranes (EM) are found in these vessels. The outermost layer is the *tunica adventitia* (TA), present in all blood vessel types but capillaries. These smallest vessels consist only of a monolayer of endothelial cells surrounded by pericytes (P) embedded in the basement membrane (BM). Illustration created with BioRender.com.

Concerning their structural composition, blood vessels show an architecture of concentric layers of cellular and non-cellular components (see figure 1.3). The innermost layer of the blood vessel wall is the *tunica intima*. It consists of a monolayer of endothelial cells on a basement membrane and subendothelial connective tissue. As interface between the vessel lumen and the tissue, endothelial cells control the passage of substances and cells and the gas exchange. Capillaries only consist of this inner layer with pericytes embedded in the basement membrane. The middle layer, the *tunica media*, consists

mainly of smooth muscle cells, elastic and collagen fibres. This layer has contractile properties and is generally thicker in arterial vessels than in venous. The outermost layer of blood vessels is the *tunica adventitia*, composed of fibroblasts in a loose connective tissue [23, 28–30].

Except the epidermis, the skin is highly supplied with blood via a dense vascular network. In addition to its nutritional function, it is also important for thermoregulation and acts as a blood reservoir. The skin vascular system is structured into two plexuses [20, 22, 31]. Arteries and veins within the hypodermis supply and drain the deep vascular plexus, located in the reticular dermis near the subcutis [23]. The deep horizontal plexus is composed of arterioles and venules with diameters up to 100 µm [31]. Via their muscular part, they control the blood circulation and therefore the thermoregulation of the skin. These vessels have numerous tributaries supplying the skin appendages but also ascending vertically through the dermis to interconnect with the superficial horizontal plexus [23, 31–33]. This plexus is localised in the papillary dermis. Arterioles here show an outside diameter of 17 to 26 µm with an inner endothelial cell tube of 7.5 to 12 µm. From this dense network of small arterioles and venules, capillary loops extend into the dermal papillae, supplying the epidermis with oxygen and nutrients. These small capillaries have an outside diameter of 7.5 to 10 µm and a lumen diameter of 3.5 to 6 µm [31]. Post-capillary venules being the most prominent type of blood vessels in the superficial vascular plexus act as blood reservoir and dissipate the heat [23].

1.1.2 Current skin models and their applications

Artificial substitutes mimicking human skin are a versatile tool for various research and medical purposes. Their broad use ranges from grafts for the treatment of patients with excessive skin injuries [9, 11] to *in vitro* test systems for basic and pharmacological research [15–17]. In this thesis, the focus will be on skin models used in research, therefore skin equivalents for the use on patients are not discussed.

Skin equivalents for *in vitro* applications are widely used in numerous research areas. They are used in basic research to unravel fundamental processes in the skin such as pigmentation [34] and the reaction of skin to sunlight [35, 36]. Furthermore, it is possible to mimic diseased skin by employing patient-derived cells to elucidate the developmental process and to test potential therapies [17]. There are models mimicking psoriasis [37, 38], malignant melanoma [39] or wound healing [40], just to name a few. Another huge application scenario is toxicological testing. Numerous chemical, pharmaceutical or cosmetic compounds need to be tested in regard to their safety. For this reason, Draize

et al. developed an assay in 1944 that uses albino rabbits to test the harm of substances applied topically on the skin [41]. Due to ethical and scientific reasons, current policies tend to replace animal experimentation for *in vitro* testing. In 2013, a complete marketing ban on cosmetics with ingredients that have been tested on animals became effective in the EU, pointing out the necessity of *in vitro* test systems [42].

Epidermal skin models

The simplest approach to build a three-dimensional (3D) skin equivalent *in vitro* is reconstructed human epidermis (RHE). These models constitute the epidermal part of human skin. They are comprised of human epidermal keratinocytes seeded on a collagen scaffold or a porous synthetic membrane. During culture at the air-liquid interface and triggered by a calcium gradient in a specialized medium, the cells differentiate and build up a stratified epidermis [43]. Due to its relatively simple setup, RHE is highly standardized and scalable to be produced in large quantities. Today, RHE is commercially available and sold by many companies under various trademarks such as Episkin™ and Skinethic™ from L'Oréal (Nice, FR), Epiderm™ from MatTek Corporation (Ashland MA, US) or epiCS® from CellSystems (Troisdorf, DE). These models are widely used for skin irritation and corrosion testing [15], with some of them being validated by the EU to be used in tests according to official guidelines from the Organisation for Economic Cooperation and Development (OECD) (test guidelines 431 for *in vitro skin* corrosion [44] and 439 for *in vitro* skin irritation [45]).

Full-thickness skin models

As RHE only depicts the outermost layer of the skin, approaches were made to mimic the anatomy of human skin *in vivo* further by adding a dermal compartment. The so created full-thickness skin equivalents (FTSEs) contain a dermal part, usually comprised of some kind of matrix seeded with fibroblasts, and an epidermal part. For the dermal part, different scaffolds are possible. Synthetic scaffolds such as poly(lactic-co-glycolic acid) (PLGA) [46, 47], polycaprolactone (PCL) [48] or porous polystyrene [49, 50] are used for their mechanical resilience. They are commercially available, biocompatible and do not bear the risk of interspecies pathogen transfer [48]. However, they are not of natural origin and therefore lack cellular adhesion molecules. Biological scaffolds promise a higher cell viability, biocompatibility and a better imitation of skin *in vivo*. They are often used as hydrogels, being easy to cast and enabling the embedding of cells within the scaffold. The most commonly used is collagen type I [51–53], but also other natural

macromolecules are employed such as chitosan [54], gelatin and hyaluronic acid [55, 56] or fibrin [57, 58]. These hydrogels possess high water holding capacity and structural resemblance to the ECM [59]. Other biological scaffolds include deepidermalized human dermis [60,61] or decellularized porcine small intestine submucosa [62]. Another approach to generate the dermal part of FTSEs is the self-assembly technique, in which fibroblasts are seeded in sheets and cultured for several weeks to produce their own matrix. With this method it is possible to generate totally human skin models without any kind of scaffold [63–65].

Commercially available products for FTSEs are for example EpiDermFT™ from MatTek Corporation (Ashland MA, US), Phenion® FT Skin Model from Henkel AG & Co. KGaA (Düsseldorf, DE) or the skin equivalent by Epistem Ltd. (Manchester, UK).

In recent years, a new technology for the fabrication of skin equivalents for clinical applications as well as for research purposes emerged: Several studies showed the applicability of 3D bioprinting to generate multilayered human skin *in vitro*, employing different kinds of natural or synthetic matrices and including keratinocytes and fibroblasts [66–68].

FTSEs are very useful to investigate dermatological questions regarding the interplay of cells of the epidermis and dermis. They can be further adapted to the scientific need by introducing additional cell types such as patient-derived cells, immune cells or endothelial cells [15].

1.1.3 Vascularization as a demanding task in skin tissue engineering

A key challenge of all engineered tissues is vascularization. Almost every tissue needs to be vascularized for proper nutrient and oxygen supply of the cells as the maximum diffusion range is generally considered as only 200 µm [69, 70]. Thus, more complex and bigger tissue equivalents need proper vascularization for the cells to remain viable.

During embryonic development, vessels are formed by vasculogenesis and angiogenesis [30, 69, 71]. Vasculogenesis occurs in early embryonic development by *de novo* vessel formation [30]. Here, angioblasts differentiate into endothelial cells, which proliferate to form a primitive capillary network in a previously avascular tissue [30, 71]. There are also postnatal vasculogenic processes, when bone marrow-derived endothelial progenitor cells enter the circulation to reach sites of tissue repair and differentiate into mature endothelial cells to build a new vascular network [72]. Angiogenesis is defined as the formation of new vessels from already existing vascular structures [69, 71]. It can be distinguished between sprouting and intussusceptive angiogenesis. In sprouting angiogenesis, endothelial cells

form sprouts originating from pre-existing vessels [71, 73]. A subtype of endothelial cells, the tip cells, guide and lead the vessel sprout, determining the direction. Neighbouring stalk cells proliferate and thereby lengthen the sprout and form a lumen [73, 74]. In intussusceptive angiogenesis, new blood vessels are created by splitting an existing vessel into two by reorganisation of the vessel walls [71, 75]. Angiogenesis responds to the need for nutrients and oxygen of tissue areas devoid of vasculature [69]. Cells in hypoxic tissue secrete growth factors and chemokines such as vascular endothelial growth factor (VEGF), basic fibroblast growth factor (bFGF) or angiopoietins, activating vascular growth and remodeling [30,69]. Capillaries formed by angiogenesis can undergo subsequent arteriogenesis, in which the vascular structures mature and increase in diameter and wall thickness. During this process, mural cells are recruited and ECM is generated to stabilize the vessel [76]. Arteriogenesis is not driven by hypoxia, but rather mediated by fluid flow shear stress and activation of the endothelium [69, 76]

As explained in section 1.1.1, the dermis harbours a dense network of capillaries, pointing out the need of a vascular system for skin equivalents to mimic the *in vivo* situation. For clinical applications, a proper vascularization of skin grafts to cover big wounds is absolutely crucial. The newly implanted skin equivalent needs to be supplied via the patient's blood vessels as soon as possible to survive, otherwise graft necrosis may occur [77, 78]. The ingrowing of existing vessels from the host into the implant is a suitable possibility for the new tissue to be vascularized, but this process takes a lot of time. Therefore, already prevascularized skin equivalents would help improve the care and healing of these wounds as the inosculation of already existing vessels is much faster [69, 77, 79, 80].

But also for *in vitro* applications, vascularized skin models would provide many benefits. Many application scenarios for skin models limited now, would be conceivable with a functional vascularization. A vascular network would not only allow for oxygen and nutrient supply, but also improve the model's resemblance of skin *in vivo* and thereby enhance the relevance as a test system. Skin models with vascularization would enable studies on drug absorption and penetration via the skin into the blood stream, an important test setting for pharmaceutical and cosmetic formulations [81, 82]. The other way round, it would be possible to apply drugs systemically via perfusion through the vessels and analyse the impact on the target tissue [17]. Furthermore, endothelial cells are critical components during the initiation and progression of inflammatory skin processes and allergies as they can secrete several chemokines and cytokines and are able to recruit immune cells [83, 84]. Thus, vascularized skin models would provide ideal test settings to study inflammatory skin diseases such as atopic dermatitis [85] or

psoriasis [31, 37]. Additionally, the vascular system plays an important role in several diseases and pathologic states such as wound healing [58] or the progression of skin cancers [63].

To address this issue, several approaches for integrating vessels into tissue engineered constructs have been proposed. Vascularization strategies take advantage of the spontaneous organisation of endothelial cells into lumen-like structures in matrices to form vascular networks. It was established that endothelial cells are able to form vascular networks, often without the addition of growth factors or other special treatment [58, 77, 80, 86–89]. First, endothelial cells assemble to form a primitive vascular network in a previously avascular tissue. This process is similar to vasculogenesis. Subsequently, this network can be further organised and remodelled, resembling angiogenesis and arteriogenesis [69].

In these vascularization approaches, human dermal microvascular endothelial cells (hdmEC) or human umbilical vein endothelial cells (HUVEC) are seeded together with fibroblasts in the dermal compartment of skin equivalents [58, 77, 89, 90] or added using a scaffold-free sheet technique, in which the desired cells are seeded layer by layer [63, 64]. These experimental procedures led to the formation of random capillary structures *in vitro*. This process can be promoted further by the use of angiogenic growth factors such as VEGF or angiopoietin-1 [91]. Using this technique for skin grafts, the growth and survival of the implant can be improved, since the already existing vascular structures within the graft inosculate with the vessels from the wound bed, ensuring a rapid blood supply [77]. For *in vitro* skin models, the situation is different. They cannot be supplied via the randomly formatted capillary network since there is no accessibility for perfusion [81]. Perfusion is not only crucial for oxygen and nutrient supply and removal of metabolic by-products, but the flow also exerts shear forces on the endothelial cells, important for their proper development and vessel maturation [30, 92].

This is why other approaches focus on generating one or multiple channels, that can be perfused by connection to a tubing system with a peristaltic pump. Linear vessels can be designed using a nylon wire or a needle that is engulfed by the matrix and subsequently removed to form a hollow channel [81, 93]. Other approaches use spatial micropatterning, decellularized tissues or 3D bioprinting to generate hollow channels [28, 69, 91, 94]. Also 3D printing of sacrificial material is used to form a place holder which can afterwards be dissolved [95]. They all have in common to generate hollow structures that can then be seeded with endothelial cells to envelop the vessel walls. For the perfusion of these models, they have to be cultured in tailored bioreactors that enable the connection to a tubing and pumping system.

1.1.4 Bioreactors for perfused tissue engineered constructs

Bioreactor systems are widely used in tissue engineering to provide optimal culture conditions for engineered constructs. They maintain and preserve the tissue construct while mimicking the natural cellular niche [96, 97]. Therefore, they have to recreate the conditions *in vivo* regarding temperature, mechanical stimuli or spatial organisation. Bioreactors have to meet the criterion of being easy in handling, most importantly, they have to keep the tissue constructs sterile to prevent contaminations, the material has to be biocompatible and non-toxic for the cells and it is advantageous if it can be sterilized to allow for multiple use [98, 99]. Bioreactors can have the most diverse designs depending on the tissue and the application [98].

In tissue engineering, perfusion bioreactors enable dynamic culture conditions with a steady supply of the tissue construct with cell culture medium. This prevents periodic changes in media composition caused by manual media changes under static culture conditions [97, 100]. For the development of vascularized tissues *in vitro*, such bioreactors can be used for perfusion of generated channels within the tissue construct by connecting the vascular structures to a tubing system with an external pump. The challenge here is to establish a tight connection of the vascular structures to the in- and outlets of the bioreactor for proper perfusion. A major advantage is the shear stress generated by the medium flow through the channel, important for endothelial development and vessel maturation [30, 92]. Several studies showed the applicability of bioreactors for the generation and culture of vascularized tissue engineered constructs. To accomplish that, channels for perfusion were generated in the dermal compartment of the models by casting a matrix around nylon wires [81], cannulas [93, 99] or sacrificial material [95] as a negative mold and subsequent removal. The generated channels could then be seeded with HUVEC or hdmEC and cultured under dynamic flow conditions.

Regarding skin tissue engineering, another challenge is the culture of the model at the air-liquid interface. Only a few studies succeeded in the incorporation of perfusable vascular structures in human skin equivalents using tailor-made bioreactors. Groeber et al. used a biological decellularized intact vessel system from porcine jejunum as scaffold for a vascular network [94]. Using this biological scaffold, a natural, hierarchically organised vascular tree could be achieved within the models. For the culture of their skin equivalent, the authors established a tailored, sophisticated bioreactor system enabling physiological medium flow and culture at the air-liquid interface for formation of a stratified epidermis. In contrast, Mori et al. used a tailor-made culture device with a grid of nylon wires in a collagen hydrogel and seeded the so formed channels with HUVEC to generate

"Skin integrated with perfusable vascular channels on a chip" [81]. They could show that the perfused vascular channels had a positive impact on the cell density in the dermal layer due to a better nutrient and oxygen supply. Furthermore, they used their model to measure the percutaneous absorption. In a follow-up study, Mori et al. added a stretching apparatus to their culture device to show the positive impact of mechanical stimuli on the dermis and the epidermis [101]. Abaci et al. used microfabrication to generate microchannels of sacrificial material in a controlled geometry [102]. They successfully incorporated induced pluripotent stem cells (iPSC)-derived endothelial cells into the perfused channels of the skin equivalent, facilitating the potential application as skin grafts. Kim et al. developed a 3D printing platform to print the culture device and cell-laden bioinks simultaneously to generate a perfusable skin equivalent composed of epidermis, dermis and subcutis [103]. Using this method, they were able to generate straight and convoluted channels, that were seeded with HUVEC and perfusable. However, in all these approaches, the vasculature of the skin equivalent consisted of one or several macrochannels lacking a physiological microvascularization. Recently, Salameh et al. published a skin model with a complex perfusable vascular network combining central channels for perfusion with a microvascularization approach [82]. They used the culture device from Mori et al. [81] with nylon wires to generate three central channels and included in a "sandwich" technique a monolayer of HUVEC within the dermal compartment to induce vasculogenesis. They showed the applicability of their perfused vascularized skin model for skin permeability testing as well as for systemic exposure of compounds and conclude, that their model better mimics skin physiology and opens more possibilities for *in vitro* applications.

One of such applications could be the investigation of malignant melanoma. The vasculature is strongly involved in melanoma progression, but most *in vitro* tumor models do not include the vascular system and thus do not represent a tissue-specific environment [63]. Hence, vascularized skin models offer new possibilities to enhanced melanoma modeling *in vitro*.

1.2 Malignant melanoma

Malignant melanoma (MM) is the most dangerous type of skin cancer. Although accounting for only 4 % of newly diagnosed skin tumors, it is responsible for 90 % of skin cancer-related deaths [63, 104, 105]. In Germany, the incidence of MM has increased fivefold in the last 5 decades [106]. The high mortality rate of MM is due to its aggressive and early metastasis as well as the development of therapy resistance [107, 108]. More

than two thirds of all melanoma can be detected in an early stage of progression, providing a high survival rate for patients. Nevertheless, once spread to distant organs, prognosis is poor [104, 106].

1.2.1 Etiology and development

MM arises from the pigment-producing cells in the skin, the melanocytes, by stepwise transformation [104, 105, 107, 108]. As melanocytes occur not only in the skin, the disease can also affect other body sites such as the eyes or, rarely, the digestive tract. However, the most frequently occurring form is cutanous melanoma [109]. Melanoma development is, as for any kind of cancer, a multifactorial process. The most important exogenous risk factor for melanoma is exposure to ultraviolet radiation. Congenital risk factors include the skin type, a family history of melanoma as well as the amount of benign nevi. Furthermore, a previous MM increases the risk to develop a new one [105–107].

MM develops gradually from normal melanocytes. The different stages of melanoma progression are described in the Clark model (see figure 1.4) [110]. The first step is the proliferation of normal melanocytes to form a benign nevus. Although the control of growth is already disrupted in these cells, this stage is still a physiological state. Benign nevi rarely progress to cancer. But if several factors come together, dysplastic nevi are formed. They can arise from existing benign nevi or from new lesions. In the radial-growth phase, the cells proliferate within the epidermis and the tumor increases in size. The next step is the vertical-growth phase, when the transformed cells pass the basement membrane and invade the dermis. This leads finally to melanoma metastasis with melanoma cells infiltrating blood and lymph vessels and thereby spreading throughout the body to distant organs [105, 110].

The stepwise transformation of melanocytes to melanoma cells is driven by mutations in several oncogenes and tumor suppressor genes. The oncogenes v-raf murine sarcoma viral oncogene homolog B (BRAF) and the neuroblastoma RAS viral (v-ras) oncogene homolog (NRAS) are often affected. BRAF and NRAS are both proteins of the mitogen-activated protein kinase (MAPK) signaling pathway, involved in cell growth, proliferation, differentiation and migration [111–113]. The binding of extracellular ligands like growth factors to a receptor tyrosine kinase activates the cascade of the MAPK pathway, finally resulting in a cellular response. An activating mutation of one of these proteins leads to permanent signaling of the pathway and thereby to uncontrolled proliferation of the cells [109]. The numbers vary slightly in literature, reporting that BRAF mutations were seen in around 60 % of melanomas [112, 114] and NRAS muations in 15-17 % [114, 115].

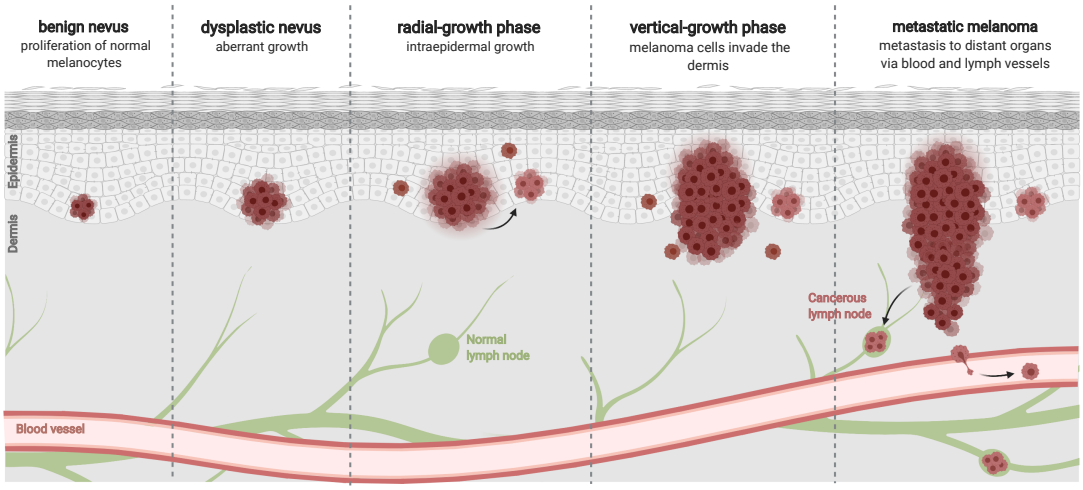

Figure 1.4: Melanoma development. Melanoma development is a multistep process. Beginning as a benign nevus of structurally normal melanocytes, different factors trigger aberrant growth resulting in a dysplastic nevus. During the radial-growth phase, cells acquire the ability to proliferate intraepidermally. The vertical-growth phase is characterized by melanoma cells invading the dermis, finally leading to metastasis to distant organs via invasion of blood and lymph vessels. Illustration adapted from "Melanoma Staging", by BioRender.com (2021). Retrieved from https://app.biorender.com/biorender-templates.

The most common mutation in BRAF is the V600E mutation, which means that valin is substituted to glutamic acid in codon 600 of exon 15, followed by V600K where the valin is changed to lysin [113, 115]. The discovery of specific driver mutations in activating signaling pathways as cause for the development of MM opened up the establishment of new therapies targeting these proteins. Novel drugs such as BRAF or MEK inhibitors have been shown to significantly improve prognosis for patients and are nowadays routinely used in the clinic [113]. Nevertheless, the tumors often establish resistance mechanisms over time. This emphasizes the need to understand the mechanisms of MM development and to develop new therapies for better survival chances and cure of the patients.

1.2.2 Melanoma models

To study melanomagenesis and the efficacy and safety of potential new therapeutics, various model systems have been established.

A large part of today's knowledge about melanoma cells comes from work done with adherent cells in two-dimensional (2D) cell culture assays. These monolayer cultures are advantageous in regard to simplicity, convenience and costs and for preliminary high-throughput screens [5]. However, beyond investigation of basic principles of tumor

cell biology, these cell cultures depict only a reductionist approach as they do not take into account the spatial formation of tumors *in vivo* and the complex tumor microenvironment, that has been shown to be crucial for tumor behaviour [5, 116, 117].

In contrast, to investigate melanoma in their *in vivo* environment, animal models are employed. Until today, different animal models have been used to study melanoma development and to assess the outcome of drugs in preclinical phases [117]. Human tumor xenografts implanted in immunosuppressed mice allow the study of primary tumors and metastases and also the implementation of patient-derived model systems. Furthermore, genetically engineered mouse models have been established, allowing to study the influence of genetic alterations on the outcome of melanoma development and progression [5].

Besides 2D cell cultures and animal models opposed at the far margins of the spectrum, 3D *in vitro* models represent a good compromise between the lack of a microenvironment in monolayer cell cultures and the high and unpredictable complexity of experimentation in living animals [118].

In recent years, various 3D melanoma models have been established. The simplest approach are spheroid models, already established in the early 1970s by Sutherland et al. [119]. Spheroids are globular aggregates of multiple cells that can be generated using different techniques from tumor cells alone or in co-culture with other cells. These spheroids better simulate the tumor conditions *in vivo* as they enable cell-cell contacts and the formation of a heterogenous tumor mass caused by an oxygen and nutrient gradient [5, 117, 120]. They can be used for drug screening or implanted into different matrices to study melanoma growth and invasion. However, spheroids only depict the tumor and not the surrounding tissue, therefore neglecting the interactions of tumor cells with neighbouring normal cells and the ECM.

To mimic further the environment in which melanoma naturally develops, the above mentioned skin models provide suitable settings. By seeding melanoma cells together with keratinocytes on top of the dermal equivalents, many studies showed the generation of tumors in FTSEs [50, 63, 64, 121–123]. Other authors showed the incorporation of melanoma spheroids in the dermal part of FTSE, mimicking cutaneous melanoma metastases [39]. It has been established, that the incorporated melanoma cells show similarities in their growth and invasion properties to the tumors from which they originated [5, 39, 64]. Thus, melanoma skin models can be employed to investigate melanoma progression and spreading. Furthermore, they are used as preclinical test systems for new anti-tumor therapies, and are also conceivable to be used in personalized medicine with cells isolated from a patient's melanoma [50, 63, 117].

However, even these models are not able to mimic human skin and therefore the

environment of MM in total. Already in 1971, Judah Folkman postulated that tumors could not grow without the formation of new blood vessels and that they therefore secrete angiogenic factors to stimulate neovascularization [124]. This was when the idea of anti-angiogenic therapies for tumors was born. In fact, the vascular network is involved in tumor progression and an important part of the tumor microenvironment [63]. In order to supply the growing tumor mass, the tumor needs vascularization [125]. The tumor vasculature is developed by angiogenesis via sprouting endothelial cells from nearby vessels, and to a lesser extent by vasculogenesis, in which vessels start to form from circulating cells [126]. To initiate and maintain these processes, the tumor secretes growth factors to attract endothelial cells for capillary formation that will supply the melanoma [124, 125]. This pathological angiogenesis leads to abnormal vessels regarding structure and function. Due to an imperfect lining of endothelial cells and abnormal vessel walls, the vessels are unstable and leaky. The tumor vascular network is chaotic without the hierarchical structure of normal vessels. This renders it unfunctional and results in avascular, hypoxic voids and a chaotic blood flow [30, 127]. Furthermore, the tumor needs the vasculature for its last developmental state, metastasis. A decisive aspect of melanoma progression and its aggressiveness is the invasion of tumor cells into blood and lymph vessels and the concomitant spreading throughout the body to distant organs. To study this last step in melanoma development, skin models with a functional vasculature are needed. They could also be employed as test system to study anti-angiogenic therapies. First approaches were made by Gibot et al. [64] and Bourland et al. [63], who used cell sheet technology to generate a 3D melanoma skin equivalent with incorporated HUVEC or hdmEC, respectively. They established capillary networks within the melanoma skin models and therefore provided a more natural microenvironment for the tumor. However, these vascular structures cannot be perfused, thereby limiting the application possibilities for investigating tumor metastasis.

1.3 Aim of the thesis

Tissue engineered skin equivalents are broadly used, in the clinic as skin grafts as well as for *in vitro* testing. However, most of the established skin models lack a vasculature, limiting their applicability. In recent years, several approaches aimed at this problem, but so far there are no skin equivalents with a functional, i. e. perfusable vasculature. But without a vasculature, a vital aspect of the tissue environment is missing. This becomes especially apparent for modeling diseases affecting or interacting with the vascular system. One of such pathologies is malignant melanoma. This skin cancer uses lymph and blood

vessels for its dissemination throughout the body to form distant metastases. Furthermore, the tumor interacts with the cells of the vascular system to form new vessels for its own supply. Up to date, different skin models mimic melanoma *in vitro* but without a proper vasculature, they cannot recapitulate the final step of melanoma progression, i. e. metastasis formation. Thus, studies on melanoma metastasis rely on animal models. However, due to scientific, economic and ethical reasons animal experimentation should be replaced.

Therefore, the aim of this thesis is to find vascularization strategies for FTSEs that can be used as a test system to study melanoma development and metastasis and thus serve as an alternative to animal models. To target this goal, this thesis consists of two parts (see figure 1.5).

In the first part, vascularization strategies for FTSEs shall be investigated. Therefore, two approaches are pursued: By seeding endothelial cells in co-culture with fibroblasts in the dermal part of the FTSEs, the self-assembly capacity of endothelial cells is exploited to generate capillary-like structures within the FTSE. Here, an optimized seeding strategy and cell density have to be evaluated. Perfusion is achieved via molding a central channel seeded with endothelial cells in the collagen hydrogel using a tailor-made bioreactor. Combining both strategies shall enable the generation of a perfused, vascularized skin model. After a tissue maturation phase, it is hypothesized that the capillary-like structures within the dermis connect themselves to the central vessel and thereby enable the generation of a perfusable network.

The second part of this thesis aims at the establishment of melanoma FTSEs. The models will be generated by seeding melanoma cells within the epidermis of FTSEs. The successful integration will be characterized histologically.

As an overall goal, the combination of the vascularized FTSE and the melanoma model shall create a sophisticated melanoma skin model to enable the investigation of the interactions of the melanoma with the vasculature and to mimic melanoma metastasis. Hence, the vascularization strategies for FTSEs are applied to study the progression of malignant melanoma, closing the circle of the two parts of this thesis.

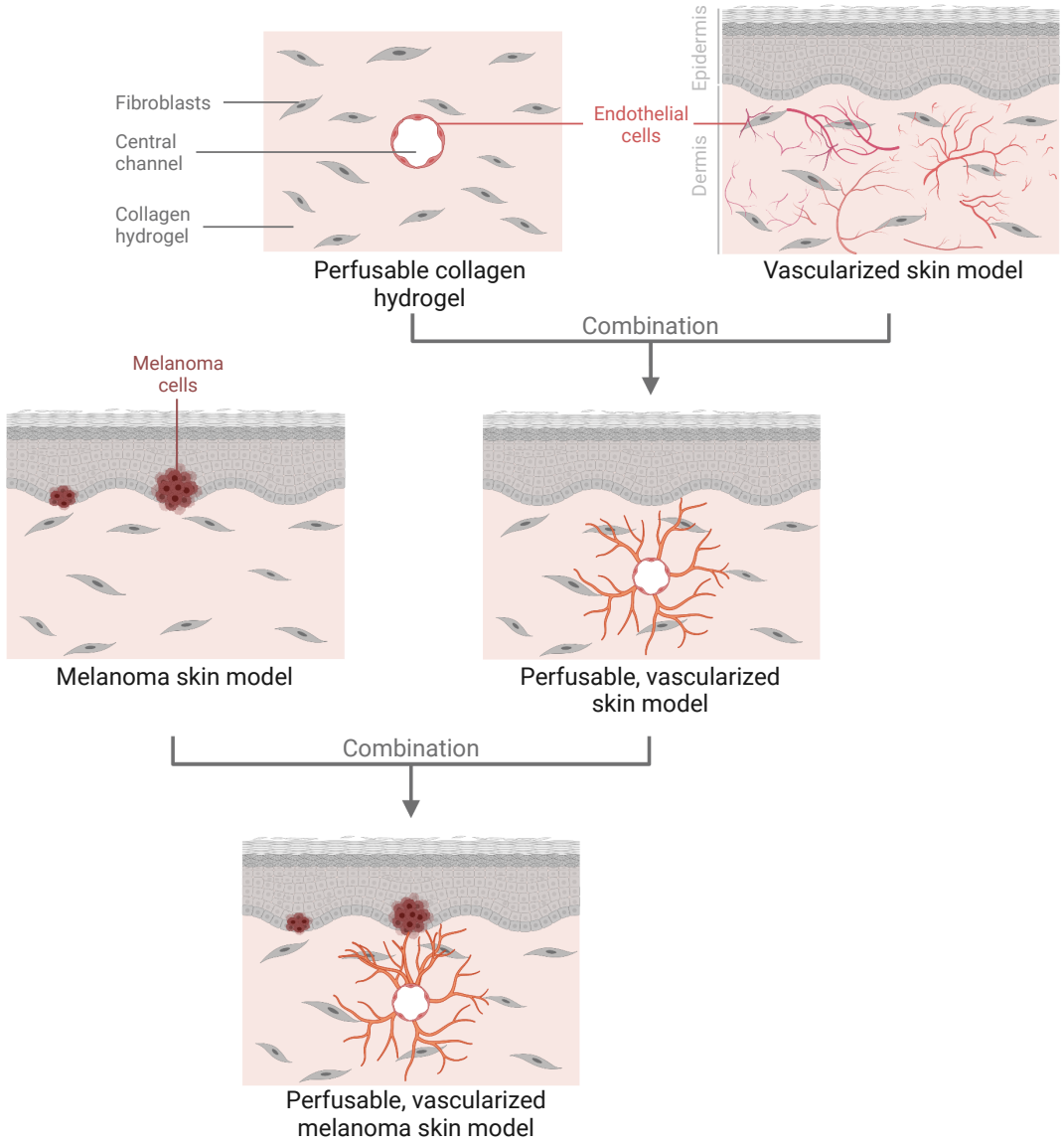

Figure 1.5: Schematic outline of the thesis. Different models have to be established towards a model for investigation of melanoma progression. On the one side, a vascularized skin model shall be generated by combining a capillary network with a central channel within the models for perfusion. On the other hand, melanomas are integrated in the skin models. Combining both models will lead to a vascularized skin model for studying melanoma-endothelial interactions and metastasis. Illustration created with BioRender.com.

2 Materials

2.1 Reagents

Table 2.1: Table of reagents

Designation	Manufacturer
2-Propanol	Sigma-Aldrich, St. Louis (US)
3-(4,5-Dimethyl-2-thiazolyl)-2,5-diphenyl-2H-tetrazolium bromide (MTT)	Sigma-Aldrich, St. Louis (US)
4',6-diamidino-2-phenylindole (DAPI) (1 mg/ml)	Thermo Fisher Scientific, Waltham (US)
Acetic acid 100 %	Carl Roth, Karlsruhe (DE)
Accutase ready-to-use	Thermo Fisher Scientific, Waltham (US)
Antibody dilution solution	DCS Innovative Diagnostic-Systems, Hamburg (DE)
Ascorbyl-2-phosphate	Sigma-Aldrich, St. Louis (US)
Bovine serum albumin (BSA)	Santa Cruz Biotechnology, Dallas (US)
Calcium dichloride ($CaCl_2$) dihydrate	Sigma-Aldrich, St. Louis (US)
CD31 MicroBead Kit	Miltenyi Biotec, Bergisch Gladbach (DE)
CellTiter-Glo® Luminescent Cell Viability Assay	Promega GmbH, Walldorf (DE)
Chondroitin sulfate	Sigma-Aldrich, St. Louis (US)
Citric acid monohydrate	Agilent Dako, Santa Clara (US)
Collagen type IV from from human placenta	Sigma-Aldrich, St. Louis (US)
Collagenase 0.19 U/mg	Serva Electrophoresis GmbH, Heidelberg (DE)
Decorin, recombinant human protein	Abcam, Cambridge (UK)
Descosept	Dr. Schumacher, Malsfeld-Beiseförth (DE)
Dimethyl sulfoxide (DMSO)	Sigma-Aldrich, St. Louis (US)
Dispase 1.83 U/mg	Thermo Fisher Scientific, Waltham (US)
DMEM + GlutaMAX 4.5 g/l D-glucose	Thermo Fisher Scientific, Waltham (US)
DMEM high glucose	Thermo Fisher Scientific, Waltham (US)
DMEM powder	Thermo Fisher Scientific, Waltham (US)
Entellan	Merck, Darmstadt (DE)
Eosin	Morphisto, Frankfurt am Main (DE)
Epilife medium	Thermo Fisher Scientific, Waltham (US)

Table of reagents (continued)

Designation	Manufacturer
Ethanol 99 %	Sigma-Aldrich, St. Louis (US)
Ethylenediaminetetraacetric acid disodium salt dihydrate (EDTA) solution 0.5 M pH = 8.0	Sigma-Aldrich, St. Louis (US)
Foetal calf serum (FCS)	Biochrom, Berlin (DE)
Foetal calf serum (FCS)	Bio & Sell, Feucht (DE)
FibroLife Serum-Free Medium Complete Kit	Lifeline Cell Technologies, Frederick (US)
Fibronectin from human plasma	Sigma-Aldrich, St. Louis (US)
Fluoresceindiacetate	Sigma-Aldrich, St. Louis (US)
Fluoromount with DAPI	Thermo Fisher Scientific, Waltham (US)
Haematoxylin	Morphisto, Frankfurt am Main (DE)
HEPES	Sigma-Aldrich, St. Louis (US)
Hydrogen peroxide 30 %	Merck, Darmstadt (DE)
Human keratinocyte growth supplement (HKGS)	Thermo Fisher Scientific, Waltham (US)
Keratinocyte growth factor (KGF)	Thermo Fisher Scientific, Waltham (US)
Paraffin	Carl Roth, Karlsruhe (DE)
Penicillin / Streptomycin (100 U/mL Pen, 10 mg/mL Strep)	Sigma-Aldrich, St. Louis (US)
Phosphate buffered saline with $MgCl_2$ and $CaCl_2$ (PBS^+)	Sigma-Aldrich, St. Louis (US)
Phosphate buffered saline without $MgCl_2$ and $CaCl_2$ (PBS^-)	Sigma-Aldrich, St. Louis (US)
Pronase 1 mg/ml I	Roche Diagnostics, Rotkreuz (CH)
Propidium iodide	Sigma-Aldrich, St. Louis (US)
Roti-Histofix (Paraformaldehyde 4 %)	Carl Roth, Karlsruhe (DE)
RPMI 1640 + GlutaMAX	Thermo Fisher Scientific, Waltham (US)
Sodium bicarbonate ($NaHCO_2$)	Carl Roth, Karlsruhe (DE)
Sodium hydroxide (NaOH) 1 M	Carl Roth, Karlsruhe (DE)
SuperVision 2 HRP Kit	DCS Innovative Diagnostic-Systems, Hamburg (DE)
Tris(hydroxymethyl)-aminomethan (Tris)	Carl Roth, Karlsruhe (DE)
Triton-X 100	Carl Roth, Karlsruhe (DE)
Trypan blue 0.4 %	Sigma-Aldrich, St. Louis (US)
Trypsin / EDTA 0.5 %	Thermo Fisher Scientific, Waltham (US)
Tween-20	Sigma-Aldrich, St. Louis (US)
VascuLife VEGF-Mv Medium Complete Kit	Lifeline Cell Technologies, Frederick (US)
Versene	Thermo Fisher Scientific, Waltham (US)
Xylol	Sigma-Aldrich, St. Louis (US)

2.2 Consumables

Table 2.2: Table of consumables

Designation	Manufacturer
Air filter for bioreactor, Minisart	Sartorius Stedim Biotech GmbH, Göttingen (DE)
Aluminium foil	Carl Roth, Karlsruhe (DE)
Autoclave bags	Hartenstein, Würzburg (DE)
Biopsy pads	VWR, Radnor (US)
Cell culture plate 12 well (deep)	Greiner Bio-One, Frickenhausen (DE)
Cell culture plate 6 well	Corning, New York (US)
Cell sieve 100 µm	Greiner Bio-One, Frickenhausen (DE)
Cell sieve 30 µm	Miltenyi Biotec, Bergisch Gladbach (DE)
Centrifuge tube 15 ml, 50 ml	Greiner Bio-One, Frickenhausen (DE)
Combitip 2.5 ml, 5 ml, 10 ml, 25 ml	Eppendorf, Hamburg (DE)
Corning Costar Snapwell inserts 0.4 µm for 6 well plates	Corning, New York (US)
Corning Costar Snapwell plate 6 well	Corning, New York (US)
Cover slip 24 x 60 mm	Thermo Fisher Scientific, Waltham (US)
Cryotube 2 ml	Greiner Bio-One, Frickenhausen (DE)
Culture flasks T25, T75, T150	TPP, Trasadingen (DE)
Culture flask T175	Greiner Bio-One, Frickenhausen (DE)
Embedding cassettes	VWR, Radnor (US)
E-plates View 96 for xCELLigence	ACEA Biosciences Inc., San Diego (US)
Filter 0.2 µm, 0.45 µm	Sarstedt, Nümbrecht (DE)
Filter paper	Labonord, Mönchengladbach (DE)
Fluorodish	World Precision Instruments, Sarasota County (US)
Gloves	Hartmann, Heidenheim (DE)
LS and MS columns with ferromagnetic spheres	Miltenyi Biotec, Bergisch Gladbach (DE)
Luer valve (needlefree, swabable)	Nordson Medical, Loveland (US)
Menzel glass microslides	Thermo Fisher Scientific, Waltham (US)
Microplate 6 well, 12 well, 24 well	TPP, Trasadingen (DE)
Microplate 96 well U-bottom	Greiner Bio-One, Frickenhausen (DE)
Microtome blade S35	Pfm medical, Köln (DE)
Parafilm "M" laboratory film	Bemis, Neenah (US)
Pasteur pipette 230 mm	Brand, Wertheim (DE)
Peripheral venous catheter	B. Braun, Melsungen (DE)
Petri dish 100	TPP, Trasadingen (DE)
Pipet tips 0.1 - 10 µl, 10 - 200 µl, 100 - 1 250 µl	NerbePlus, Winsen/Luhe (DE)

Table of consumables (continued)

Designation	Manufacturer
Polysine microslides	Thermo Fisher Scientific, Waltham (US)
Scalpel blades	Bayha, Tuttlingen (DE)
Serological pipettes 5 ml, 10 ml, 25 ml, 50 ml	Greiner Bio-One, Frickenhausen (DE)
Silicone tubes	IDEX Health & Science GmbH, Wertheim (DE)
Sterile plastic reservoir	Kisker Biotech, Steinfurt (DE)
Syringes with Luer Lok 5 ml, 10 ml, 20 ml	BD Bioscience, Franklin Lakes (US)
Three-way valve	B. Braun, Melsungen (DE)
Reaction tubes 1.5 ml, 2 ml	Sarstedt, Nümbrecht (DE)
Weighing dishes (polystyrene)	Brand, Wertheim (DE)

2.3 Instruments

Table 2.3: Table of instruments

Designation	Manufacturer
Aspiration system Vacuboy	Integra Biosciences, Biebertal (DE)
Centrifuge	Thermo Fisher Scientific, Waltham (US)
Cold-storage room 4 °C	Genheimer, Höchberg (DE)
Compression motor	TERM Würzburg (DE)
Confocal microscope TCS SP8	Leica, Wetzlar (DE)
Cryo tank	German-Cryo, Jüchen (DE)
Electronic balance	Kern, Balingen-Frommern (DE)
Embedding machine	Thermo Fisher Scientific, Waltham (US)
Freezer -20 °C	Liebherr, Biberach (CH)
Freezer -80 °C	Kendro, Oberschleißheim (DE)
Fume hood	Prutscher Laboratory Systems, Neudörfl (AT)
Hand tally counter	NeoLab, Heidelberg (DE)
Heating cabinet 37 °C	Medite, Burgdorf (DE)
Heating cabinet 60 °C	Medite, Burgdorf (DE)
Ice machine AF-80	Scotsman, Milan (IT)
Incubator Heracell 240i	Thermo Fisher Scientific, Waltham (US)
Incubator with pump for bioreactors	TERM Würzburg (DE)
Labelling device for embedding cassettes	Vogel, Senftenberg (DE)
Labelling device for microslides	Vogel, Senftenberg (DE)
Lypholisateur Alpha 2-4 LSC plus	Christ, Osterode am Harz (DE)

Table of instruments (continued)

Designation	Manufacturer
Magnetic stirrer	VWR, Radnor (US)
Microscope	Zeiss, Oberkochen (DE)
Microscope Evos	Thermo Fisher Scientific, Waltham (US)
Microscope Keyence Biorevo BZ-9000	Keyence, Neu-Isenburg (DE)
Microtome SM 2010R	Leica, Wetzlar (DE)
Mulitstep pipette	Eppendorf, Hamburg (DE)
Multichannel pipette	Eppendorf, Hamburg (DE)
Orbital shaker	VWR, Radnor (US)
Paraffin embedding module	Leica, Wetzlar (DE)
pH meter	Mettler Toledo, Giessen (DE)
Pipette 0.5 -10 µl	Eppendorf, Hamburg (DE)
Pipette 10 - 100 µl	Eppendorf, Hamburg (DE)
Pipette 100 - 1 000 µl	Eppendorf, Hamburg (DE)
Pipetting aid Accu-jet Pro	Brand, Wertheim (DE)
Plate reader Infinite® 200 PRO	Tecan Trading AG, Männedorf (CH)
Refrigerator 4 °C	Kirsch, Willstätt-Sand (DE)
Rocking platform	NeoLab, Heidelberg (DE)
Safety cabinet Safe2020	Thermo Fisher Scientific, Waltham (US)
Spinner flask	Corning, Wiesbaden (DE)
Steam cooker	Braun, Kronberg/Taunus (DE)
Timer	Carl Roth GmbH, Karlsruhe (DE)
Ultracentrifuge Avanti J-26xp	Beckman Coulter, Krefeld (DE)
Ultrapure water system	Millipore, Schwalbach (DE)
Vacuum pump	VWR, Radnor (US)
Vortex shaker	Carl Roth GmBH, Karlsruhe (DE)
Water bath	Memmert, Büchenbach (DE)
xCELLigence RTCA SP	ACEA Biosciences Inc., San Diego (US)

2.4 Software

Table 2.4: Table of software

Designation	Manufacturer
BioRender	BioRender, Toronto (CA)
BZ-II Viewer (BZ-9000)	Keyence, Neu-Isenburg (DE)
Compression Software	TERM Würzburg (DE)
GraphPad PRISM 9	GraphPad Software, La Jolla (US)
ImageJ	National Institutes of Health, Bethesda (US)
Microsoft Office Excel	Microsoft Corporation, Redmond (US)
TeXShop	Richard Koch, Max Horn, Dirk Olmes
xCELLigence RTCA Software Pro	ACEA Biosciences Inc., San Diego (US)

2.5 Laboratory equipment

Table 2.5: Table of laboratory equipment

Designation	Manufacturer
Beakers 250 and 1 000 ml	Schott, Mainz (DE)
Casting molds for paraffin blocks	Labonord, Mönchenglattbach (DE)
Compression reactor	TERM Würzburg (DE)
DRS Dermapen, 32 x 1 mm needles	DRS Edueo, Berlin (DE)
Forceps	Fine Science Tools FST, Heidelberg (DE)
Funnel	Hartenstein, Würzburg (DE)
Grease pen	Agilent Dako, Santa Clara (US)
Laboratory bottles 1 l, 250 ml, 100 ml, 50 ml	Schott, Mainz (DE)
Luer-Lock connectors	Nordson medical, Fort Collins (US)
MACS MultiStand	Milteny Biotec, Bergisch Gladbach (DE)
Magnetic stir bar and rod	Hartenstein, Würzburg (DE)
Measuring cylinder 100 ml	Vitlab, Großostheim (DE)
Measuring cylinder 500 ml	Vitlab, Großostheim (DE)
Metal cannulas 16 G and 18 G	NeoLab, Heidelberg (DE)
Metal carrier basket	Merceteo, München (DE)
MiniMACS and MidiMACS (magnets)	Milteny Biotec, Bergisch Gladbach (DE)
Mr. Frosty freezing aid	Thermo Fisher Scientific, Waltham (US)
Neubauer counting chamber	Hartenstein, Würzburg (DE)
Protective gloves against cold	VWR, Darmstadt (DE)
Pumping tubes	Cole-Parmer GmbH, Wertheim (DE)

Table of laboratory equipment (continued)

Designation	Manufacturer
Safety goggles	NeoLab, Heidelberg (DE)
Scalpel blades	Bayha, Tuttlingen (DE)
Scalpel holder	Bayha, Tuttlingen (DE)
Sealing ring	Arcus GmbH, Seevetal (DE)
Spatula	Hartenstein, Würzburg (DE)
Spray bottle	Hartenstein, Würzburg (DE)
Staining jar acc. Hellendahl	Paul Marienfeld GmbH & Co.KG, Lauda-Königshofen (DE)
Stainless steel autoclaving container	Fine Science Tools, Heidelberg (DE)
Tube rack	NeoLab, Heidelberg (DE)
Mediumflasche für Bioreaktor	Schott, Mainz (DE)

2.6 Antibodies

Table 2.6: Table of primary antibodies

Antibody	Manufacturer	Article number	Dilution	Host	Antigen retrieval
CD31	Agilent Dako, Santa Clara (US)	M0823	1:100	mouse	none
Collagen IV	Sigma-Aldrich, St. Louis (US)	C1926	1:500	mouse	20 min pronase at room temperature
Cytokeratin 10	Agilent Dako, Santa Clara (US)	M7002	1:100	mouse	none
Cytokeratin 14	Sigma-Aldrich, St. Louis (US)	HPA023040	1:1000	rabbit	none
Decorin	Abcam, Cambridge (UK)	ab175404	1:200	rabbit	none
Hmb-45	Agilent Dako, Santa Clara (US)	M0634292	1:50	mouse	none
Ki-67	Abcam, Cambridge (UK)	ab16667	1:100	rabbit	none
Melan-A	Agilent Dako, Santa Clara (US)	M7196	1:50	mouse	heat pH 9
S100 beta	Abcam, Cambridge (UK)	ab52642	1:500	rabbit	heat pH 9
Vimentin	Abcam, Cambridge (UK)	ab92547	1:1000	rabbit	none

Table 2.7: Table of secondary antibodies

Antibody	Manufacturer	Article number	Dilution	Host
Alexa Fluor 647 donkey anti-mouse	Thermo Fisher Scientific, Waltham (US)	A31571	1:400	donkey
Alexa Fluor 555 donkey anti-mouse	Thermo Fisher Scientific, Waltham (US)	A31570	1:400	donkey
Alexa Fluor 555 donkey anti-rabbit	Thermo Fisher Scientific, Waltham (US)	A31572	1:400	donkey
Alexa Fluor 488 donkey anti-rabbit	Thermo Fisher Scientific, Waltham (US)	A21206	1:400	donkey

2.7 Cell culture media

Table 2.8: Table of cell culture media composition

Description		Composition
DMEM	10 %	FCS
	5 %	Penicillin-Streptomycin (100x)
		in DMEM + GlutaMAX + 4.5 g/l D-glucose
E1	1 %	Human Keratinocyte Growth Supplements
	1 %	Penicillin-Streptomycin (100x)
		in EpiLife Basal Medium
E10	1 %	Human Keratinocyte Growth Supplements
	1 %	Penicillin-Streptomycin (100x)
	1.44 mM	Calcium chloride
	73 µg/ml	Ascorbyl-2-phosphate
	10 ng/ml	keratinocyte growth factor
	10 %	FibroLife
		in EpiLife Basal Medium

Table of cell culture media composition (continued)

Description		Composition
FibroLife	5 ng/ml	recombinant human bFGF
	5 µg/ml	recombinant human insulin
	50 µg/ml	Ascorbic acid
	7.5 mM	L-Glutamine
	1 µg/ml	Hydrocortisone Hemisuccinate
	2 %	FCS
		in FibroLife Basal Medium
RPMI	10 %	FCS
	5 %	Penicillin-Streptomycin (100x)
		in RPMI 1640 + GlutaMAX
VascuLife	5 ng/ml	recombinant human VEGF
	5 ng/ml	recombinant human EGF
	5 ng/ml	recombinant human bFGF
	15 ng/ml	recombinant human IGF-1
	10 mM	L-Glutamine
	1 µg/ml	Hydrocortisone Hemisuccinate
	0.75 U/ml	Heparin Sulfate
	50 µg/ml	Ascorbic Acid
	5 %	FCS
	1 %	Penicillin-Streptomycin (100x)
		in VascuLife Basal Medium

2.8 Buffers and solutions

Table 2.9: Table of buffers and solutions

Description		Composition
Blocking buffer	0.03 %	Triton-X-100
	5 %	BSA
		in PBS^-
Collagenase solution	500 U/ml	collagenase
		in DMEM high glucose
Dispase solution	2 000 U/l	dispase
		in PBS^-
Gel neutralisation solution (GNS)	50 µg/ml	chondroitin sulfate
	90 mM	HEPES
	3 %	FCS
		in DMEM high glucose (2x)
		pH 8.5
MACS-buffer	2 mM	EDTA
	0.5 %	BSA
		in PBS^-
Methocel stem solution	12 g/l	methylcellulose
		in VascuLife Basal Medium
Tris/EDTA buffer	100 mM	Tris
	10 mM	EDTA
		in aqua dest.
		pH 9.0
Trypsin/EDTA 0.05 %	10 %	0.5 % trypsin/EDTA
		in PBS^-
Washing buffer	0.05 %	Tween 20
		in PBS^-

3 Methods

3.1 Cell culture

All cell culture related work was performed under sterile conditions in a safety cabinet. Used materials have been sterilised by autoclaving, unless they have already been provided sterile by the manufacturer. If not already sterile, media and buffers were sterile filtered and prewarmed to 37 °C prior to usage if not annotated otherwise. Cells and models were cultured in a humidified incubator at 37 °C and 5 % CO_2. Centrifugation steps were carried out at 300 x g for 5 minutes at room temperature, if not annotated otherwise.

3.1.1 Isolation and culture of primary human skin cells

Preparation of human skin biopsies for cell isolation

For isolation of primary human skin cells, juvenile foreskin biopsies from donors aged 1-5 years were used. The skin samples were obtained with the consent of the legal guardian and with approval of the local ethical board of the University of Würzburg (vote 182/10). The biopsies were washed with PBS^+ 3 times and examined optically. Inflamed areas were cut off and discarded, likewise adipose and connective tissue were removed with a scalpel. After the biopsy was washed again with PBS^+, it was cut into 2 x 4 mm stripes and incubated in 10 ml dispase (2 U/ml) for 16-18 hours at 4 °C. Subsequently, the epidermis could be separated from the dermis mechanically with forceps. Epidermal and dermal stripes were collected separately in PBS^+. The epidermis was used to isolate keratinocytes, while fibroblasts and endothelial cells were gained from the dermis as illustrated in figure 3.1.

Isolation and culture of human epidermal keratinocytes

The epidermal stripes were used for isolation of human epidermal keratinocytes (heK). Therefore, the stripes were washed with PBS^- and enzymatically digested with 10 ml prewarmed 0.05 % Trypsin/EDTA. During incubation at 37 °C for 5 minutes, the stripes were held in suspension by swivelling and vortexing the tube several times. The enzymatic

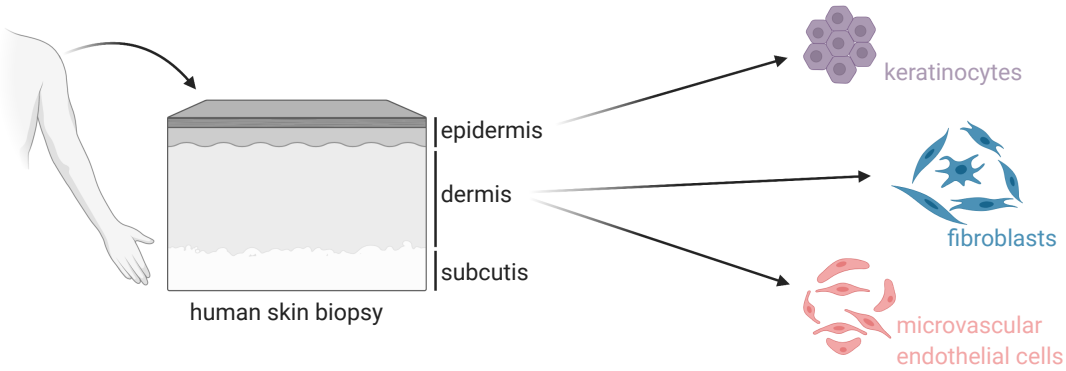

Figure 3.1: Schematic and simplified representation of the cell isolation from human skin biopsies. Keratinocytes are isolated from the epidermis, whereas fibroblasts and endothelial cells are isolated from the dermis. Illustration created with BioRender.com.

digestion was stopped by adding 1 ml fetal calf serum (FCS). To break off the keratinocytes from the partially digested tissue, the pieces were resuspended strongly for 5 minutes by pipetting the suspension up and down. The obtained solution of cells and remaining tissue pieces was transferred into a 50 ml tube via a cell sieve with a pore size of 100 µm. After washing the cell sieve for three times with 5 ml PBS^+, the cell suspension was centrifuged. The resulting pellet was resuspended in 1-5 ml E1 cell culture medium. The cell number was determined using trypan blue and a Neubauer improved cell counting chamber (see section 3.1.6). 10 000-20 000 heK/cm^2 were seeded in T175 cell culture flasks in E1 cell culture medium. Medium was changed for the first time after 2-4 days to allow for the keratinocytes to adhere properly. Further medium changes were carried out every other day, until the cells reached a confluency of 70-80 %.

Isolation and culture of human dermal microvascular endothelial cells

The dermis stripes were used for isolation of hdmEC. The stripes were washed with 10 ml versene and enzymatically digested with 10 ml 0.05 % Trypsin/EDTA for 40 minutes at 37 °C. After the enzymatic reaction was stopped by adding 1 ml FCS, the dermis pieces were transferred to a petri dish with prewarmed VascuLife medium. To extract the hdmEC from the dermis pieces, the stripes were gently scratched out several times from each side using a scalpel. The remaining stripes were stored in PBS^- for the following isolation of human dermal fibroblasts (hdF), while the cell suspension was transferred into a 50 ml tube via a cell sieve with a pore size of 100 µm. After washing the petri dish and the cell sieve for three times with 5 ml VascuLife, the cell suspension was centrifuged. The

cell pellet was resuspended in 1-2 ml VascuLife and the cell number was determined using trypan blue and a Neubauer improved cell counting chamber as described in section 3.1.6. 12 000 hdmEC/cm^2 were seeded in T25 cell culture flasks in 3 ml VascuLife. Medium was changed for the first time after 3-4 days and afterwards every 2-3 days. HdmEC were cultured until they reached a confluency of 70-80 %.

Isolation and culture of human dermal fibroblasts

The scratched out dermis stripes were used for isolation of hdF. Therefore, they were minced into small pieces until reaching a mash-like consistency and enzymatically digested with 10 ml collagenase (500 U/ml) for 45 minutes at 37 °C. During incubation, the suspension was vortexed every 10 minutes. After centrifugation, the pellet was resuspended in 10 ml Dulbecco's Modified Eagle's Medium (DMEM) culture medium. Subsequently, the dermis mash was pelleted again by centrifugation and resuspended in 2 ml DMEM. The suspension was transferred to a with DMEM moistened T75 cell culture flask and the small dermis pieces were distributed homogenously across the cell culture surface allowing the fibroblasts to grow out of the tissue. The next day, 6 ml DMEM were added carefully to the flask without detaching the dermis pieces from the surface. Medium was first changed after 4-5 days and afterwards every 2-3 days. As the fibroblasts grew out of the dermis pieces, remaining tissue pieces were washed out during medium changes. HdF were cultured until they reached a confluency of 80-90 %.

3.1.2 Endothelial cell purification

Due to the isolation process, endothelial cell cultures may be contaminated with hdF. To obtain a hdmEC culture as pure as possible, magnetic-activated cell sorting (MACS) was performed using MACS technology of Miltenyi Biotec (Bergisch-Gladbach, Germany). For a positive selection, hdmEC were labeled with anti-CD31 antibodies linked to magnetic nanoparticles. Placed in a strong magnetic field, labeled cells were hold back in the column while unlabeled cells flowed through. Separation was performed according to the manufacturer's instructions. Briefly, hdmEC in passage 0 were detached and counted (see sections 3.1.5 and 3.1.6). Pelleted cells were incubated with the magnetic nanoparticle-linked antibody against CD31 for 15 minutes on ice. Remaining antibody was washed off by centrifugation and cells were resuspended in MACS-buffer. For separation, the cell suspension was transferred to a pre-wetted MACS-column matching the cell number placed in the magnetic field. Cells attached to the nanoparticles were retained in the column while unlabeled cells ran through. The column was rinsed with MACS-buffer

three times and then removed from the magnetic field to elute the CD31-positive hdmEC. The cells were sedimented by centrifugation, resuspended in VascuLife medium and either seeded into cell culture flasks for further expansion or frozen for storage.

3.1.3 Culture of human umbilical vein endothelial cells

Human umbilical vein endothelial cells (HUVEC) were purchased from CellSystems GmbH (Troisdorf, Germany). HUVEC were seeded at a density of 3 000 cells/cm^2 and cultured in VascuLife medium with medium exchanges every two to three days until reaching a confluency of 70-80 %.

3.1.4 Culture of melanoma cells

Melanoma cell line SK-MEL-28 was kindly provided by Prof. Dr. Nick Hayward, Queensland Institute for Medical Research (Brisbane, Australia). Melanoma cell line BLM was kindly offered by Prof. Dr. Marc Schmidt, Department of Dermatology at the University Hospital Würzburg (Würzburg, Germany). Melanoma cells were seeded at a density of 3 000 cells/cm^2 and cultured in RPMI medium. Medium was exchanged every two to three days until reaching 80-90 % confluency.

3.1.5 Cell passaging

When cells reached a confluency of 70-90 % depending on the cell type, they were passaged which means they were detached from the culture flask surface and reseeded in a lower density. This is necessary for the cells to proliferate as they stop dividing and growing, start to differentiate or detach from the cell culture surface if there is no more space left. Therefore, the medium in the cell culture flasks was aspirated and the cells were washed once with PBS$^-$. For detachment, heK were incubated with 0.04 ml/cm^2 accutase for 10-15 minutes at 37 °C, whereas all other cell types were detached using 0.05 % trypsin/EDTA solution (0.06 ml/cm^2) for 5-10 minutes at 37 °C. Detachment of the cells was controlled microscopically during incubation. Trypsin had to be inactivated after incubation by adding of 10 % FCS. The cell suspensions were then transferred to a tube and flasks were rinsed once with PBS$^-$ to collect remaining cells. Subsequently, cells were sedimented by centrifugation and the resulting pellet was resuspended in the according cell culture medium. The cell count was determined (see section 3.1.6) and cells were used for experiments or reseeded into cell culture flasks for further expansion. HeK and hdF were seeded at a density of 4 000 cells/cm^2 in E1 medium or DMEM, respectively. HdmEC and HUVEC were seeded at a density of 3 000 cells/cm^2 in VascuLife. SK-MEL-28 and

BLM were seeded at a density of 3 000 cells/cm^2 and cultured in RPMI medium. HeK were used for experiments in passage 3, hdF, hdmEC and HUVEC in passages 3 to 5. For melanoma cell lines, the passage number was not determined.

3.1.6 Cell counting

The cell concentration of suspensions was determined by counting the cells using a Neubauer improved cell counting chamber. Therefore, the cell suspension was mixed with 0.4 % trypan blue solution in a ratio of 1:1 to 1:10 depending on the cell density. Cells were counted in all four quadrants of the counting chamber employing a light microscope. The mean value of the quadrants was calculated and multiplied by 10 000 (Neubauer chamber volume factor) and the dilution factor of trypan blue to obtain the cell count per ml (see following equation).

$$\text{mean value of counted cells in four quadrants} \times 10^4 \times \text{dilution factor} = \text{cell count/ml}$$

3.1.7 Cryopreservation and thawing of cells

For cryopreservation, $3 * 10^6$ cells/ml (heK) or $1 * 10^6$ cells/ml (hdF, hdmEC, HUVEC and melanoma cells) in their respective cell culture medium additionally containing 10 % dimethyl sulfoxide were put in a cryotube and initially frozen at -80 °C using a freezing container with a freezing rate of 1 °C/minute. After 24 hours, the cryotubes were transferred to the gas phase of liquid nitrogen below -130 °C for long-term storage.

Frozen cells were quickly thawed by adding 1 ml of prewarmed cell culture medium to the cryotube and pipetting up and down. The resulting cell suspension was diluted in 8 ml of the respective cell culture medium. For heK, this cell suspension was split up in four T175 cell culture flasks containing 18 ml prewarmed E1 cell culture medium. All other cell types were sedimented by centrifugation, the resulting pellet was resuspended in 1 ml cell culture medium and transferred to a T150 cell culture flask containing 19 ml of the respective prewarmed medium. Cells were incubated at 37 °C and 5 % CO_2 and medium was changed the next day.

3.2 Collagen isolation

Collagen type I was isolated from rat tails from 8-10 week old rats. Frozen rat tails were thawed in PBS$^-$ and disinfected by immersing in 70 % ethanol. Tails were always kept in PBS$^-$, not to dry out. After the tails were skinned, vertebra were broken successively

beginning at the end of the tail and thereby the tendons were pulled out. The isolated tendons were cut off the vertebra and adhering fat and connective tissue were removed. Afterwards, tendons were washed in PBS^- three times. For collagen dissolution, tendons of 100 rat tails were incubated for 10 minutes in 70 % ethanol for disinfection, washed with PBS^- three times and cut into small pieces. Tendon fibres were freeze-dried and 0.1 % acetic acid was added to a concentration of 10 mg/ml. For dissolution, the solution was stirred in a spinner flask for 7 days at 4 °C. To remove unsoluble fibres, the collagen solution was centrifuged for 1 hour at 14 000 x g. The supernatant was dispensed to aliquots for storage at 4 °C.

3.3 Preparation of collagen hydrogels

Collagen hydrogels were prepared for various purposes: Sprouting assays and skin equivalents are based on collagen hydrogels, as are the perfused collagen hydrogels. Furthermore, collagen hydrogels were generated to assess vascularization strategies. In general, collagen hydrogels were prepared by mixing collagen solved in 0.1 % acetic acid with gel neutralisation solution (GNS) in a 2:1 volumetric ratio. Cells in the respective needed concentration could be added beforehand to the GNS. The GNS is a buffer solution at pH 8.5 containing 2x DMEM to nourish cells within the hydrogel. By mixing the acetic collagen solution with the basic GNS the pH was shifted to neutral, enabling the polymerisation of the collagen fibres to form a collagen gel. In order to avoid air bubbles and to facilitate mixing and dispensing of the viscous collagen gel, this step was performed using a syringe system: The respective volumina of GNS and collagen solution were filled in two 20 ml syringes with Luer-Lok. The syringes were connected using a three-way valve and by alternating draining and filling of the syringes the collagen solution was mixed gently with the GNS to obtain a homogenous neutralised collagen solution. This solution was dispensed quickly in the respective culture devices using either on of the syringes or a multistep pipette. The neutralised collagen solution was then incubated for 1 hour under normal culture conditions for polymerisation of the collagen. The solidified collagen gel could then be used in further experimental setups. Due to the initial collagen concentration of 10 mg/ml and the mixing with GNS in a 2:1 ratio, the final collagen concentration of the gel was 6.7 mg/ml, henceforth referred to as low-density collagen gel. To reach higher collagen concentrations and prevent collagen contraction, the polymerised hydrogels were mechanically compressed either by a compression motor or by adding weights on top of the models. Thereby the volume of the collagen hydrogel was reduced by a factor ranging from 2 to 6.6 and thus the collagen

concentration was increased by that factor. In doing so, final collagen concentrations of up to 45 mg/ml could be achieved, henceforth referred to as high-density collagen gel.

3.4 Sprouting assay

To evaluate the ability of the endothelial cells to sprout in the dermal equivalent of the models, a sprouting assay with varying collagen concentrations was performed. For this, as a first step spheroids had to be formed from the hdmEC. Therefore, hdmEC in passage 2 to 4 were detached and the cell count was determined (see sections 3.1.5 and 3.1.6). $2.5 * 10^5$ cells were added to a mixture of 40 ml VascuLife and 10 ml methocel stem solution. 100 µl of this cell suspension were carefully pipetted to each well of a 96-well-plate with U-bottom, avoiding air bubbles. After 24 hours of incubation at 37 °C, 5 % CO_2 and a relative humidity of 95 %, hdmEC formed spheroids. Spheroids and the surrounding medium were harvested by pipetting, collected in a centrifugation tube and spun down by centrifugation. The pellet was loosened by scraping the tube over a bumpy surface and resuspended in 3 ml GNS. For microscopy applications, the used collagen had to be prepared by filtrating with a pore size of 0.45 µm. Different concentrations of the collagen were achieved by dilution with 0.1 % acetic acid. The filtrated collagen and the GNS containing the hdmEC spheroids were gently mixed in a 2:1 ratio, avoiding air bubbles or foam generation. 1 ml of this mixture was pipetted into each well of a 12-well-plate. After 1 hour polymerisation of the collagen gel at 37 °C, 200 µl VascuLife were added on top of the gels. Spheroids were cultured under normal culture conditions. After 24 hours, the sprouting behaviour of the hdmEC was assessed microscopically using the EVOS microscope. The assay is shown schematically in figure 3.2. Images of 10 representative spheroids per condition were taken and the cumulative length of all sprouts of one spheroid was determined using ImageJ.

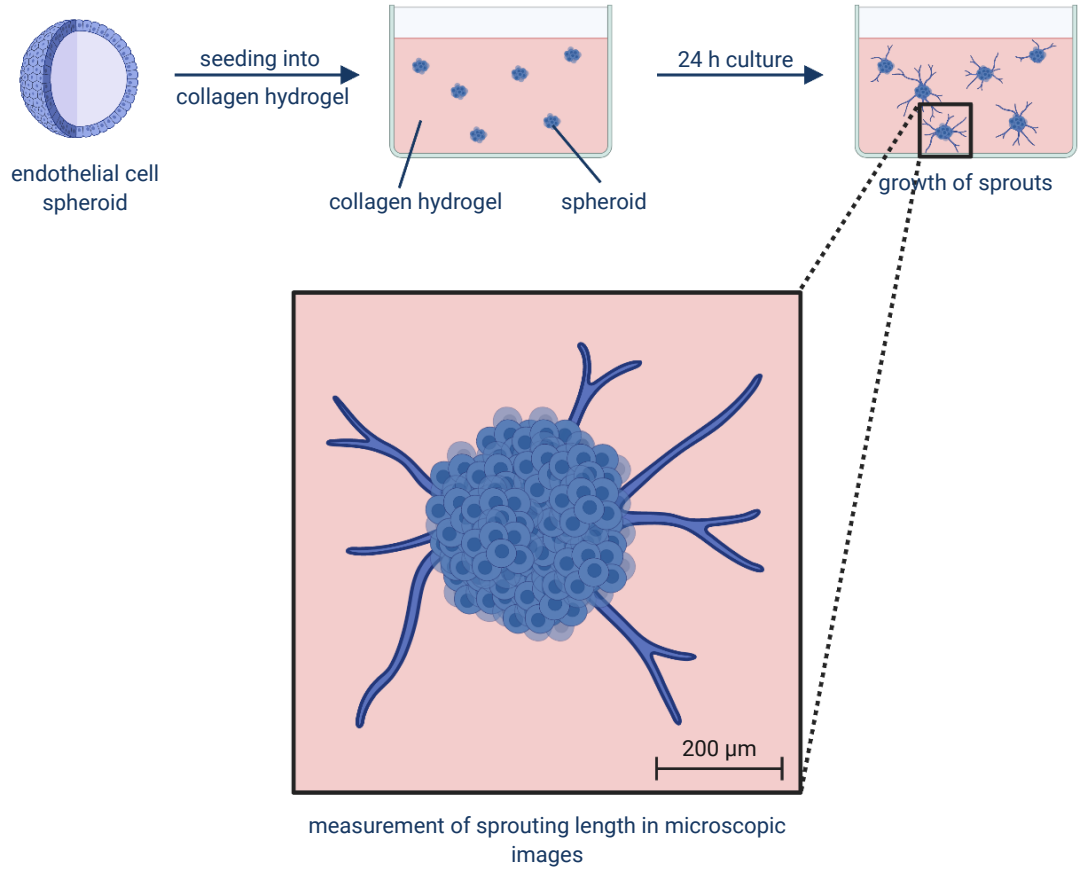

Figure 3.2: Schematic representation of a sprouting assay. Endothelial cell spheroids are seeded into collagen hydrogel. During culture time, sprouts are forming, growing out of the spheroids. After 48 h of culture, microscopic images are taken and the cumulative sprouting length is measured. Illustration created with BioRender.com.

3.5 Generation of full-thickness skin equivalents

The generation of full-thickness skin equivalents (FTSEs) was based on a previously published protocol [51] and further adapted. FTSEs were comprised of a dermal compartment built up of collagen type I hydrogel containing hdF, and of an epidermal compartment based on heK. A batch of FTSEs consisted of 12 models, therefore numbers and volumes are given for this amount. For smaller batch sizes, numbers and volumes were scaled down accordingly.

For generation of the dermal part, hdF in passage 2 to 4 were detached and the cell count was determined (see sections 3.1.5 and 3.1.6). As the final concentration of hdF should be 45 000 hdF/model, $7.71 * 10^5$ hdF were resuspended in 4 ml GNS. The so

prepared GNS was mixed with 8 ml 10 mg/ml collagen type I from rat tail using a syringe system as described in 3.3. Before solidification, 700 µl of the hdF-containing collagen gel were pipetted in Snapwell inserts, which had been punctured with a derma pen and placed in the laboratory internal compression reactor beforehand. The collagen gels polymerised during 1 hour of incubation at 37 °C. Thereafter, they got mechanically compressed either by a compression motor or by adding weights on top of the compression reactor (1 000 g for 50 minutes in total) to a final volume of 113 µl. In doing so, a final collagen concentration of 41.3 mg/ml was achieved. The final concentration of hdF was about $4 * 10^5$ cells/ml. The dermal equivalents were placed in 6 well plates with 5 ml DMEM per well and cultured submerged for 7 days. Medium was changed every 2 to 3 days.

In preparation to build up the epidermal part, the medium was changed to E10 1 day prior to seeding heK on top of the collagen gels. HeK in passage 2 were detached and counted (see sections 3.1.5 and 3.1.6). For 12 models, $6 * 10^6$ cells were resuspended in 3 ml E10. By pipetting 250 µl of this suspension on top of the drained collagen gel, a cell count of 500 000 heK/model was achieved. After 2 hours of incubation at 37 °C and 5 % CO_2 to allow for the keratinocytes to settle down, wells were filled with 5 ml E10. Models were cultured submerged for 24 hours, then the medium on top of the models was removed and the medium level in the wells was lowered to 2.5 ml for further culture of the models at the air-liquid interface. Models were cultured in that fashion for 21 days with medium changes ever 2 to 3 days. A simplified schematic overview of the process is given in figure 3.3.

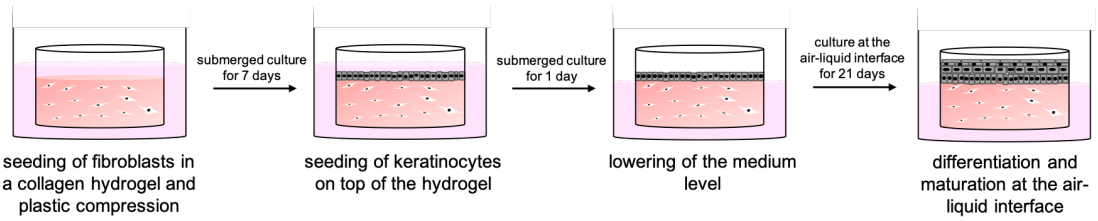

Figure 3.3: Schematic representation of the generation of full-thickness skin equivalents. Human dermal fibroblasts are seeded in a matrix of collagen type I. After polymerisation, the collagen hydrogel is plastically compressed and is cultured under submerged conditions for 7 days. Human epidermal keratinocytes are seeded on top of the dermal part and are cultured under submerged conditions for 1 day. Then, the medium level is lowered at the same level as the surface of the model. During culture at the air-liquid interface, the keratinocytes differentiate and form a mature and stratified epidermis.

3.5.1 Generation of full-thickness skin equivalents with hdmEC

To integrate endothelial cells into the FTSE, hdmEC in passage 2 to 4 were detached and the cell count was determined (see sections 3.1.5 and 3.1.6). HdmEC were added to the dermal part of the FTSE in concentrations of $4 * 10^5$ cells/ml to $6.4 * 10^6$ cells/ml, corresponding to 45 000 to 720 000 hdmEC/model. Thus, for 12 models $7.71 * 10^5$ to $12.3 * 10^6$ hdmEC were resuspended in 4 ml GNS additionally to the hdF. All other steps were performed accordingly to the protocol for the generation of FTSEs (see section 3.5) with the only change, that the dermal equivalents were cultured in VascuLife instead of DMEM.

3.5.2 Generation of full-thickness skin equivalents with melanoma

Melanoma cells were incorporated in the epidermal part of the FTSE. The dermal part was generated as described for FTSEs (see section 3.5). For the epidermal part, additionally to keratinocytes, melanoma cells were detached and the cell count was determined (see sections 3.1.5 and 3.1.6). Melanoma cells were added to the suspension of heK in a ratio of 1:50, which means 500 000 heK and 10 000 melanoma cells per model. Thus, for 12 models, 120 000 melanoma cells were resuspended together with $6 * 10^6$ heK in 3 ml E10. All further steps were carried out according to the generation of FTSEs.

3.6 Generation of perfused collagen hydrogels

3.6.1 Silicone tube setup

The first and simplest setup for generation of a perfused collagen hydrogel was a silicone tube as mold for the collagen with a wire run lengthwise through the tube as negative mold for the channel (shown in figure 4.18). The wire was hold in place with the Luer-connectors sealing the ends of the tube. With these connectors, the tube could be connected to the tubing system for perfusion. The whole setup was assembled and autoclaved before usage. The approximately 4 cm long silicone tube was filled with 1 ml neutralised collagen solution (a mixture of 10 mg/ml collagen type I from rat tail and GNS in a ratio of 2:1 as described in section 3.3), engulfing the wire. After polymerisation for 1 hour at 37 °C, the wire was removed, thereby creating a central channel within the collagen hydrogel. A cell suspension of $2 * 10^6$ hdmEC/ml in VascuLife was injected into the channel until it was filled with the suspension and it dripped out the other side. The collagen hydrogels were cultured statically for 4 hours at 37 °C and 5 % CO_2. For perfusion culture, the silicone tube harbouring the collagen hydrogel was connected to

the tubing system via the Luer-connectors. Dynamic flow conditions were achieved with a peristaltic pump, feeding medium from the reservoir through the channel with a flow velocity of 0.89 ml/min. The perfused collagen hydrogels were cultured at 37 °C and 5 % CO_2 for up to 5 days.

3.6.2 Channel chamber setup

The second setup for creating a perfusable channel in a collagen hydrogel was a 3D printed channel chamber (see figure 4.20). The workflow was the same as for the silicone tube setup described in section sec:Silicone tube setup with two amendments: The amount of collagen solution filled in the channel chamber was 2 ml and $4 * 10^6$ hdmEC/ml were seeded into the channel.

3.6.3 Bioreactors

For generation and culture of a perfused collagen hydrogel, two different bioreactors (design B and C) were designed and 3D printed via stereolithography. The bioreactor parts were sterilized using plasma-sterilization, assembled and the bioreactor was prepared by insertion of the cannula of a peripheral venous catheter. HdF in passage 2 to 4 were detached and the cell count was determined (see sections 3.1.5 and 3.1.6). HdF were resuspended in GNS to a concentration of $6 * 10^5$ cells/ml. Collagen type I from rat tail was mixed with the hdF containing GNS at a volumetric ratio of 2:1 and filled into the prepared bioreactor. For the bioreactor design B, 6 ml collagen gel were cast into the bioreactor body, and for design C 9 ml. After 1 hour at 37 °C, the collagen hydrogel was polymerized and was then mechanically compressed using a laboratory internal compression motor. Using this technique, the collagen hydrogel was compressed by a factor of 2, this means the volume was diminished to half of the original size and therefore the collagen concentration and the cell concentration were doubled. Hence, a final collagen concentration of 13.3 mg/ml and a final hdF concentration of $4 * 10^5$ cells/ml were achieved. Regarding the bioreactor design C, the compression chimney was removed. Both bioreactor types were then sealed and the collagen hydrogel was cultured under static conditions at 37 °C and 5 % CO_2. The next day, the cannula of the peripheral venous catheter was carefully removed, thereby creating a central channel for perfusion. Via the Luer connectors of the peripheral venous catheters, the bioreactor was connected to the silicone tubes of the fluidic system containing a medium reservoir filled with 30 ml VascuLife. A constant medium flow of 2.67 ml/min was achieved using a pump. Cultured at 37 °C and 5 % CO_2, the collagen hydrogel was saturated with VascuLife,

before the next day, the channel was seeded with hdmEC. Therefore, the bioreactor was disconnected from the fluidic system and $2 * 10^6$ hdmEC in 250 µl VascuLife were injected into the channel. After 4 hours of static incubation at 37 °C to allow for the hdmEC to adhere, the bioreactor was reconnected to the fluidic system. Medium in the reservoir was changed and the flow velocity was set to 0.89 ml/min. The next two days, the flow velocity was increased stepwise to 2.67 ml/min. The collagen hydrogel was cultured in the bioreactor and perfused under constant flow conditions for up to 14 days. The medium was exchanged weekly.

3.7 Coating for adhesion of endothelial cells

To test if coating the culture surface with ECM-proteins could improve the adhesion of hdmEC, wells of a 96 well-plate were coated with various concentrations of collagen type I, collagen type IV, fibronectin or a combination of collagen type IV and fibronectin. Both collagens were solved in 0.1 % acetic acid to a concentration of 1 mg/ml. They were further diluted with 0.1 % acetic acid to concentrations of 0.4 and 0.2 mg/ml. Fibronectin lyophilisate was dissolved in ultrapure water to a concentration of 0.5 mg/ml and further diluted to the used concentrations of 0.1 mg/ml and 0.05 mg/ml. To coat the culture surface, 50 µl of the respective concentration of the protein solutions were added to each well. Well plates were incubated over night at 37 °C. After the incubation time, the wells were washed carefully with PBS^- and seeded with 5 000 hdmEC in 100 µl VascuLife per well. After 2 to 3 hours incubation time for the cells to settle down, the adhesion rate of the hdmEC on the differently coated surfaces was assessed.

3.8 Viability assessment

There are several possibilities to test for cell and tissue viability. All of the here described assays are end-point analysis as the cells get destroyed.

3.8.1 Live/dead staining

Cell viability can be determined by double-staining with fluoresceindiacetate (FDA) and propidium iodide (PI). FDA passively diffuses through the cell membrane and is there converted to fluorescein. Therefore, only viable cells are stained in a bright fluorescent green. PI passes only through damaged cell membranes and intercalates with DNA and RNA to form a bright red fluorescent complex. Since it cannot penetrate intact cell membranes, only nuclei from damaged and dead cells are stained [128] [129].

For the double-staining, 1 µl FDA (0.5 mg/ml in acetone) and 9 µl PI (0.05 mg/ml in PBS^-) were diluted in 990 µl PBS^-. Hydrogels with cells were washed with PBS^- and incubated with the prepared staining solution for 5 minutes at room temperature in the dark. The samples were washed again and immediately assessed by fluorescence microscopy.

3.8.2 MTT assay

Another method for evaluation of cell viability is the staining with 3-(4,5-dimethylthiazol-2-yl)-2,5-diphenyltetrazolium bromide (MTT). The yellow tetrazolium salt MTT enters the cell and is reduced to the unsoluble formazan salt, which appears as purple-blue crystals within the cell. This reaction takes place in the mitochondria of metabolically active cells, therefore only viable cells will be stained dark blue. For quantification, the formazan precipitate can be dissolved in isopropyl alcohol and the optical density can be measured at 570 nm. With the cell-laden collagen hydrogels in this thesis, a qualitative analysis was performed by washing the hydrogels with PBS^+ and subsequent incubation in MTT solution (1 mg/ml in PBS^+) for 1 hour at 37 °C. Afterwards, the hydrogel was washed again and assessed macroscopically.

3.8.3 Luminescence cell viability assay

With the CellTiter-Glo® Luminescence Cell Viability Assay (Promega GmbH, Germany) viability was determined via the level of adenosine triphosphate (ATP) in the cells. By addition of the reagents, the cells are lysed and the released ATP is then the substrate for a luciferase reaction. The produced luminescence is therefore proportional to the number of viable cells which can be quantified using a standard curve. The assay was performed according to the manufacturer's instructions. The luminescence was measured at a wavelength of 560 nm using the plate reader Infinite® 200 Pro (Tecan Trading AG, Switzerland).

3.9 Adhesion measurement via real-time cell analysis

The xCELLigence real-time cell analysis (RTCA) system (ACEA Biosciences Inc., US) was used to monitor in real-time the adhesion of endothelial cells on different coatings. Therefore, the wells of an E-plate 96 View (ACEA Biosciences Inc., US) were coated with different ECM-proteins and seeded with 5 000 hdmEC as described in section 3.7. The plate was put immediately in the xCELLigence device within an incubator. Via

the integrated electrodes of the well plate, the impedance in every well was measured automatically every 3 minutes for 3 hours. The xCELLigence RTCA Software Pro provided by the manufacturer plotted the impedance expressed as cell index over the time. To determine the adhesion rate of the cells, the slope of the plotted curves was calculated.

3.10 Histological and immunohistological characterization

3.10.1 Fixation and preparation of the models

For histological analysis, tissue models were fixated and embedded in paraffin to generate histological sections. First, FTSE and collagen hydrogels were removed from their culture vessels after 21 or 14 days, respectively. FTSE were carefully cut out of the Snapwells, while the perfused collagen hydrogels were removed from the bioreactors by disassembling the bioreactor. Both, FTSE and perfused collagen hydrogels, were fixated overnight at 4 °C using 4 % paraformaldehyde. The models were placed between two biopsy pads in an embedding cassette and drained in deionised water for several hours. An embedding machine transferred the cassettes automatically and stepwise from water over ethanol, propanol and xylene to paraffin. The single steps are listed in table 3.1.

Table 3.1: Program of the paraffin embedding machine

Time	Solution	Description
1 h	deionised water	washing out of fixation solution
1 h	50 % Ethanol	dehydration
1 h	70 % Ethanol	dehydration
1 h	80 % Ethanol	dehydration
1 h	96 % Ethanol	dehydration
1 h	2-Propanol I	dehydration
1 h	2-Propanol II	dehydration
1 h	Xylene I	dehydration
1 h	Xylene II	dehydration
1.5 h	Paraffin I	paraffin embedding
1.5 h	Paraffin II	paraffin embedding

Subsequently, the models were removed from the embedding cassettes, halved if necessary and embedded in a mold with warm paraffin wax. The solidified paraffin blocks

were used to generate histological sections of 3.5 µm on glass slides (uncoated slides for HE-staining and polysine-adhesion slides for immunohistochemical stainings) for further analytical staining.

3.10.2 Deparaffination and rehydration of tissue sections

The slides were left to dry in a heating cabinet at 37 °C overnight. They were then incubated in a heating cabinet at 60 °C for 1 hour to melt the paraffin, before they were transferred into Xylene for deparaffination and subsequent rehydration as depicted in the following table:

Table 3.2: Deparaffination and rehydration

Time	Solution	Description
10 min	Xylene I	Deparaffination
10 min	Xylene II	Deparaffination
3 times dipping	96 % Ethanol I	Rehydration
3 times dipping	96 % Ethanol II	Rehydration
3 times dipping	70 % Ethanol	Rehydration
3 times dipping	50 % Ethanol	Rehydration
dipping until turbulences disappear	deionised water	Washing

3.10.3 HE staining

For a histological overview, sections were stained with hematoxylin and eosin (HE). Sections were deparaffinized and rehydrated (see 3.10.2) and then stained according to the following protocol:

Table 3.3: HE staining

Time	Solution	Description
6 min	Hematoxylin	staining of basophilic structures/cell nuclei
dipping	deionised water	washing
5 min	tab water	bluing
6 min	Eosin	staining of cell cytoplasm
dipping	deionised water	washing
2 min	70 % Ethanol	dehydration

HE staining (continued)

Time	Solution	Description
2 min	96 % Ethanol	dehydration
5 min	2-Propanol I	dehydration
5 min	2-Propanol II	dehydration
5 min	Xylene I	dehydration
5 min	Xylene II	dehydration

Finally, the slides were mounted with the non-aqueous mounting medium Entellan and covered with coverslips.

3.10.4 Immunohistological staining

For immunohistochemical stainings, the SuperVision 2 HRP Kit (DCS Innovative Diagnostic-Systems) was used. With this technique, a specific antigen is labeled with horseradish peroxidase (HRP) which catalyzes the oxidation of 3,3'-diaminobenzidine (DAB) to form a brown precipitate. This chromogen can be visualized using light microscopy.

For preparation, the sections were deparaffinized and rehydrated (see section 3.10.2) and the slices were encircled with a grease pen. The slides were placed in a wet chamber to prevent the slices from falling dry. The staining was conducted according to the manufacturer's protocol. Primary antibodies were diluted in antibody dilution solution. The respective dilutions are given in table 2.6. The single steps of the staining protocol are listed in the following table:

Table 3.4: Immunohistological staining

Time	Solution	Description
5 min	PBS-Tween	washing
10 min	3 % H2O2	blocking of endogenous peroxidases
5 min	PBS-Tween	washing
30 min	Blocking buffer	blocking of unspecific binding targets
overnight at 4 °C	primary antibody	binding of epitope
3 x 5 min	PBS-Tween	washing
10 min	Polmer enhancer	linker
3 x 5 min	PBS-Tween	washing
20 min	HRP-Polymer	linking HRP-polymer to antibody

Immunohistological staining (continued)

Time	Solution	Description
3 x 5 min	PBS-Tween	washing
3-5 min	DAB solution	incubation with chromogen
5 min	PBS-Tween	washing
6 min	Hematoxylin	staining of cell nuclei
5 min	tab water	bluing
dipping	deionised water	washing
2 min	70 % Ethanol	dehydration
2 min	96 % Ethanol	dehydration
5 min	2-Propanol I	dehydration
5 min	2-Propanol II	dehydration
5 min	Xylene I	dehydration
5 min	Xylene II	dehydration

After dehydration, the slides were mounted with Entellan and covered with coverslips. Brightfield images were acquired using the microscope Keyence Biorevo BZ-9000.

3.10.5 Immunofluorescence staining

To identify specific cellular markers, tissue sections were stained by immunofluorescence (IF). Just as with the DAB staining, the sections were deparaffinized and rehydrated (see 3.10.2). If the used antibodies required antigen retrieval, the slides were either cooked for 20 minutes in a steam cooker in Tris/EDTA buffer at pH 9 (antibody against melan-A and S100 beta) or incubated with pronase for 20 minutes at room temperature (antibody against collagen IV). Afterwards, the slides were transferred to deionised water and the single slices were encircled with a grease pen. The slides were washed in washing buffer and put into a wet chamber which also ensured to perform the staining in the dark. The IF staining was performed according to the following protocol:

Table 3.5: Immunofluorescence staining

Time	Solution	Description
20 min	blocking buffer	blocking of unspecific binding targets
overnight at 4 °C	primary antibody	binding of epitope
3 x 5 min	PBS-Tween	washing
60 min	secondary antibody	binding of primary antibody
3 x 5 min	PBS-Tween	washing

Primary and secondary antibodies were diluted in antibody dilution solution. The respective dilutions are given in table 2.6. After the last washing step, the slides were mounted using Fluoromount with DAPI and covered with coverslips. Fluorescence images were acquired using the microscope Keyence Biorevo BZ-9000 with the respective filter sets.

3.10.6 Whole mount immunofluorescence staining

For immunofluorescence staining, collagen hydrogels were cut out of the inserts and placed in a 24-well-plate. The staining was performed according to table 3.6. For incubation steps, the samples were put on a shaker. Primary and secondary antibodies were diluted in antibody dilution solution. The respective dilutions are given in table 2.6.

Table 3.6: Whole mount immunofluorescence staining

Time	Solution	Description
overnight at 4 °C	4 % paraformaldehyde	fixation
overnight at 4 °C	PBS$^-$	washing out fixative
60 min	blocking buffer	blocking of unspecific binding targets
overnight at room temperature	primary antibody	binding of epitope
3 x 10 min	PBS-Tween	washing
overnight at room temperature	secondary antibody	binding of primary antibody
simultaneous	DAPI 1 µg/ml	staining of cell nuclei
3 x 10 min	PBS-Tween	washing

The samples were kept in PBS$^-$ until image acquisition using the confocal microscope TCS SP8.

3.11 Image analysis

To assess the effect of adding different concentrations of endothelial cells into the dermal part of vFTSEs in regard to their network building capacity, the formed endothelial structures were quantified in stained cross-sections using ImageJ. Per concentration ten microscopic images of immunohistochemical stainings for CD31 in 20x magnification were analysed using the ImageJ macro shown in figure 3.4. The exposure time was the same for all images. For quantification, the RGB-image was transferred to the CMYK color model. The yellow channel depicted the positive staining signal and was chosen

```
name=getTitle;
run("RGB to CMYK");
run("Stack to Images");
selectWindow("Y");
rename(name);
//run("Threshold...");
setThreshold(0.1800, 1000000000000000000000000000000.0000);
run("Measure");
```

Figure 3.4: ImageJ macro for quantification of endothelial structures. Microscopic images of immunohistochemical stainings for CD31 of vascularized FTSEs were analyzed using this macro in ImageJ. RGB images were converted to CMYK. For the yellow channel a threshold with a minimum of 0.1800 was applied and the thresholded area was measured.

for threshold analysis. The minimum threshold was set to 0.1800 for every image to guarantee comparability. The thresholded area was measured and was related to the total area of the dermis, which was measured by hand.

3.12 Statistical Analysis

All data are depicted as mean with standard deviation (SD). Statistical analyses were performed using the software GraphPad PRISM 9 (GraphPad Software Inc., US). Data were tested for normality. To compare two data sets meeting the criterion for normal distribution, an unpaired t test was performed. For more than two not normally distributed data sets, the Kruskal-Wallis test with subsequent Dunn's multiple comparisons test was performed. P-values < 0.05 were considered significant, marked with an asterisk.

4 Results

In this thesis, the establishment of vascularized FTSE was investigated. On the one hand, FTSE were seeded with hdmEC in the dermal part to develop a capillary-like network. Therefore, different conditions for the hdmEC to sprout and form lumen-like structures in the collagen hydrogel were tested. On the other hand, a central channel was generated and seeded with hdmEC to form a vessel for perfusion. Here, different kinds of perfusion bioreactors of increasing complexity were tested. As metastasis relies on the vasculature, vascularized skin models represent a useful tool for investigating this process. For this purpose, the implementation of melanoma in the FTSE and the potential crosstalk between the tumor and the vasculature were addressed.

4.1 Assessment of vascularization strategies in collagen hydrogels

In the first part of this work, the suitability of the collagen matrix used to generate vascularized skin models was investigated. For integration of hdmEC in the dermal part of FTSEs, it was necessary to evaluate the applicability of the used matrix for hdmEC to grow and sprout in and to find an appropriate seeding strategy for the hdmEC.

4.1.1 Sprouting ability of endothelial cells in collagen hydrogel

To test whether the primary hdmEC were able to sprout in the collagen type I hydrogel, sprouting assays were performed (described in section 3.4). Sprouting assays are a versatile tool to study angiogenesis *in vitro* in a 3D environment. The well-established and robust method is used to study the influence of genetic alterations and pharmacological compounds on capillary-like tube formation of endothelial cells [130–133]. In this thesis, it is used to investigate if the collagen type I matrix is suitable for endothelial cell sprouting. Preformed spheroids of hdmEC were seeded in a collagen hydrogel and formed sprouts outgrowing the spheroid after 24 h of culture (see figure 4.1). Once this was achieved, several collagen concentrations were tested. Increasing collagen concentrations from

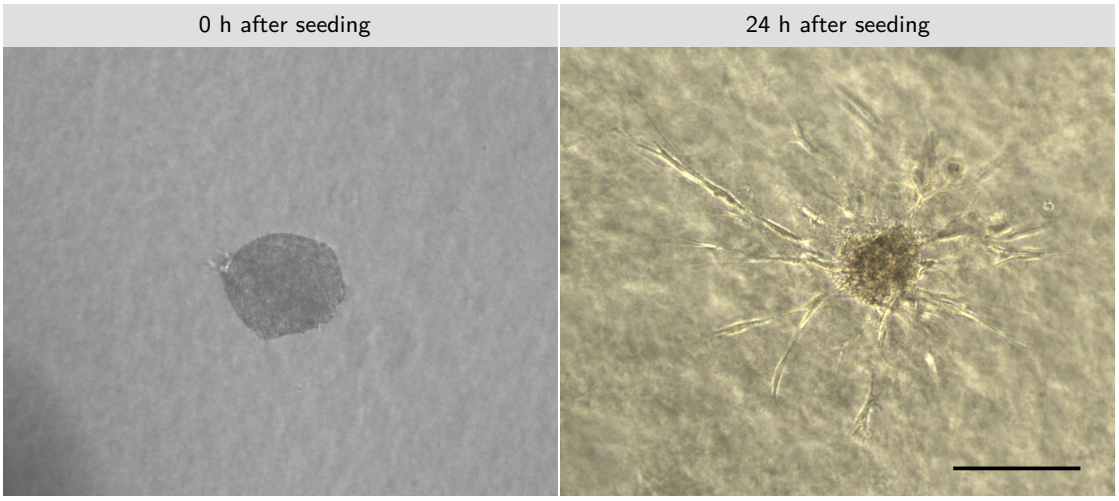

Figure 4.1: Sprouting of endothelial cells in a collagen hydrogel. Endothelial cell spheroids were seeded in a collagen hydrogel. Directly after seeding, the spheroids are visible within the collagen hydrogel, but without sprouts. 24 h later, sprouts growing out of the spheroid are numerous. Scale bar = 200 µm.

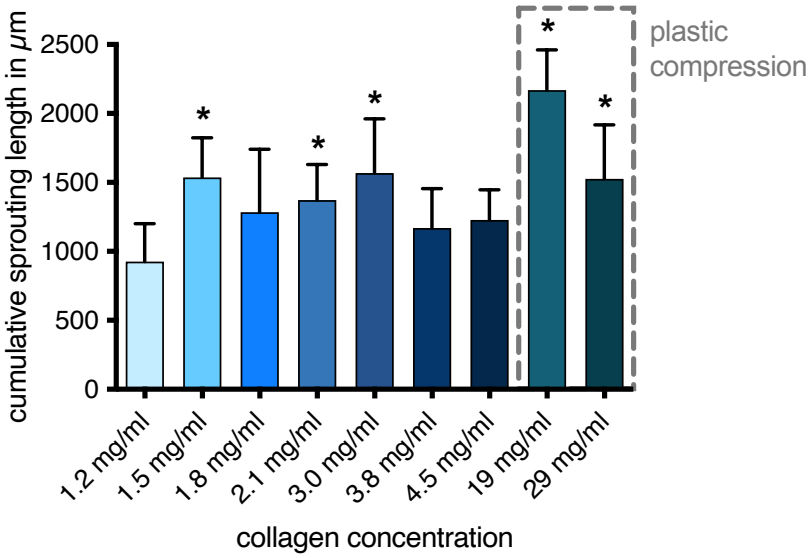

Figure 4.2: Cumulative sprouting length of endothelial cell spheroids in collagen hydrogels of different concentrations. Endothelial cell spheroids were seeded in collagen hydrogels of increasing collagen concentrations, ranging from 1.2 to 29 mg/ml. After 24 h of culture, microscopic images were taken and the cumulative sprouting length of 10 spheroids per concentration was measured. Data are shown as mean with standard deviation. *Ordinary one-way ANOVA with Dunnett's multiple comparisons test comparing each concentration with the initial concentration of 1.2 mg/ml, * $p < 0.05$.*

1.2 mg/ml to 4.5 mg/ml were found to be suitable for successful endothelial cell sprouting and resulted in cumulative sprouting lengths of 925 to 1 568 µm, what is depicted in figure 4.2. As the FTSEs are comprised of compressed collagen hydrogel to gain higher collagen concentrations and to prevent the hydrogel from shrinkage, sprouting assays with mechanically compressed high-density collagen hydrogels (like described in section 3.5 "Generation of full-thickness skin equivalents") were performed. Endothelial cell spheroids embedded in hydrogels with collagen concentrations of 19 mg/ml and 29 mg/ml resulted in cumulative sprouting lengths of 2 169 and 1 527 µm, respectively (right bars in figure 4.2). The viability of the endothelial cells in the spheroids after compression was confirmed via a live/dead staining. 24 h after seeding and compression, the endothelial cells showed sprouting and were viable as FDA was converted to the green flourescent fluorescein. Only a few cells in the core of the spheroid were stained red with PI, indicating dead cells (see figure 4.3).

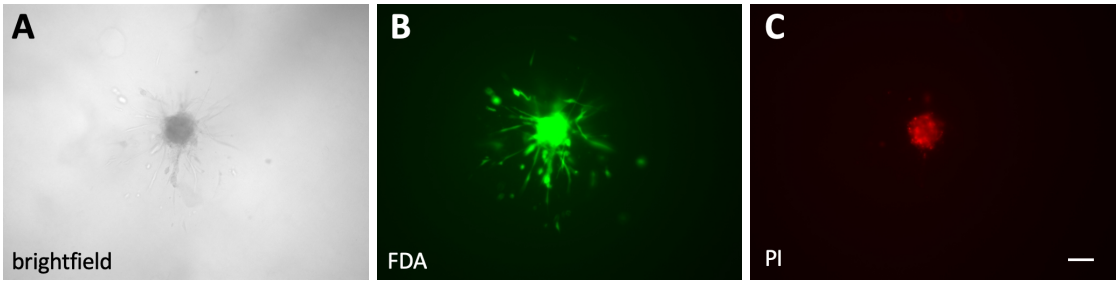

Figure 4.3: Live/dead staining of an endothelial cell spheroid with sprouts after 24 h of culture in a collagen hydrogel. The sprouts outgrowing the spheroid after 24 h are visible in the brightfield image (A). Living cells are stained with FDA (green, B), whereas dead cells are stained with PI (red, C). Scale bar = 100 µm.

4.1.2 Influence of other matrix components

The connective tissue of the dermis is not just composed of collagen type I, but also of other collagens, elastic fibres and extrafibrillar matrix components such as glycosaminoglycans, proteoglycans, and glycoproteins [134]. One of these components is the small leucine-rich proteoglycan decorin, involved in collagen fibrillogenesis [135]. To test whether adding this proteoglycan to the here used collagen type I hydrogel can influence the stability and suitability of the hydrogel to better mimic the dermal part of the skin, hdF-laden collagen hydrogels of 2 different collagen concentrations containing additionally 5 µg/ml decorin were produced and cultured for 3 weeks. During culture time, the weight of 3 hydrogels per condition was measured to detect differences in the shrinkage of the gels.

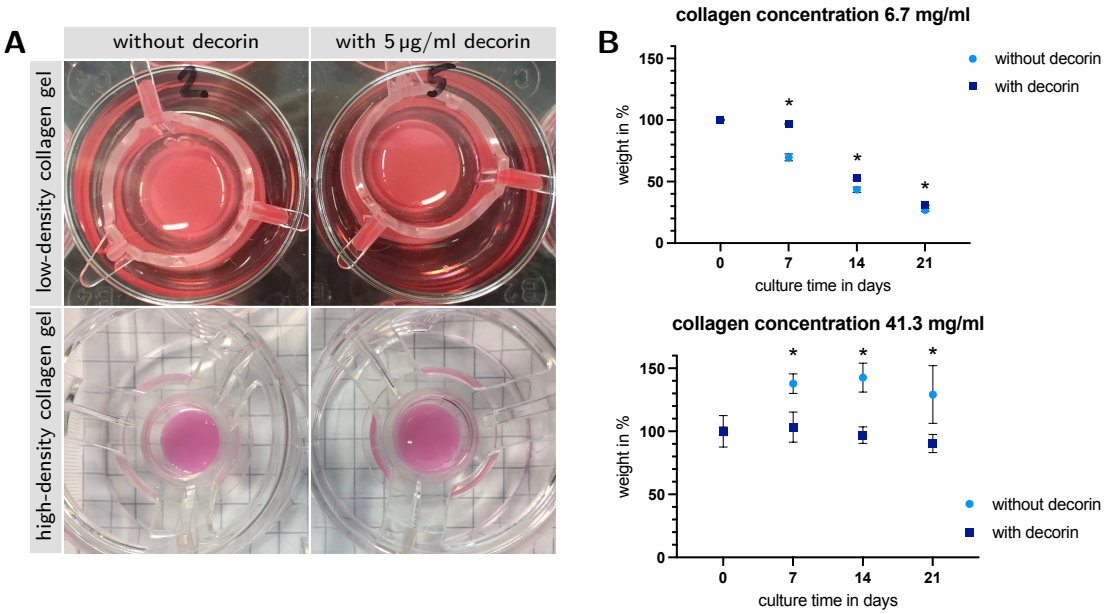

Figure 4.4: Analysis of influence of decorin on shrinkage of collagen hydrogels. Macroscopic images of cell-laden collagen hydrogels with or without decorin (A). Weight measurement of the collagen hydrogels during culture time. The mean weight at day 0 was set as 100 % to emphasise weight changes during culture time (B). *Unpaired t test comparing the mean of 3 hydrogels with and 3 hydrogels without decorin for each time point, * $p < 0.05$.*

For this analysis, the cell culture medium was completely removed from the hydrogels by aspiration. This step was prone to measuring errors, as the liquid could not always be aspirated equally for each model, and was the reason for standard deviations.

Low-density collagen hydrogels with a collagen concentration of 6.7 mg/ml showed shrinkage during culture time. This effect was observed macroscopically as the collagen hydrogels detached from the insert walls, and also in terms of the weight (see figure 4.4). Beginning at 0.98 g at day 0, the weight of the low-density collagen hydrogels without decorin decreased gradually until day 21 to a weight of 0.26 g, which is 26.8 % of the initial weight. For the low-density collagen hydrogels with decorin, the weight was 1.00 g at day 0, gradually decreasing until day 21 to 0.31 g, being 30.8 % of the initial value. For every time point, the weight of the hydrogels with decorin was higher than without decorin, especially noticeable at day 7. This difference between collagen hydrogels with and without decorin was statistically significant at days 7, 14 and 21.

In general, the high-density collagen hydrogels with a collagen concentration of 41.3 mg/ml were lighter than the low-density collagen hydrogels due to the production process. Low-density collagen hydrogels were prepared using a volume of 1 ml

collagen, whereas high-density collagen hydrogels were produced by compressing 700 µl collagen to a volume of 113 µl. Consequently, the weight of the high-density and the low-density collagen hydrogels was different. High-density collagen gels had a mean weight of 0.14 g for hydrogels without decorin and 0.20 g for the hydrogels with decorin at day 0. During culture time the hydrogels with decorin lost 10 % of weight, whereas the hydrogels without decorin gained weight to a final value of 130 % of the initial value at day 0. Differences between these two conditions were statistically significant at day 7, 14 and 21. The macroscopic images did not show any differences.

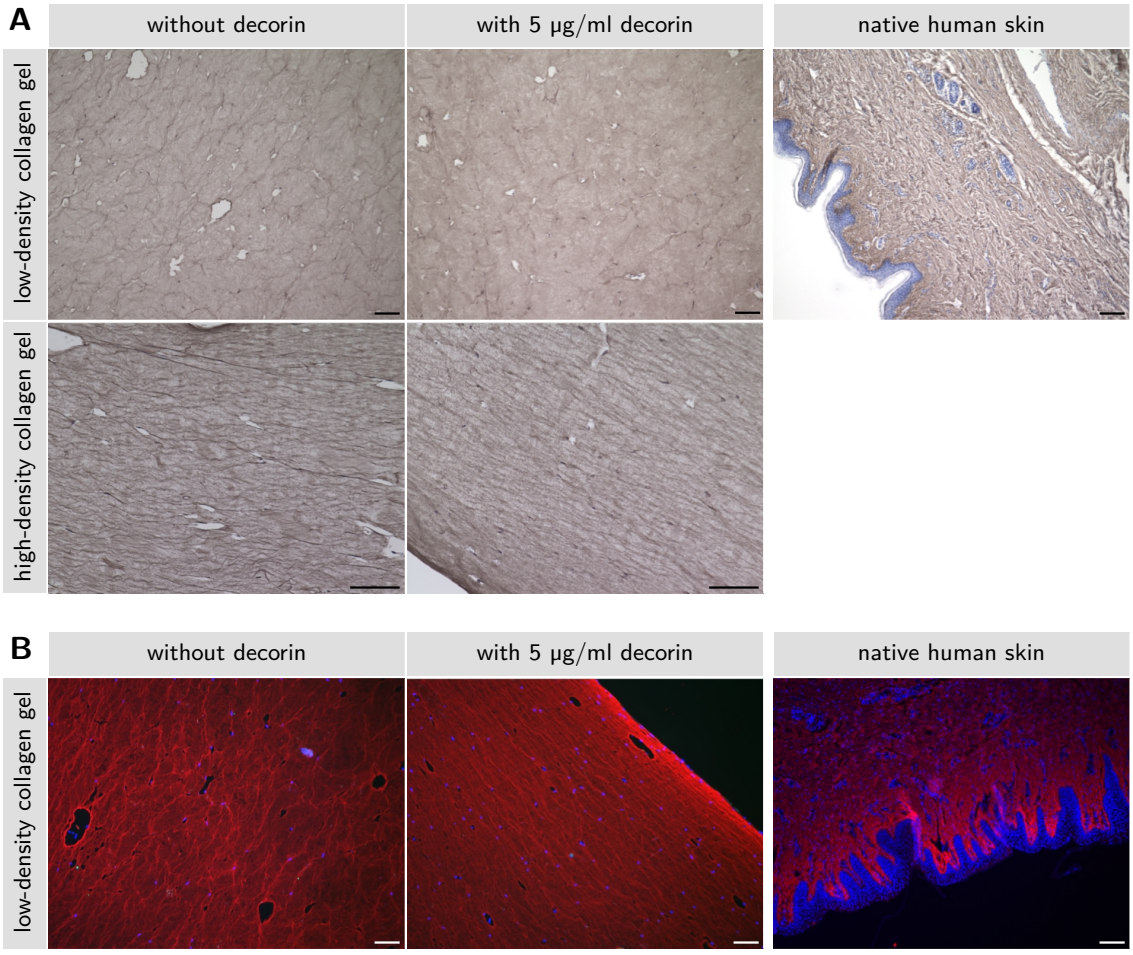

Figure 4.5: Histological analysis of collagen hydrogels with and without decorin. (A) Immunohistological staining for decorin of cross-sections of hdF-laden collagen hydrogels in two concentrations with or without 5 µg /ml decorin and cultured for three weeks. Native human skin was stained for comparison. (B) Immunofluorescence staining of the same hydrogels and native human skin for decorin (red). Cell nuclei were stained with DAPI (blue). Scale bars = 100 µm.

Immunohistochemical stainings for decorin revealed no differences, neither between high-density and low-density collagen hydrogels, nor between hydrogels with or without decorin (see figure 4.5 A). A positive staining for decorin was observed uniformly distributed all over the hydrogel. Staining of decorin was similar for all conditions, indicating that the used collagen type I already contained amounts of decorin. Moreover, decorin-staining of the collagen hydrogels is comparable to the staining of decorin in native skin. Immunofluorescence staining for decorin of the same specimen revealed the same (see figure 4.5 B).

4.1.3 Seeding strategy for endothelial cells in collagen hydrogels

To add endothelial cells to collagen hydrogels, several approaches are conceivable. Endothelial cells can be seeded on the surface or the bottom of a collagen gel or they can be incorporated into the matrix. The latter can be achieved by adding the cells in suspension when casting the collagen gel. Hereby, the number of endothelial cells, the co-culture with other cells and the configuration of the endothelial cells is vital.

Spheroids have the advantage that the cells are already in a spatial formation and have cell-cell-contacts. Besides, cells in a spheroid do not need enzymatic detachment prior to experimentation. Hence their surface proteins remain intact. Therefore, seeding endothelial cell spheroids instead of single cells into the collagen hydrogel could be beneficial to form connected structures. This hypothesis was tested by seeding endothelial cell spheroids and single cells in a high-density collagen type I hydrogel. Spheroids were generated as described in section 3.4 and collagen gels were prepared as described in section 3.3. The same cell count of about 550 000 endothelial cells/ml was used for both, the hydrogels with spheroids and the hydrogels with single cells. The collagen hydrogels were compressed to a final concentration of 31 mg/ml. Per condition, three collagen gels were generated. After a culture time of three weeks, hydrogels were fixated and a whole mount staining was conducted. Immunofluorescence staining revealed no differences in the development of connected structures (see figure 4.6). The cells in both conditions seemed to be equally distributed throughout the hydrogel.

As mentioned earlier, the co-culture with other cells in the collagen hydrogel is an important aspect for the endothelial cells. For lymphatic endothelial cells, Marino et al. showed the need of the presence of fibroblasts for the endothelial cells to assemble into capillary-like structures [89]. According to these findings, collagen hydrogels were generated with either hdmEC only or hdmEC in co-culture with hdF. 100 000 hdmEC/ml or 100 000 hdmEC/ml together with 100 000 hdF/ml were seeded in a low-density collagen

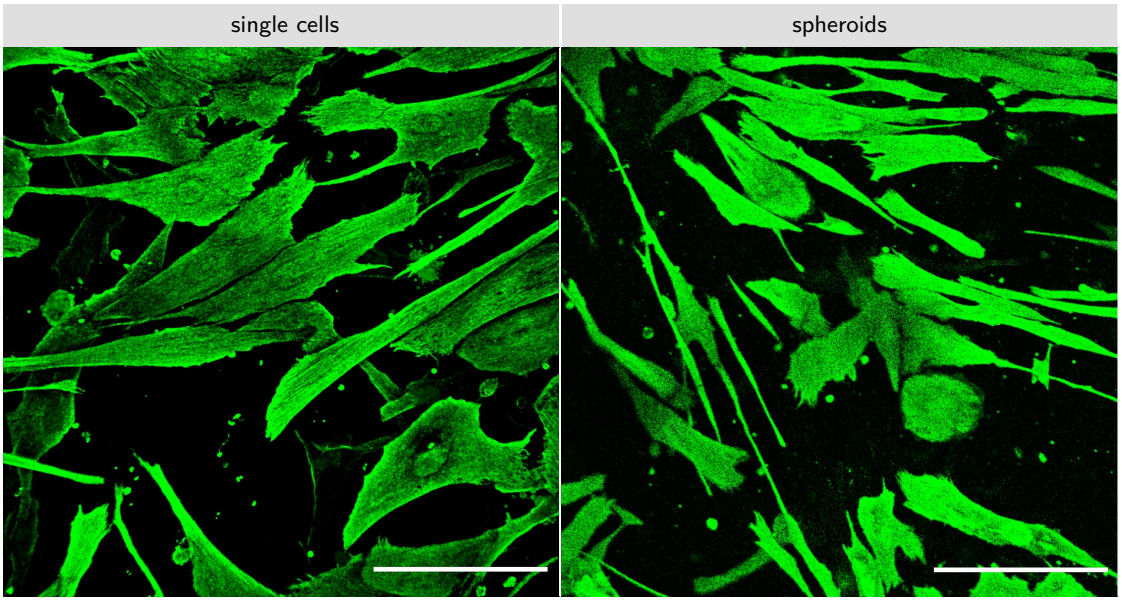

Figure 4.6: Seeding of spheroids vs. single cells. Whole mount staining for vimentin visualized endothelial cells in a high-density collagen hydrogel. Cells were either seeded as single cells or as preformed spheroids and cultured for 3 weeks. Scale bars = 100 µm.

hydrogel with a collagen concentration of 6 mg/ml. The collagen hydrogels were cultured for 7 and 21 days, respectively, and the influence of the fibroblasts on the endothelial cells was assessed by immunohistologically stainings for CD31, an endothelial cell marker.

Figure 4.7 contrasts the results for the seeding of the endothelial cells alone or in co-culture with fibroblasts. At day 7, small CD31-positive lumen-like structures were visible only for the co-culture. These structures were also visible and to some extent larger at day 21. For the endothelial cells alone, there were no such structures, despite the presence of CD31-positive cells. Furthermore, the collagen hydrogel with hdmEC only seemed to be less stable, as the hydrogel appeared ruptured at day 21.

Summarizing these results, co-culture with fibroblasts seems to be beneficial for the endothelial cells to form lumen-like structures in a collagen hydrogel. Recapitulating the findings of Marino et al. and in order to investigate the spatial conformation of the endothelial structures in the hydrogels, low-density collagen hydrogels with a collagen concentration of 3.3 mg/ml and seeded with 60 000 hdmEC/ml and 40 000 hdF/ml were cultured for 21 days and subsequently analysed using whole mount staining for CD31. The left picture in figure 4.8 shows the arrangement of the endothelial cells into partial cord-like structures.

In section 4.1.1 it was shown that endothelial cells sprout very well in high-density

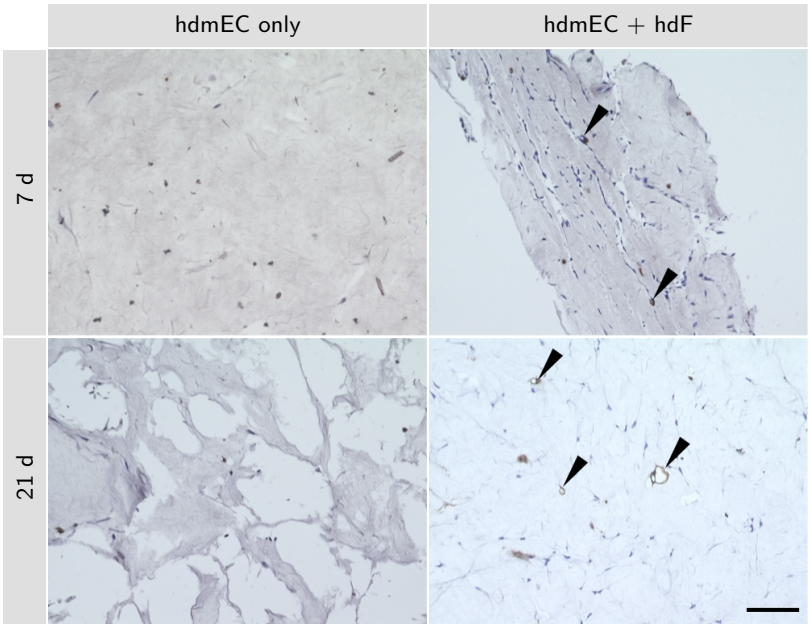

Figure 4.7: Seeding of endothelial cells only or in co-culture with fibroblasts. Endothelial cells were seeded in a collagen hydrogel alone or in co-culture with fibroblasts. Immunohistochemical staining for CD31 revealed endothelial formation of lumen-like structures only in co-culture with hdF (arrowheads). Scale bar = 100 µm.

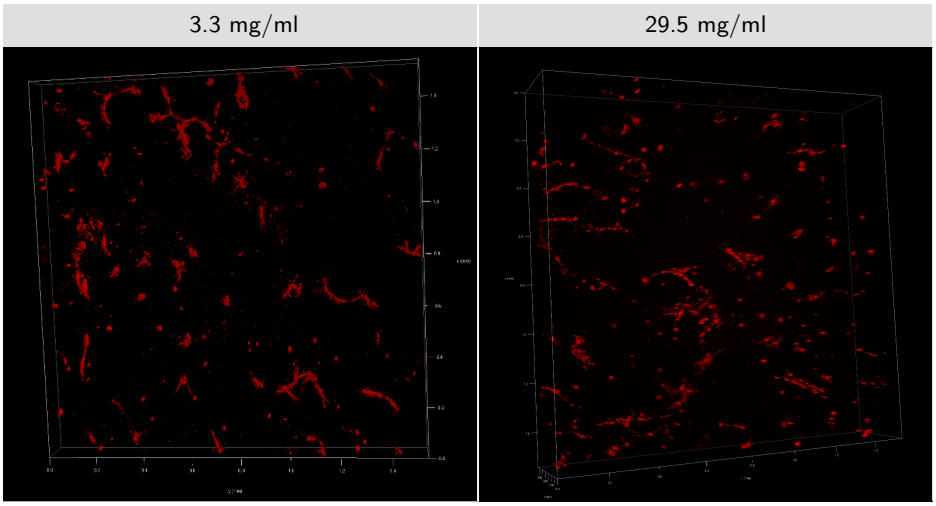

Figure 4.8: 3D spatial conformation of endothelial cells in a collagen hydrogel. HdmEC and hdF were seeded in a collagen hydrogel with a collagen concentration of 3.3 mg/ml or 29.5 mg/ml and cultured for 21 days. Whole mount staining was performed using an antibody against CD31 (red) and confocal microscopic pictures were stacked for a 3D reconstruction. Ticks at scale are 0.2 mm.

collagen hydrogels. Therefore the above described experiment was conducted with the single change that the collagen hydrogel was compressed to achieve a higher concentration. Even in a high-density collagen hydrogel with a concentration of 29.5 mg/ml, partial cord-like structures were visible and spatially arranged in the hydrogel (see right picture in figure 4.8).

Taken together, these preliminary tests proved the suitability of the used collagen hydrogel to incorporate hdmEC. Even in the high-density collagen hydrogel, that is used to generate FTSEs, hdmEC were viable and showed a great sprouting capability. Adding decorin as further ECM component to the collagen hydrogel showed no benefit in the here used concentration. It could be shown that the seeding of single endothelial cells is sufficient to form small, lumen-like structures within the hydrogel and that the co-culture with fibroblasts is necessary.

4.2 Establishment of a vascularized full-thickness skin equivalent based on a high-density collagen hydrogel

Based on the results described above, hdmEC should be integrated in a high-density collagen hydrogel to generate the vascularized dermal part of a FTSE. Therefore, it was investigated how the incorporation of endothelial cells into previously established FTSEs could be achieved. By seeding hdmEC into the dermal part of FTSEs, it was hypothesised that the cells would self-assemble to lumen-like structures to form a rudimentary capillary network.

4.2.1 Determination of the optimal endothelial cell density in FTSEs

First experiments demonstrated the feasibility of seeding hdmEC together with hdF in the dermal part of FTSE. After 4 weeks of culture, the presence of the endothelial cells in the dermal part of the FTSE was determined by immunofluorescence staining for CD31. By seeding $4 * 10^5$ hdmEC/ml additionally to the $4 * 10^5$ hdF/ml, few lumen-like structures were detectable in HE-stained cross-sections. They were proven to be of endothelial origin by immunofluorescence staining of CD31 (see figure 4.9).

As these structures were quite sparsely, it was tested if adding more hdmEC to the models would affect the outcome favourably. First, the number of endothelial cells in the models was doubled resulting in a density of $8 * 10^5$ hdmEC/ml. This did not much affect the prevalence of lumen-like structures, as shown in figure 4.10 by immunohistological staining of CD31. Hence, the number of added endothelial cells was stepwise increased.

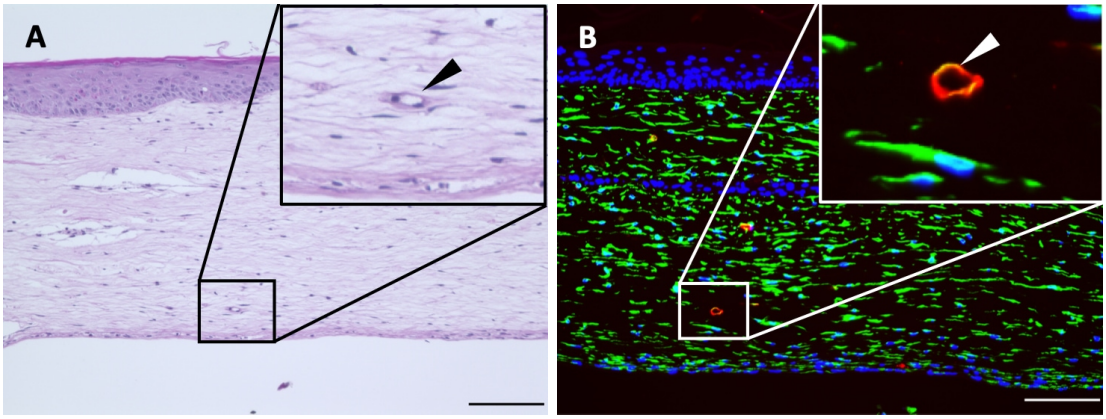

Figure 4.9: Histological assessment of vascularized FTSE. HdmEC were seeded together with hdF in the dermal part of FTSE, each in a concentration of $4 * 10^5$ cells/ml. After 4 weeks of culture, lumen-like structures were observable in HE-stained cross-sections (A). The endothelial origin of these structures was confirmed by an immunofluorescence staining for CD31 (red) and vimentin (green), cell nuclei were stained with DAPI (B). Arrowheads indicate lumen-like structures. Scale bars = 100 µm.

Cell concentrations of $2.6 * 10^6$ to $6.4 * 10^6$ hdmEC/ml achieved large and widespread endothelial structures with lumen-like appearance (see figure 4.10 A). These structures were quantified using image analysis as explained in section 3.11. In brief, the area of positively stained structures was measured and related to the total area of the dermis. For each condition, 10 images of 3 vFTSEs were measured. This analysis revealed a significant increase of endothelial structures within the dermis for models with $2.6 * 10^6$ hdmEC/ml or more compared to models with $4 * 10^5$ or $8 * 10^5$ hdmEC/ml (see figure 4.10 B). Differences between the conditions with $2.6 * 10^6$ hdmEC/ml or more were not significant.

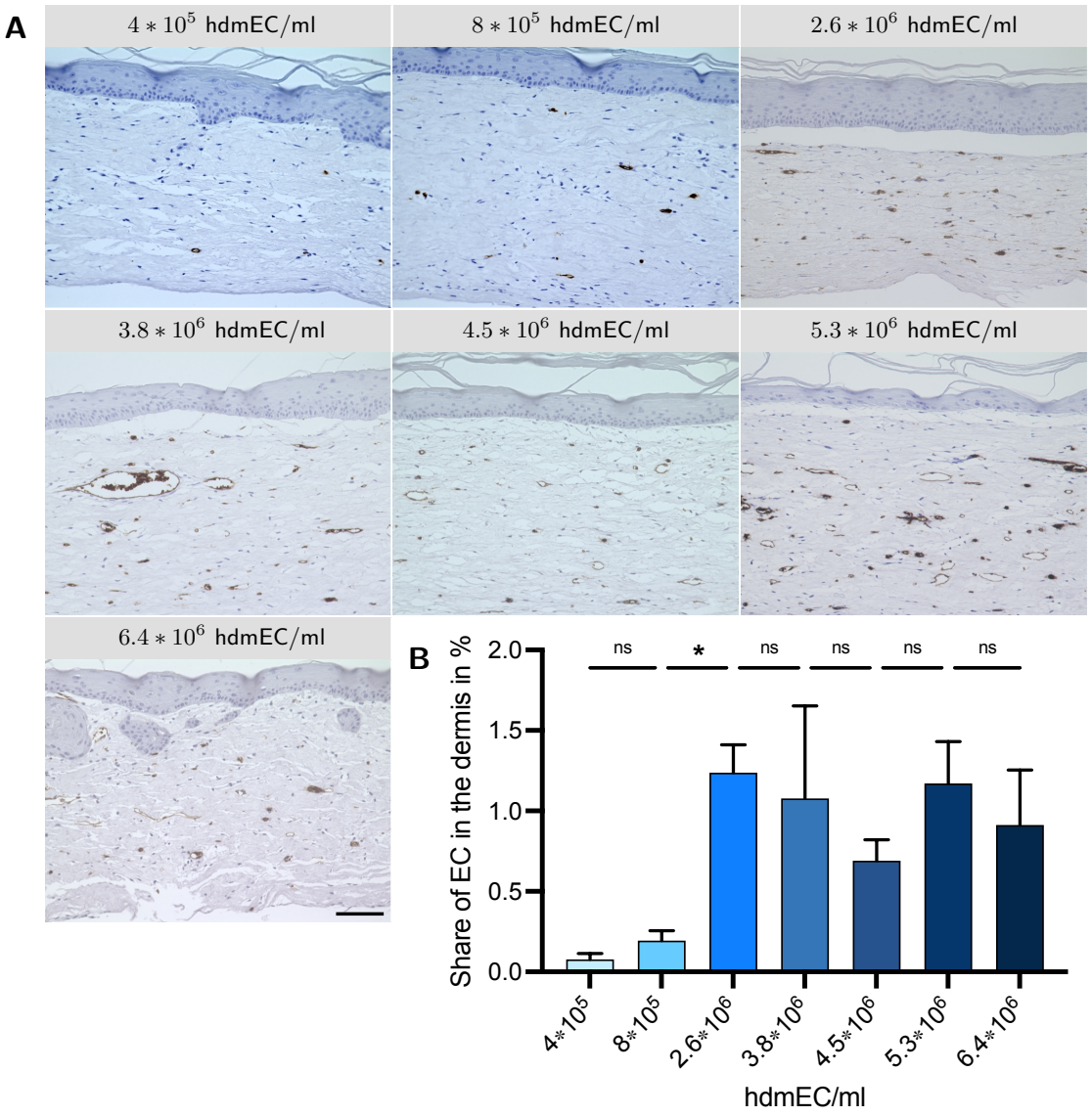

Figure 4.10: Histological assessment of vascularized FTSE with increasing numbers of hdmEC. The indicated concentration of hdmEC was seeded together with $4 * 10^5$ hdF/ml in the dermal part of FTSEs. After 4 weeks of culture, lumen-like structures were detected using immunohistological staining of CD31. Scale bar = 100 µm (A). Quantification of CD31-positive areas within the dermis (B). Shown is the share of endothelial structures in relation to the total area of the dermis, which increases massively for $2.6 * 10^6$ hdmEC/ml compared to $4 * 10^5$ or $8 * 10^5$ hdmEC/ml. All conditions with $2.6 * 10^6$ hdmEC/ml or more do not differ significantly between each other. *Kruskal-Wallis test with subsequent Dunn's multiple comparisons test, 10 images of 3 vFTSEs per condition, * $p < 0.05$, ns not significant.*

4.2.2 Cell culture medium for vascularized FTSEs

The choice of cell culture medium is pivotal for the development of 3D tissue models. In this thesis, FTSEs were cultured in E10, which had been established previously to optimize the maturation of the 3D skin equivalents. However, hdmEC require a special cell culture medium adapted to their needs. In this work, VascuLife is used for hdmEC culture. Hence, integration of hdmEC in FTSEs raised the question whether a combination of both cell culture media could improve the development of endothelial structures in the FTSEs. Therefore, FTSEs with $4 * 10^5$ hdmEC/ml and $6.4 * 10^6$ hdmEC/ml were cultured in either E10 only or in a mixture of E10 and VascuLife. After 4 weeks of culture, immunohistological staining of CD31 revealed the presence of endothelial structures in the FTSE, regardless of the medium in which the models were cultured (see figure 4.11). However, the epidermis of the models cultured in the mixture of E10 and VascuLife was thinner and not as stratified as the epidermis of models cultured in E10 only. Therefore, in further experiments E10 only was used to culture vascularized FTSE.

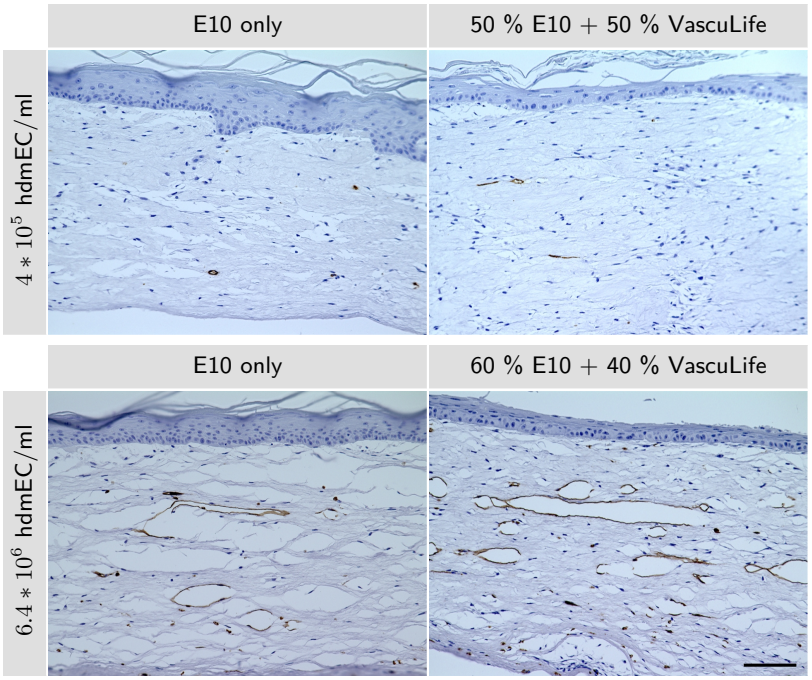

Figure 4.11: Histological assessment of vascularized FTSE cultured in different medium. FTSE with $4 * 10^5$ hdmEC/ml and $6.4 * 10^6$ hdmEC/ml were cultured in either E10 only or in a mixture of E10 and VascuLife. After 4 weeks of culture, endothelial cell structures were detected using immunohistological staining of CD31. Scale bar = 100 µm.

4.2.3 Single cells versus endothelial cell spheroids in FTSEs

Seeding spheroids instead of single cells can be beneficial as already described in section 4.1.3 for collagen hydrogels. In these experiments there was no benefit from the insertion of endothelial cell spheroids, but these experiments were conducted without hdF. With the now gained knowledge of the necessity of the co-culture with fibroblasts, this approach was also tested for FTSEs. Spheroids were generated as described in section 3.4, each consisting of about 500 endothelial cells. About 77 of these spheroids were seeded in the dermal part of FTSEs, resulting in a density of $3.4 * 10^5$ hdmEC/ml. As comparison, the same amount of endothelial cells was seeded as single cells in FTSEs. After 4 weeks of culture, immunohistological stainings of cross-sections revealed CD31-positive lumen-like structures in both conditions, which were sparsely distributed over the FTSEs (see figure 4.12).

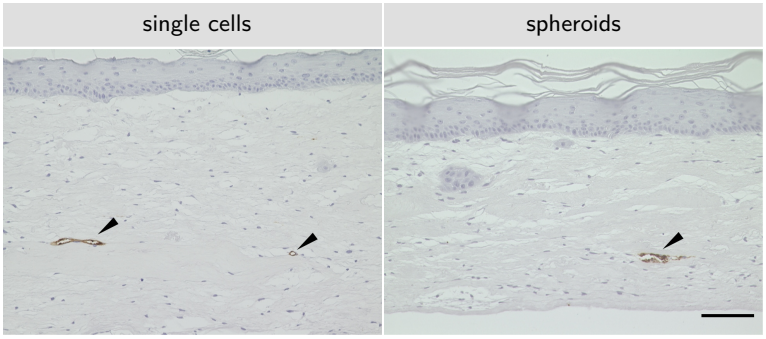

Figure 4.12: Histological assessment of vascularized FTSEs seeded with single endothelial cells or endothelial cell spheroids. The dermal part of FTSEs was seeded with about 77 spheroids, each containing about 500 hdmEC. As control served FTSEs seeded with the same amount of single endothelial cells. After 4 weeks of culture, endothelial cell structures were detected using immunohistological staining of CD31. Scale bar = 100 µm.

4.2.4 Vascularized FTSEs with human umbilical vein endothelial cells

In the literature, many vascularization approaches are conducted employing HUVEC [58,64,65,136]. They are frequently used due to their wide availability and simple isolation techniques from umbilical cords and thus their low costs. Furthermore, they proliferate easily in 2D cell culture settings and can be expanded to a great extent. Nevertheless, they originate from a vein, which is a major blood vessel, as opposed to capillaries.

To show comparability with these studies, vascularized FTSEs employing HUVEC were generated and compared with FTSEs employing hdmEC. HUVEC or hdmEC were seeded in a concentration of $4.5 * 10^6$ cells/ml in the dermal part of FTSEs (see section 3.5.1).

After 4 weeks of culture, the models were analysed histologically by immunohistological staining of CD31 shown in figure 4.13. Both, the models with hdmEC and the models with HUVEC, showed the presence of CD31-positive, lumen-like structures and in general a good morphology with a well stratified epidermis. No major differences were discernible.

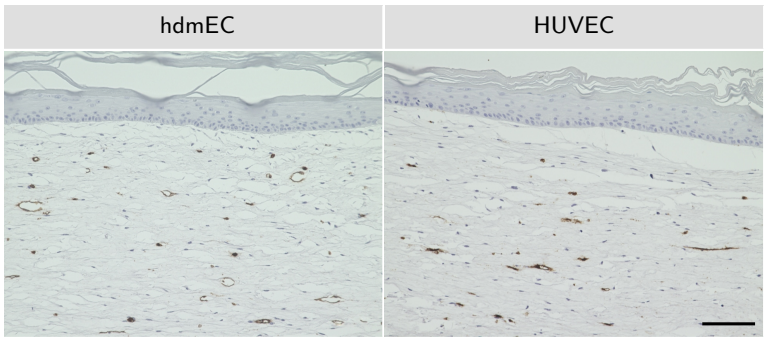

Figure 4.13: Histological assessment of vascularized FTSEs seeded with hdmEC or HUVEC. The dermal part of FTSEs was seeded with either hdmEC or HUVEC in a concentration of $4.5 * 10^6$ cells/ml. After 4 weeks of culture, endothelial cell structures were detected using immunohistological staining of CD31. Scale bar = 100 µm.

4.2.5 Characterization of vascularized FTSEs

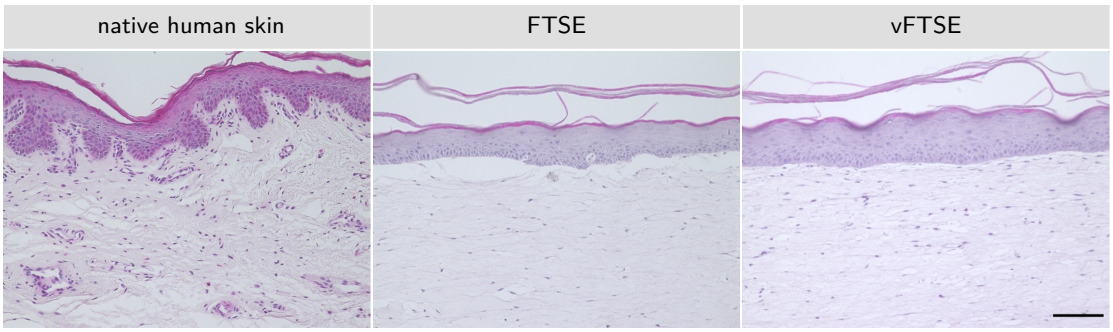

Figure 4.14: HE staining of vascularized FTSE. VFTSEs show a similar architecture to control FTSEs, with hdF seeded in the dermal part and a well stratified epidermis. Hence the incorporation of hdmEC does not impede the generation of the skin model and the maturation of the epidermis. Both models depict a simplified structure compared to native human skin. Scale bar = 100 µm.

Vascularized FTSEs were characterized by HE staining and immunohistological stainings and compared in figures 4.14 and 4.15 to normal FTSE and native human skin. The HE staining allowed an overview of the model, revealing a similar structure of FTSEs and vFTSEs. Cytokeratin 10 (CK10) and cytokeratin 14 (CK14) were used to depict

the epidermis, with CK14 as marker for basal keratinocytes and CK10 as marker for differentiated heK in subrabasal layers. Positive staining for vimentin displayed the fibroblasts, abundant in the dermal part. CD31 marked endothelial cell structures and vessels in the vascularized FTSEs as well as in the native human skin, whereas there were no signs of CD31-positive cells in the control FTSEs. Collagen type IV as part of the basal lamina was found at the dermo-epidermal junction and surrounding vessels and endothelial cell structures.

Figure 4.16 A allows a closer look at the endothelial structures within the vFTSE. Co-staining for CD31 and vimentin revealed lumen-like structures positive for CD31 (white arrowheads). Some of these structures are surrounded by vimentin-positive fibroblasts. This is comparable to the structures seen in native human skin. Figure 4.16 B shows the endothelial structures in more detail. Staining for CD31 (red) revealed the aggregation of endothelial cells into connected cord-like structures surrounded by vimentin-positive cells (green).

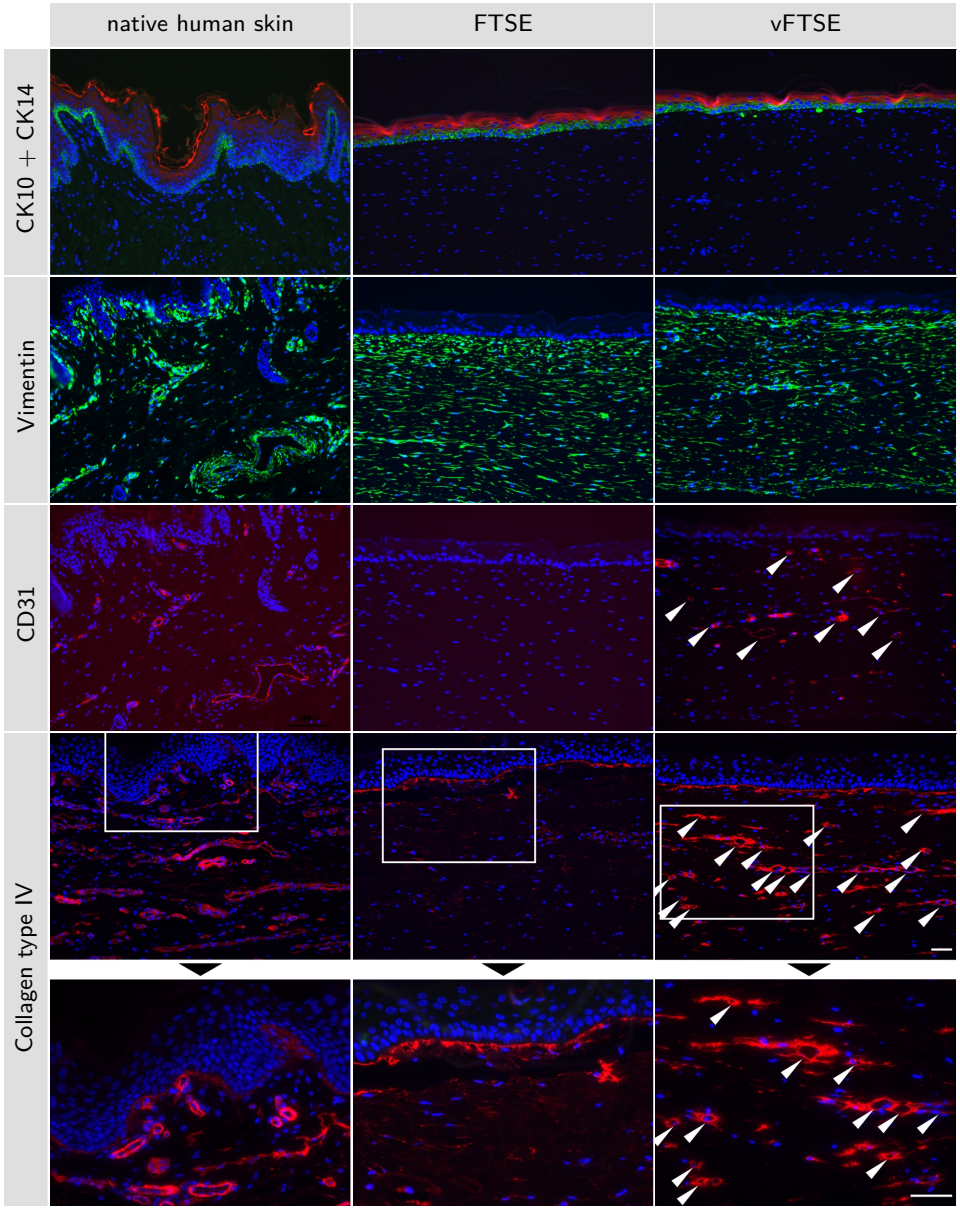

Figure 4.15: Immunofluorescence staining of vascularized FTSE compared to control FTSE and native human skin. Cytokeratin 10 (CK10, red) and 14 (CK14, green) are epidermal markers, showing the proper formation of epidermal layers in FTSE as well as in vFTSE. Vimentin (green) is distributed evenly in the dermis of both model types. In native human skin, it is accumulated around blood vessels, confirmed by a staining of endothelial cell marker CD31 (red). CD31 is absent in FTSE but positive in vFTSE, in which endothelial cells form lumen-like structures (white arrowheads). The staining of collagen type IV (red) shows the presence of a basement membrane between epidermis and dermis. It is also found surrounding vessels in native human skin and endothelial cell structures in vFTSE. Cell nuclei were stained with DAPI (blue). Scale bars = 50 µm.

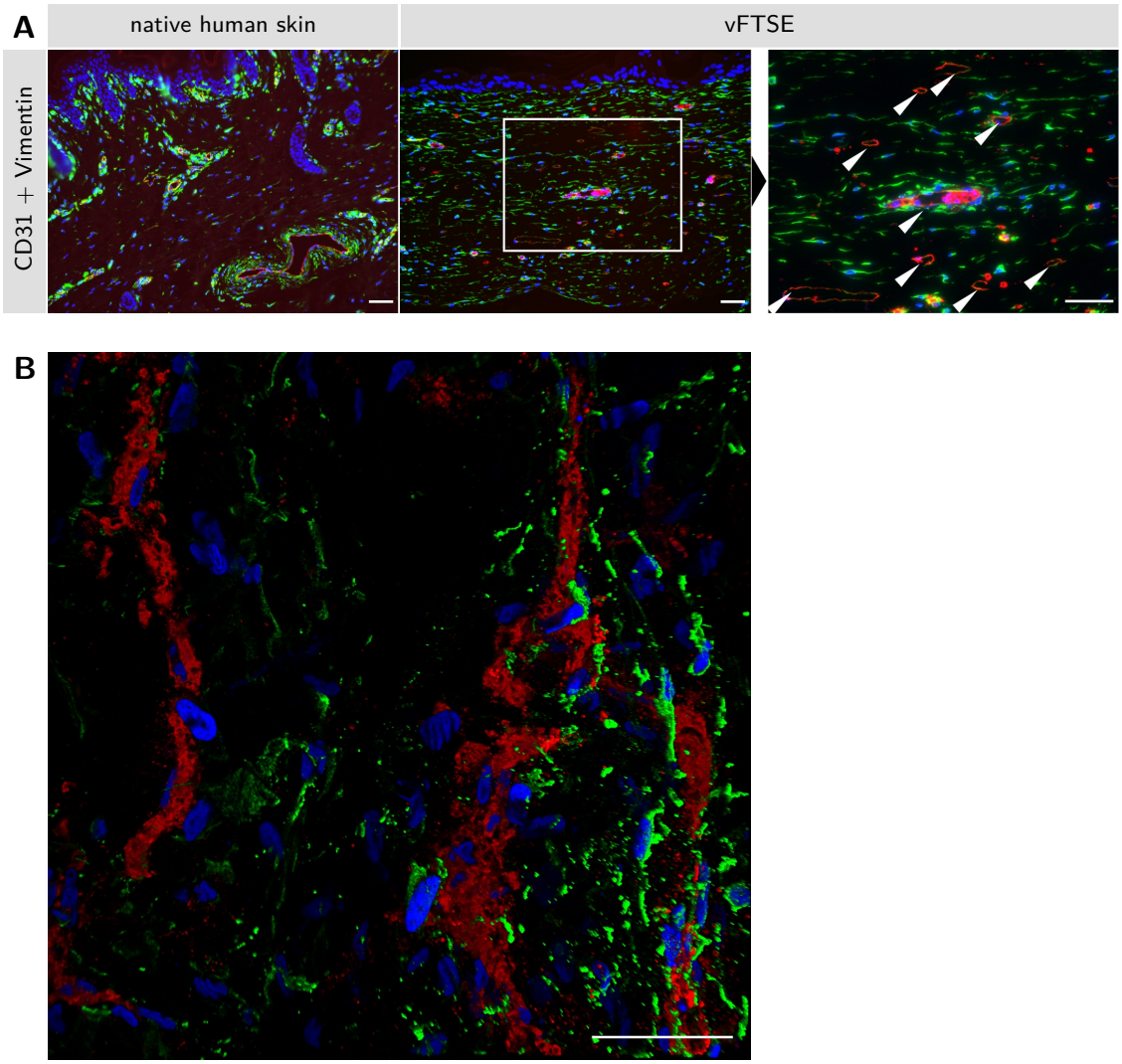

Figure 4.16: Immunofluorescence staining of endothelial structures in vascularized FTSE. (A) Detailed view of co-staining for CD31 (red) and vimentin (green) in vFTSE compared to human skin. Lumen-like structures are indicated by white arrowheads. (B) Confocal microscopic picture of staining for CD31 (red) and for vimentin (green). Cell nuclei were stained with DAPI (blue). Scale bars = 50 µm.

4.3 Development of perfused vascularized hydrogels

For generation of a perfused collagen hydrogel, several setups were tested. Common to all is, that a channel for perfusion is molded in the collagen hydrogel by casting the liquid collagen around a wire, which is removed after polymerisation, thereby creating a tubular cavity, which can be seeded with endothelial cells. Via this channel, the collagen hydrogel is perfused by connecting it to a tube system with a medium reservoir and a pump. In an attempt to facilitate endothelial cell adhesion in the channel, coating the surface was tested in preliminary experiments.

4.3.1 Coating to facilitate endothelial cell adhesion

Many cultured cell types require a coating of the culture surface with ECM proteins to improve adhesion and growth. To evaluate if coating the channel could be beneficial for adherence of endothelial cells on the lumen surface, different proteins were tested. Fibronectin is often used as coating agent in the culture of primary cells due to its cell attachment-promoting activity [137]. It is a component of the ECM with various binding sites for other proteins of the ECM and cell surface proteins from the family of integrins. Thereby, it connects cells with the fibrillary collagens I, II and III and is hence important for the attachment of cells to the ECM [138]. Collagen type IV is a component of the basement membrane, which itself is a specialised type of ECM [134, 139]. The basement membrane separates epithelial tissues from connective tissues. In the skin it can be found between the epidermis and the dermis as well as surrounding capillaries, separating the endothelium from the connective tissue of the dermis [139]. Therefore, coating the channel surface with collagen type IV could improve the generation of a vessel-like structure. As the matrix, in which the channel is cast, is built up of collagen type I, also this protein was tested as coating agent. Any other coating agent would have to have better adherence properties than collagen type I to have a beneficial effect.

To test the ability of the mentioned proteins to improve the adhesion of the hdmEC, the cells were seeded on the different coatings and their adhesion was measured using two different approaches. First, the number of adhered cells was assessed using the CellTiter-Glo®Luminescent Cell Viability Assay (Promega GmbH, Germany). Here, the number of viable cells is determined by measuring the luminescence signal from a luciferase reaction. The enzyme uses the ATP from the lysed cells, therefore, the luminescence produced is proportional to the number of viable cells and can be compared to a standard curve. The endpoint assay was performed 3 hours after seeding 5 000 hdmEC per well. Not adhered cells were removed by washing the wells carefully with PBS^-. In this way it could be

assessed how many cells had adhered since seeding and if different coatings can influence this process. Figure 4.17 A depicts the results for the measurement of 3 wells per coating. The adhesion of the hdmEC on the different coatings was compared to the adhesion on uncoated wells. Using this method, there were no significant differences between the coatings.

As this assay represents an endpoint assay, the second approach used impedance technology for continuously tracking of adherent cells. Employing the xCELLigence system (ACEA Biosciences Inc., US) it was possible to get a real-time kinetic readout by repeated measurements in a certain time frame. The system uses special well plates with integrated electrodes to measure impedance. Therefore it is possible to monitor label-free and in real-time the adhesion of cells as adhered cells will increase the impedance. Here too, 5 000 hdmEC were seeded in pre-coated wells. The impedance value for each well was automatically measured by the xCELLigence system every 3 minutes over a period of 3 hours and expressed as cell index. The cell index plotted as curve shows the increase of impedance over time due to adhering cells within the first hours. After 2 hours most of the curves flattened, which means that most of the cells had adhered. Therefore, only this time frame was considered for adhesion assessment. For determination of the rate of adhesion, the slope of the curves for every well was calculated according to the formula:

$$\text{cell index} = \text{slope} \times \text{time} + \text{intercept}$$

Figure 4.17 B shows the adhesion rates of hdmEC on the different coatings assessed via impedance measurement compared to adhesion on an uncoated surface (100 %). Per coating 6 wells were measured and averaged. All concentrations of collagen type I and 0.2 mg/ml collagen type IV showed a slightly higher adhesion rate compared to the uncoated control. The combination of collagen type IV and fibronectin showed the best adhesion rate around 150 %, whereas fibronectin alone had a lower adhesion rate compared to the uncoated control. However, these differences were not statistically significant. Figure 4.17 C shows exemplary microscopic pictures of adhered hdmEC on different coatings in the xCELLigence well plate. The electrodes for impedance measurement are visible on the left and right edges. Only a small space in the middle of the wells is left without electrodes for microscopic evaluation. Also here, wells coated with fibronectin showed less adhesion and in wells coated with the combination of collagen type IV and fibronectin many adhered hdmEC were visible.

Taken together, no coating could significantly improve the adhesion of endothelial cells in these experiments. Therefore, further experiments were conducted without coating.

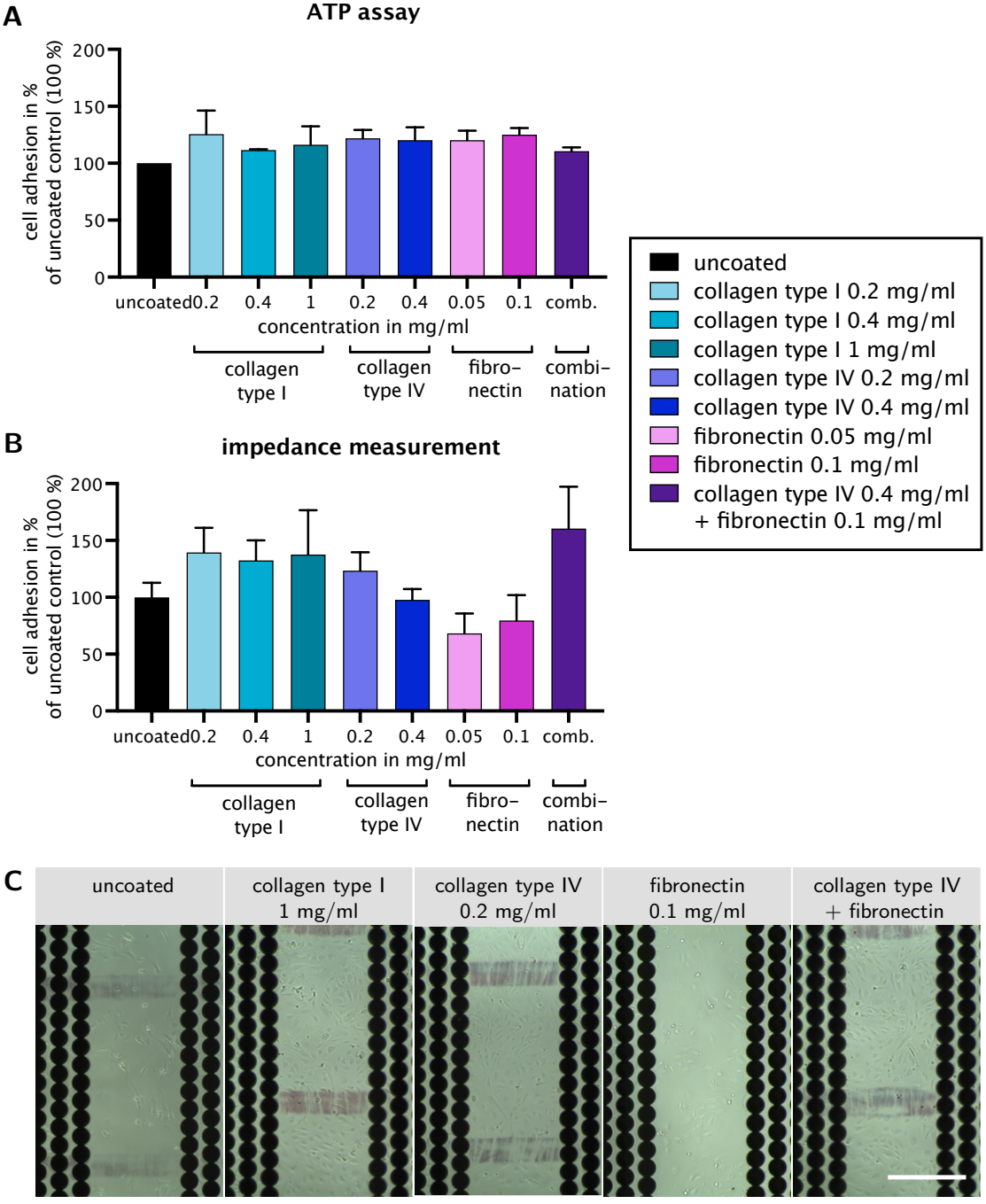

Figure 4.17: Adhesion of endothelial cells on different coatings. Measurement of adhesion of hdmEC by determination of the cell count via ATP luminescence assay (A) or by impedance analysis (B). Wells were coated with collagen type I, collagen type IV, fibronectin or a combination of collagen type IV and fibronectin before 5 000 hdmEC were seeded in each well. Adhesion was measured 3 h after seeding for the ATP luminescence assay and continuously for 2 h after seeding for impedance analysis. The adhesion in uncoated wells was set to 100 %. Per condition, 3 (A) or 6 (B) wells were measured, respectively. Exemplary microscopic pictures of adhered hdmEC in the electrode well plate of the xCELLigence are depicted in C. The electrodes for impedance measurement are visible on the left and right edges of the pictures. Scale bar = 400 µm. *Kruskal-Wallis test with subsequent Dunn's multiple comparisons test comparing each coating to the uncoated control, no statistical differences.*

4.3.2 Development series of the technical setup

Silicone tube setup

The first and smallest setup is depicted in figure 4.18. With this setup it was possible to parallelize several models as the setup was quite simple and small. Other advantages were the small amount of collagen gel needed to fill the tube and that no special parts were needed, further reducing the costs for every single model.

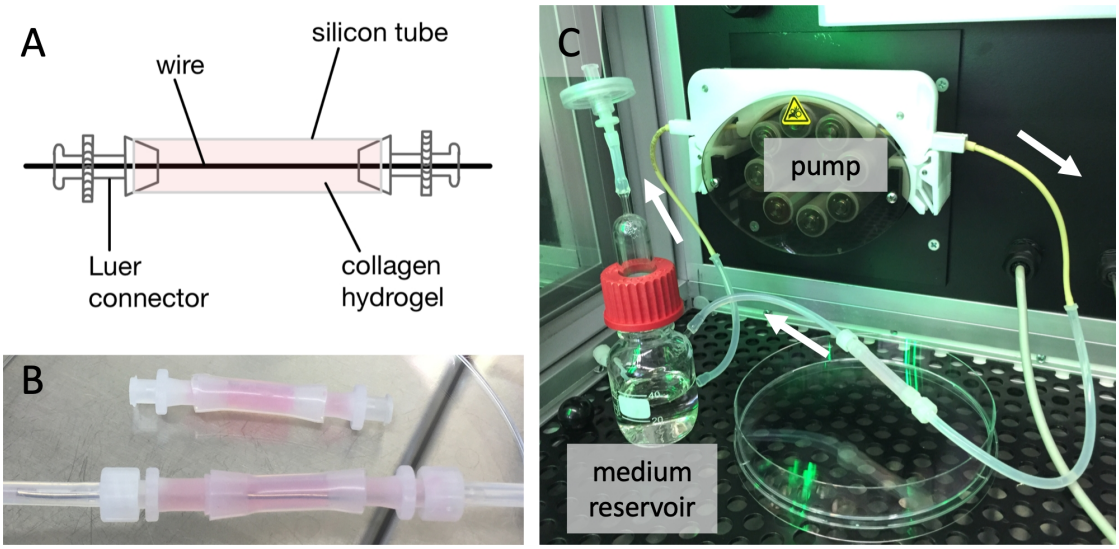

Figure 4.18: Technical silicone tube setup. (A) Schematic of the silicone tube setup with collagen hydrogel filled in. (B) Fotograph of the silicone tube setup with the wire inside (front) and the wire removed (back). (C) Complete fluidic system with peristaltic pump and medium reservoir. White arrows indicate medium flow.

It was made up of a thick silicone tube sealed with a Luer-connector on each side for connection to the tubing system. Through the Luer-connectors, a wire was shoved through the silicon tube as mold for the central channel. Collagen neutralized with GNL was filled into the tube surrounding the wire. After polymerisation of the collagen, the wire was removed, thereby creating a macroscopically visible channel (see figure 4.19 A). The surface of the created channel was seeded with hdmEC and the collagen hydrogels were incubated statically (without perfusion) over night. A subsequently conducted qualitative MTT assay showed a slight blue stain within the channel (see figure 4.19 B), proving the presence of viable hdmEC. Histological staining of cross sections of the collagen hydrogel showed an irregular formed channel within the hydrogel partly lined with hdmEC (see figure 4.19 C and C').

In the next step, the collagen hydrogels were perfused via the hdmEC-seeded channel.

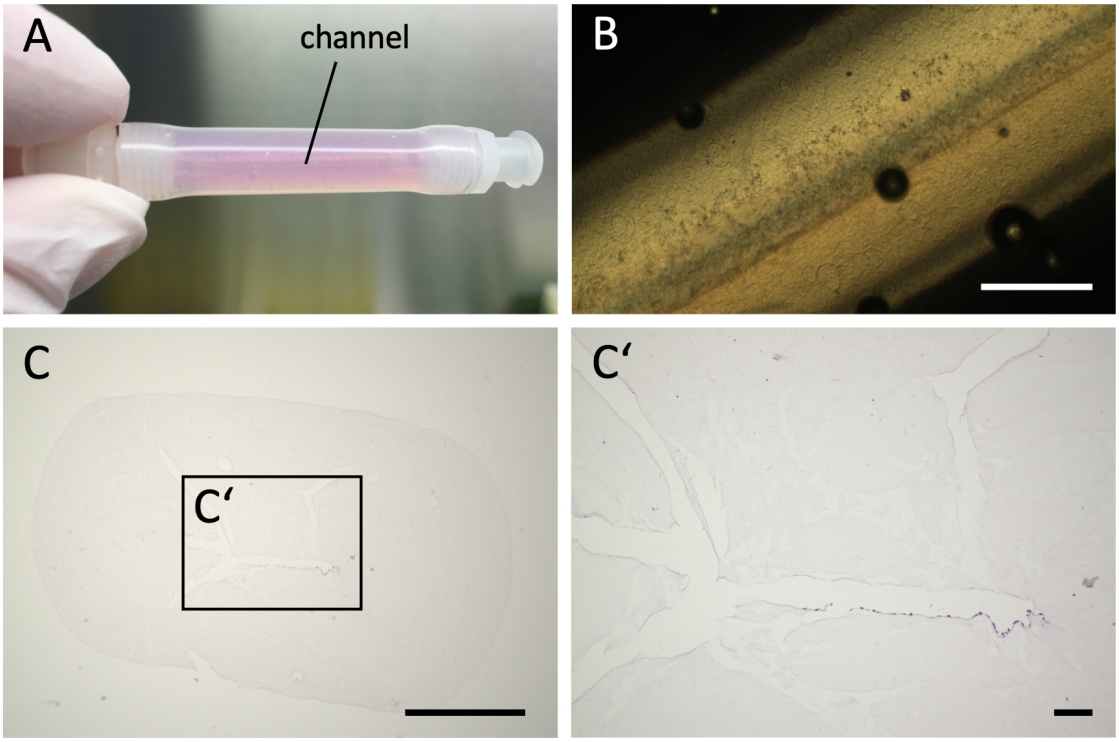

Figure 4.19: Collagen hydrogel with channel created in silicone tube. (A) Macroscopic image of the created channel after removal of the wire. (B) Qualitative MTT assay showing viable endothelial cells in the channel. (C and C') HE-stained cross section of the collagen hydrogel with channel partly lined with endothelial cells. Scale bars = 1 000 µm (B, C) and 100 µm (C').

Therefore, the silicone tube harbouring the collagen hydrogel was connected to the tubing system via the Luer-connectors. Dynamic flow conditions were achieved with a peristaltic pump, feeding medium from the reservoir through the channel (depicted in figure 4.18 C). During culture time, several problems occured with this setup: The collagen hydrogel was either flushed out of the silicone tube or shrank so that the channel collapsed and could not be perfused. Additionally, casting the collagen before and removing the hydrogel after the culture time was difficult due to the small amount of used collagen and the small components. Therefore, collagen hydrogels could not be fixated and analysed after dynamic flow culture in this setup.

Channel chamber

To get a more stable collagen hydrogel, a first rudimentary bioreactor was designed by Miriam Komma during her master thesis [140]. The customized channel chamber is built up of one compartment to fill in collagen with two opposing openings (see figure 4.20 A).

Luer-connectors in the openings permit the connection to the tubing system and also hold the wire for the generation of the channel. The bioreactor was 3D printed using fused filament fabrication (FFF), enabling easy adaption possibilities.

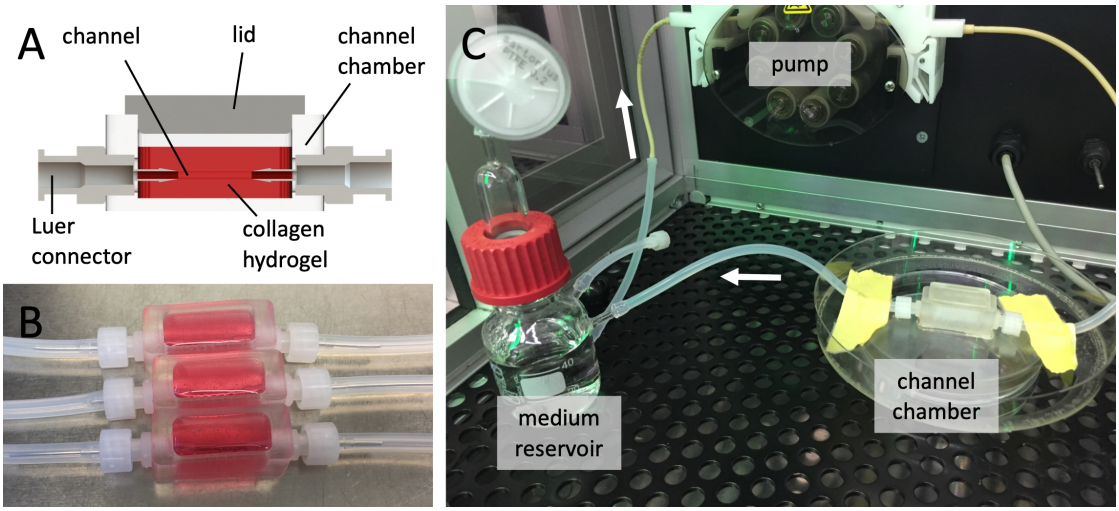

Figure 4.20: Technical channel chamber setup. (A) Schematic cut view of the 3D printed channel chamber with collagen hydrogel filled in. (B) Fotograph of the channel chamber setup with the wire inside and collagen filled in. (C) Complete fluidic system with pump and medium reservoir. White arrows indicate medium flow.

Similar to the silicone tube setup, liquid neutralized collagen was filled in the channel chamber engulfing the wire (see figure 4.20 B). After polymerisation of the collagen, the wire was removed to create the central channel. For visualization and to check its stability, the channel was flushed with 0.1 % phenol red (see figure 4.21 A). Through the collagen hydrogel, the stain was visible only in the channel, indicating its integrity. The whole collagen hydrogel was stable and easy to handle as it could be removed easily and without damage from the channel chamber (see figure 4.21 B). The channel lumen was seeded with hdmEC and the hydrogels were cultured statically over night. HE-stained cross-section revealed a compact and smooth hydrogel with a clearly visible channel. However, the channel was lined only with a few hdmEC (see figure 4.21 C and C').

By plugging the Luer-connectors in the tubing system, the channel could be perfused. The whole setup of the fluidic system can be seen in figure 4.20 C. But dynamic flow culture led to leakage problems as the lid did not close tightly enough. Therefore, analysis of the perfused collagen hydrogels was not possible.

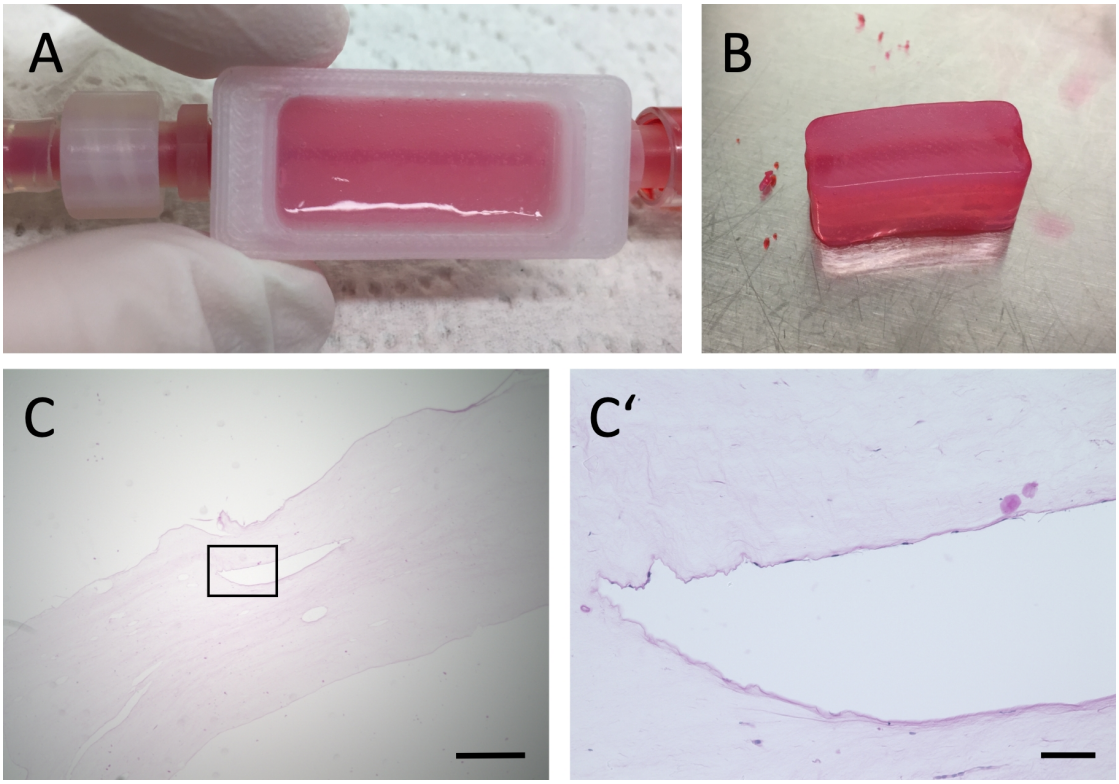

Figure 4.21: Collagen hydrogel with channel created in channel chamber. (A) Macroscopic image of the created channel after removal of the wire, visualized with phenol red. (B) Collagen hydrogel removed from the channel chamber. (C and C') HE-stained cross section of the channel. The collagen hydrogel is compact and the channel is easily distinguishable with only a few cells lining the lumen surface. Scale bars = 1 000 µm (C) and 100 µm (C').

Bioreactors

The previously described setups for creating a perfusable channel in a collagen hydrogel had one pitfall in common: Plastic compression to generate a high-density collagen hydrogel comparable to FTSE was not possible. To address this problem, more sophisticated bioreactors were developed. In this thesis, two different designs of bioreactors were tested for their suitability to generate and maintain a perfused collagen hydrogel. The bioreactors were designed by Marius Gensler and Miriam Komma during her master thesis [140]. They were 3D printed via stereolithography using Dental SG Resin (Formlabs Inc., US) as printing material. Both bioreactors consist of a bioreactor body to harbour the perfused collagen hydrogel and in both bioreactors the cannula of a peripherous venous catheter is used as negative mold for the central channel. However, they differ in their complexity. The comparison of both bioreactor designs is depicted in figure 4.22.

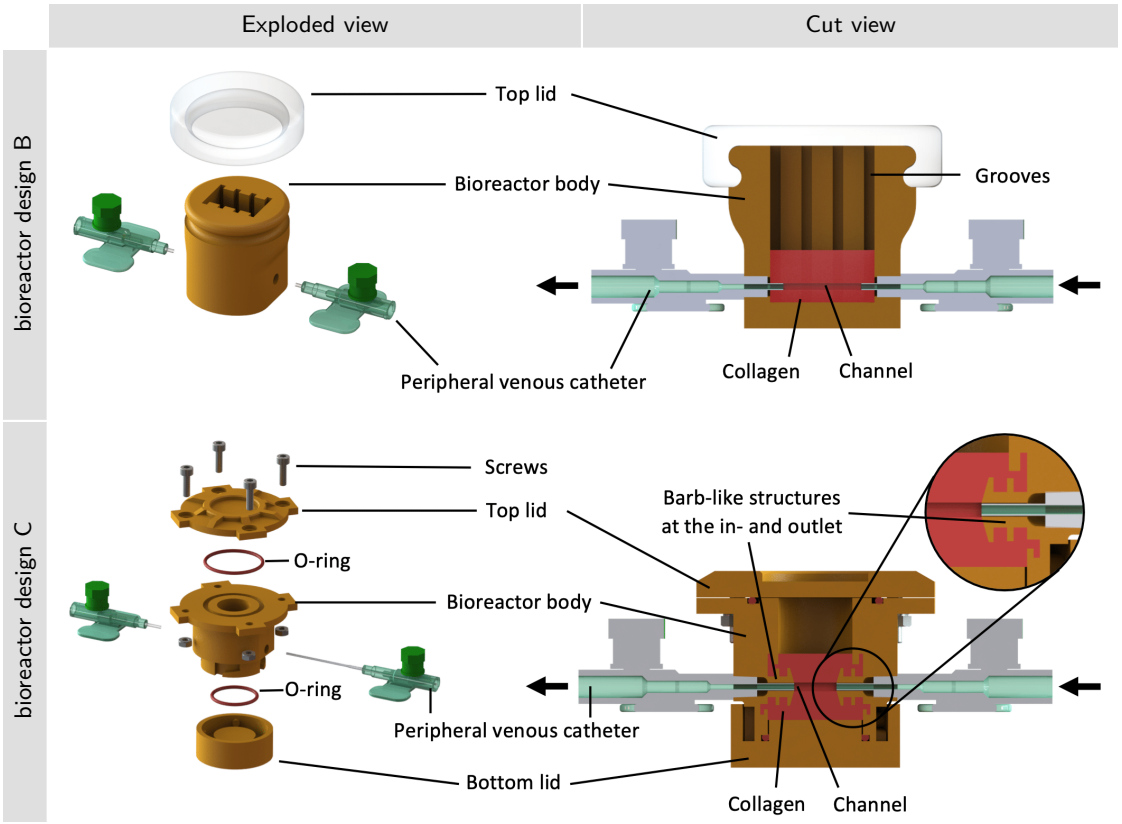

Figure 4.22: Assembly of the two bioreactors. Exploded and cut view of bioreactor design B and bioreactor design C. Both bioreactors consist of a bioreactor body in which the collagen is filled in. Two opposing inlets hold peripheral venous catheters for perfusion. The bioreactors are closed with a lid. The bioreactor design B has grooves at the inside of the bioreactor body to anchor the hydrogel and to enable squeezing out the liquid during compression. The bioreactor design C has a removable bottom lid connected to the bioreactor via a plug connection. The upper lid is fixed with screws and both lids are sealed via O-rings. Barb-like structures protrude inwards from the openings to anchor the hydrogel. Arrows indicate the medium flow. Parts of the figure adapted from [99].

Design B consists of one single part and is closed via a silicone lid. Through the two opposing openings in the bioreactor body, two peripherous venous catheters are shoved as ports for the perfusion of the channel. The cannula of one of them crosses the bioreactor centrally to create the negative mold for the channel. The base area is rectangular and about 2 cm^2. The two sites hold vertical grooves of 2 mm in depth and width. They are intended on the one hand to anchor the collagen hydrogel and on the other hand to enable squeezing out the liquid during compression.

The bioreactor design C consists of multiple pieces. The bottom lid is connected to the bioreactor body via a plug connection. For compression it can be replaced by a bottom

lid with a grid structure to allow the fluid to escape during compression. The upper lid is fixed with screws and both lids are sealed via O-rings. The base area here is round and about 1 cm^2. Several undercuts in the interior of the bioreactor body are intended to anchor and stabilise the collagen hydrogel. Also for this reason, the ports at the in- and outlet are extended inwards in the form of barb-like structures. The cannula of one of the peripherous venous catheters at the in- and outlet is inserted across the bioreactor to form the central channel.

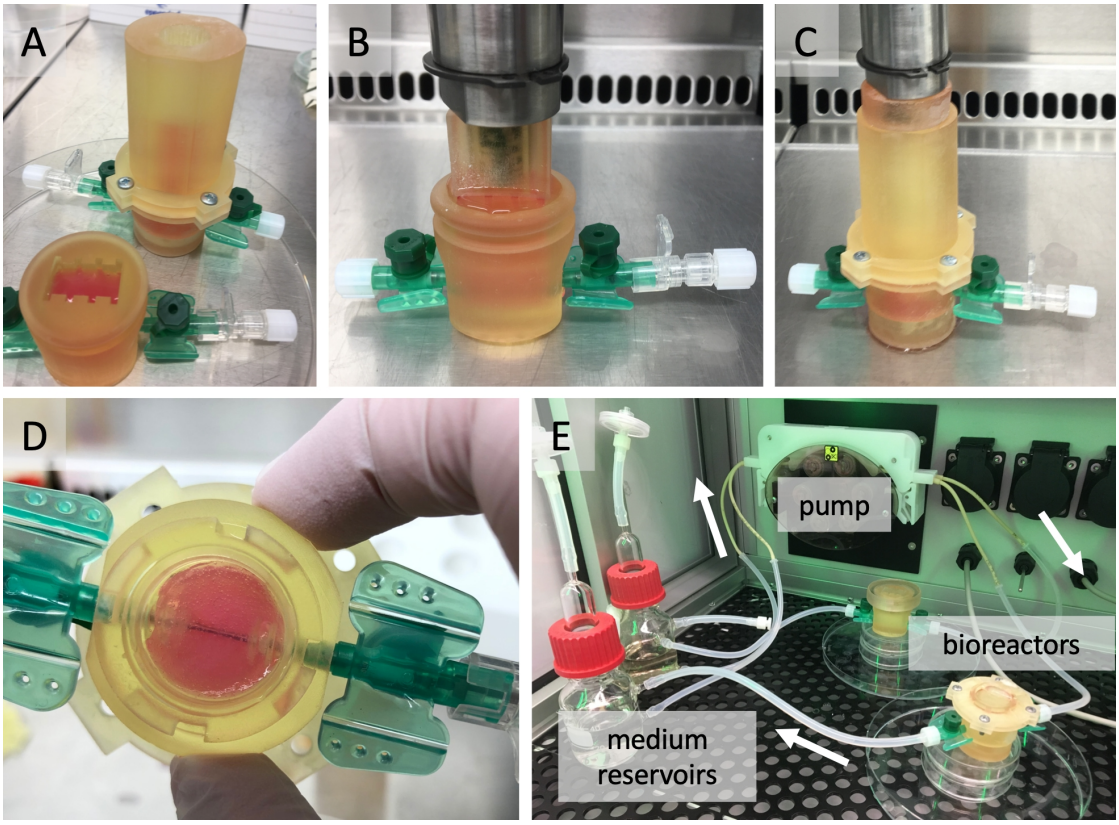

Figure 4.23: Workflow for a perfused collagen hydrogel. Both bioreactors are filled with collagen. The bioreactor design C has a chimney-like extension on top to enlarge the volume of the collagen (A). After polymerisation, the collagen hydrogels in the bioreactor design B (B) and in the bioreactor design C (C) are plastically compressed. After 24 hours of incubation, the cannula is removed (D) and the created channel is seeded with hdmEC. Collagen hydrogels in both bioreactors are cultured under dynamic flow conditions for up to 14 days (E). White arrows indicate the medium flow.

For generation of a perfused collagen hydrogel, both bioreactors were prepared and filled with cell-laden collagen as described in section 3.6.3. For the bioreactor design C, a chimney-like extension was installed at the top of the bioreactor to enlarge the

volume of the collagen to be filled in (see figure 4.23 A rear). After polymerisation, the collagen hydrogels were plastically compressed using customized stamps to a final collagen concentration of 13.3 mg/ml (see figure 4.23 B and C). Excessive fluid was squeezed out of the hydrogels reducing the initial collagen volume. The extension of bioreactor design C was removed and the grid-structured bottom lid was replaced with the closed one. Both bioreactors were sealed with their lids and the collagen hydrogel was incubated for 24 hours at 37 °C. The cannula was removed carefully (see figure 4.23 D) and the created channel was perfused with VascuLife by connecting the bioreactor to the tubing system. The next day, the channel was seeded with hdmEC. After an adhesion time of 4 hours, the bioreactors were reconnected to the tubing system and the collagen hydrogels were cultured under dynamic flow conditions for up to 14 days (see figure 4.23 E).

4.3.3 Characterization of perfused hydrogels

To verify the successful generation of the channel in the collagen hydrogel and to check its integrity and stability, the channel was flushed with 0.1 % phenol red after removal of the cannula and before seeding with hdmEC. Through the bottom of the bioreactor, the

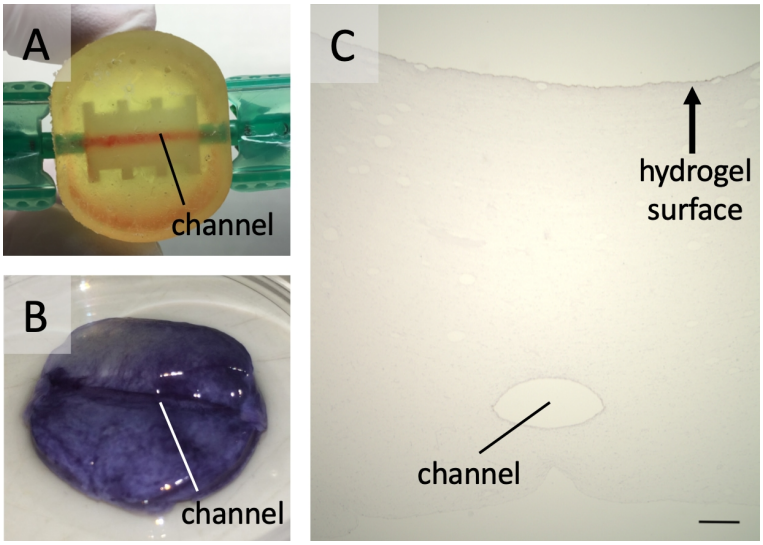

Figure 4.24: Characterisation of the perfused collagen hydrogel. The generation of a stable and perfusable channel within the collagen hydrogel was visualised by perfusion with phenol red (A). The qualitative MTT assay of the high-density collagen hydrogel indicates viable cells within the hydrogel. Furthermore, the channel is macroscopically visible (B). (C) Microscopic overview picture of a histochemically stained cross-section of the collagen hydrogel. The channel is located in the lower part and the cell-laden collagen hydrogel is smooth with some small air bubbles. Scale bar = 500 µm.

red stained channel was clearly visible within the collagen hydrogel (see figure 4.24 A). The viability of the cells within the perfused high-density collagen hydrogel was assessed by a qualitative MTT assay after 7 days of culture. The blue staining shown in figure 4.24 B indicates viable cells throughout the hydrogel. Furthermore, the central channel can be seen as slightly darker stained. For histological analysis, the bioreactors were stopped after 14 days of culture and the collagen hydrogels were fixated and embedded in paraffin. The histochemically stained cross-section at low magnification in figure 4.24 C gives an overview of the collagen hydrogel with the channel. The channel is located in the lower part of the collagen hydrogel, which appears to be smooth and without large air bubbles.

Figure 4.25 shows the channel in more detail. Both bioreactor designs were used to generate and culture perfused collagen hydrogels. Initially, experiments were performed with low-density collagen hydrogel without compression (see figure 4.25 A). When this was achieved successfully, perfused hydrogels of high-density collagen were generated by plastic compression (see 4.25 B). For both conditions in both bioreactor designs perfused channels could be generated visible in the microscopic cross-sections (marked with asterisks). Immunohistochemical staining for the endothelial marker CD31 after 14 days of perfusion culture reveals a monolayer of endothelial cells lining the lumen of the channel.

Although already shown by the immunohistochemical staining, the presence of hdmEC in the channel was verified by immunofluorescence staining of the endothelial marker CD31 (red). Fibroblasts within the collagen hydrogel were stained for vimentin (green). The images in figure 4.26 show a monolayer of endothelial cells lining the channel lumen (B and B'; lumen marked with asterisks). Additionally, small lumen-like structures of endothelial cells can be seen in proximity to the channel (white arrowheads). In comparison, images A and A' depict native human skin with small capillaries lined with endothelial cells. In both cases, fibroblasts accumulate around the vessel or channel.

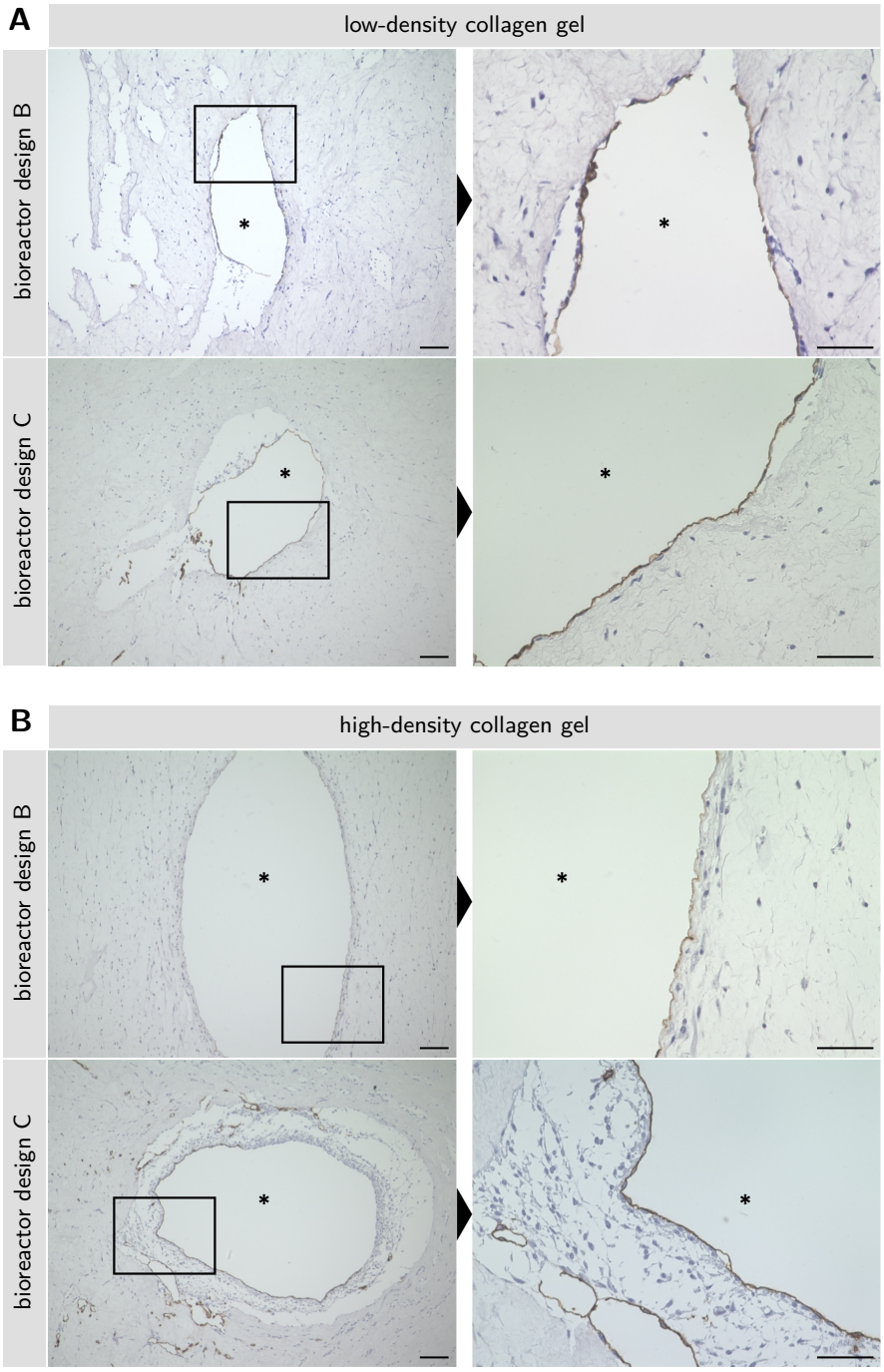

Figure 4.25: Immunohistochemical staining of endothelial cells lining the channel lumen. Perfused collagen hydrogels were generated using both bioreactor designs. Channels were generated in low-density (A) and high-density collagen gel (B) and seeded with hdmEC. Immunohistochemical staining of endothelial marker CD31 shows the cells lining the channel lumen after 14 days of perfused culture. Asterisks mark the channel lumen. Scale bars = 100 µm (left column) and 50 µm (magnifications in right column).

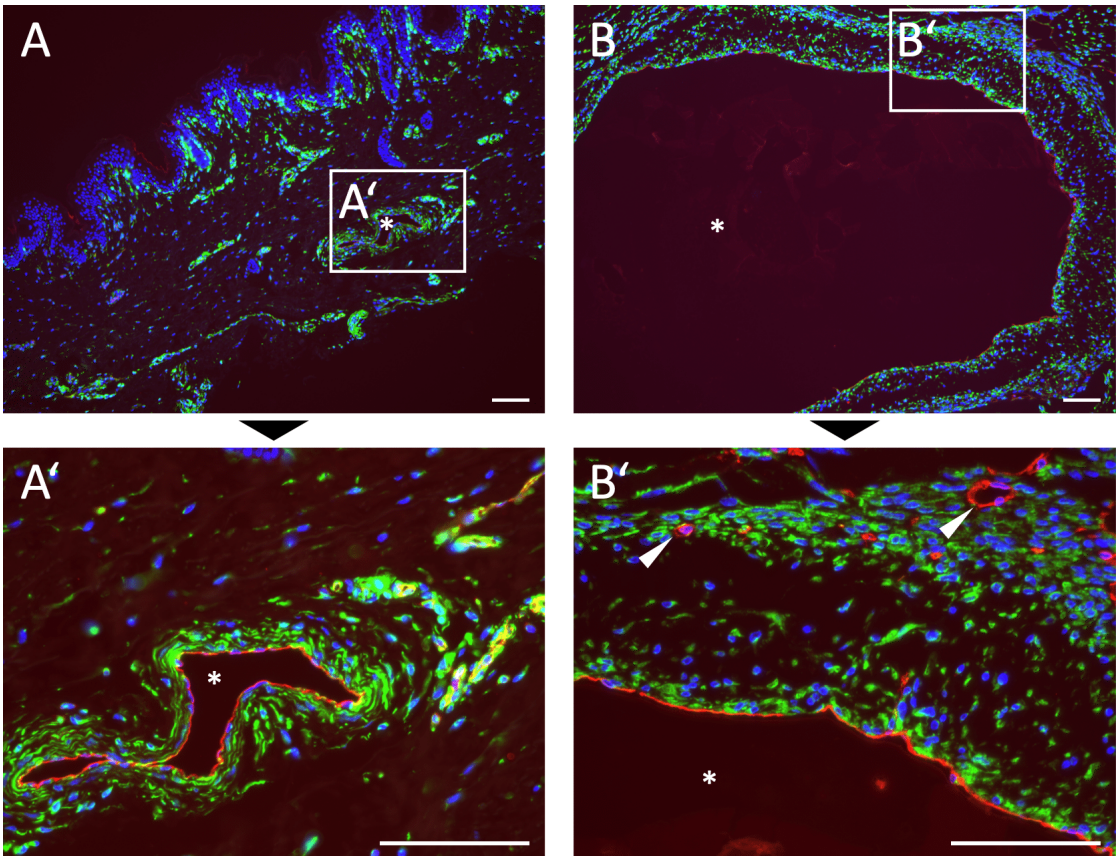

Figure 4.26: Immunofluorescence staining of endothelial cells lining the channel lumen. Immunofluorescence staining for endothelial marker CD31 (red) and fibroblast marker vimentin (green). Cell nuclei were stained with DAPI (blue). Pictures A and A' depict native skin with blood vessels lined with hdmEC. The channel created in a high-density collagen hydrogel is enveloped by hdmEC (B and B'). Additionally, small lumen-like endothelial structures are visible in the collagen gel near the channel (white arrowheads). Asterisks mark the vessel or channel lumen. Scale bars = 100 µm.

4.3.4 Integration of vascularization strategies in perfused hydrogels

As next step towards the overall goal of a vascularized perfused skin equivalent, the vascularization strategies already achieved for the FTSE as described in section 4.2 should be combined with the perfused collagen hydrogels. Therefore, high-density collagen hydrogels with a central channel seeded with endothelial cells were generated using both bioreactor designs as described in section 4.3.2. Additionally to the hdF, hdmEC were seeded in the collagen hydrogel in a final concentration of $5.7 * 10^5$ hdmEC/ml hydrogel.

Although immunohistochemical staining for endothelial marker CD31 proved the presence of endothelial cells distributed throughout the collagen hydrogel, there were no lumen-like structures (see figure 4.27) as seen for the vFTSEs (figures 4.10 and 4.15). Additionally, the pictures of the hydrogel generated in the bioreactor design B show no channel. In the hydrogel of bioreactor design C, the channel is visible, but is not lined with hdmEC. Instead, lumen-like cavities in proximity to the channel are seeded with hdmEC.

For a better resemblance of the perfused hydrogels to the FTSE, higher endothelial cell and collagen concentrations were needed. Therefore, the bioreactor design B and the compression stamp were modified to enable a higher plastic compression of the collagen hydrogel. With this modifications it was possible to compress a higher volume of collagen to a lower hight. 9 ml of cell-laden collagen were filled into the bioreactor and after polymerisation compressed to a final volume of about 1.35 ml (see figure 4.28 A, B). Thereby, the collagen concentration was increased to 36 mg/ml, comparable with the collagen concentration in FTSE. The final cell concentrations were $4 * 10^5$ cells/ml for hdF and $6.5 * 10^6$ cells/ml for hdmEC, hence corresponding to the cell concentrations in the dermal part of vFTSE. The channel was generated successfully and by perfusion with 0.1 % phenol red clearly visible through the high-density collagen (see figure 4.28 C). Since the collagen hydrogel was through the higher compression denser than the hydrogels created before, it seemed to be more stable and easier in handling. The channel was seeded with hdmEC and the perfused collagen hydrogels were cultured for 14 days. Subsequent analysis of HE stained cross-sections revealed a highly stratified or layered collagen hydrogel (see figure 4.28 D, E). The channel was visible but rather thin and without cells lining the lumen surface.

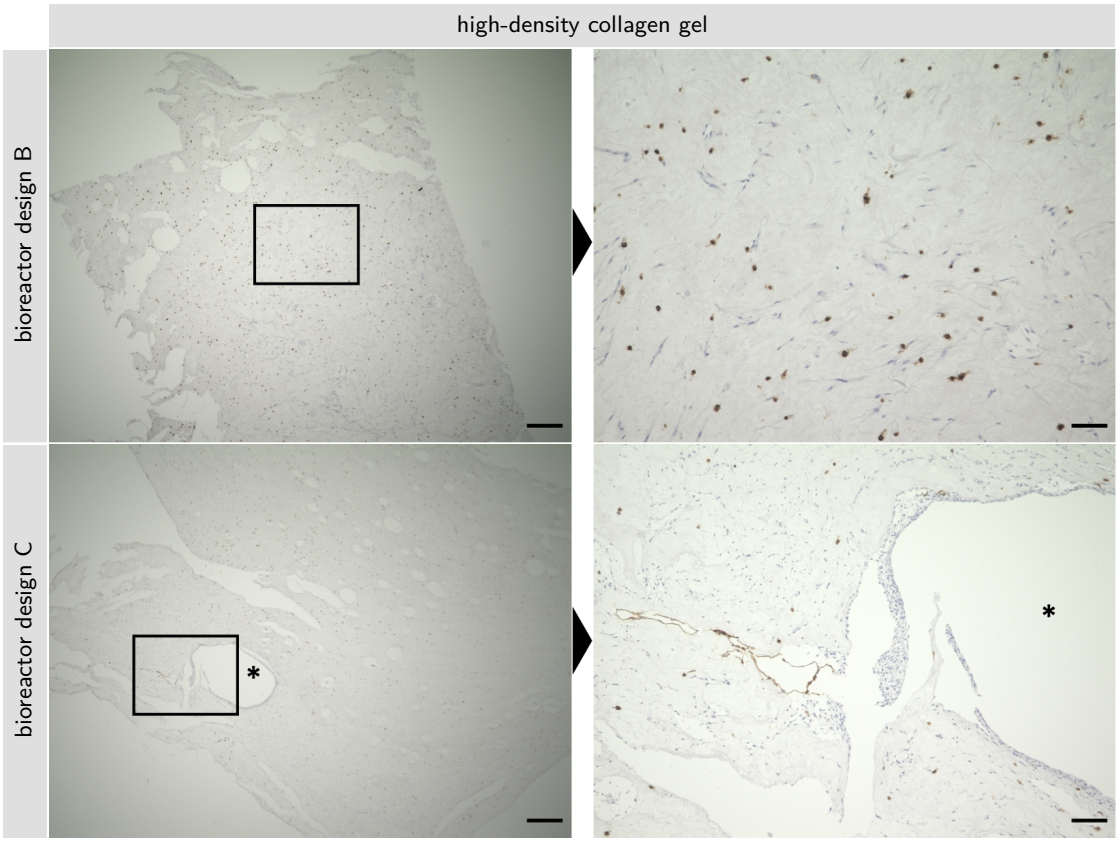

Figure 4.27: Immunohistochemical staining of endothelial cells within the perfused collagen hydrogel. Perfused high-density collagen hydrogels were generated using both bioreactor designs. The channel was seeded with hdmEC and additionally hdmEC were seeded within the collagen hydrogel. Immunohistochemical staining of endothelial marker CD31 shows the endothelial cells (brown) within the hydrogel. HdF are stained in blue. For the hydrogel generated in bioreactor design B, no channel is visible on the cross-sections. For the hydrogel generated in bioreactor design C, the channel is visible but without endothelial cells. Instead, lumen-like cavities near the channel are lined with endothelial cells. Asterisks mark the channel lumen. Scale bars = 500 µm (left column) and 100 µm (magnifications in right column).

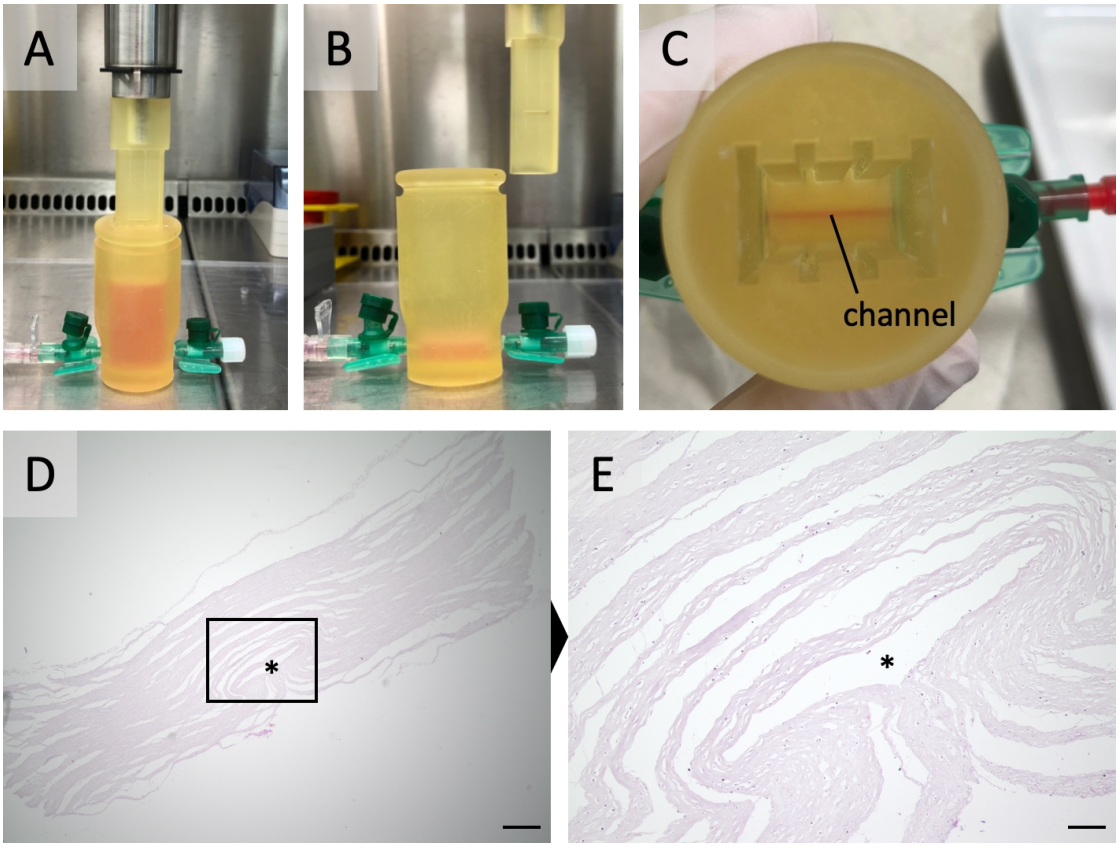

Figure 4.28: Modified bioreactor to generate collagen hydrogels with higher density. The height of the bioreactor body was increased to fill in more collagen. Likewise, the stamp was extended to enable a higher compression of the collagen hydrogel. The pictures show the bioreactor with collagen at the beginning of (A) and after plastic compression (B). The successfully generated channel was visualised by flushing with phenol red (C). HE stained cross-sections of the collagen hydrogel show the channel within the layered collagen hydrogel. There are no cells lining the channel lumen (D, E). Asterisks mark the channel lumen. Scale bars = 500 µm (D) and 100 µm (E).

4.4 Investigation of malignant melanoma in a vascularized full-thickness skin equivalent

A possible application scenario for vascularized skin models is the investigation of tumor metastasis. Malignant melanoma is considered dangerous due to its aggressiveness and early spreading to other body sites. A model mimicking the natural environment of this tumor could serve for studying its development and metastasis as well as an *in vitro* testsystem for anti-tumor therapies. Thus, the next aim was to establish melanoma full-thickness skin models to combine them then in a further step with the vascularized full-thickness skin models to generate a model for melanoma metastasis. Parts of the data presented here include results obtained by Johanna Kliche during her master thesis as part of this project [141].

4.4.1 Integration of melanoma in FTSE

On the basis of the already established FTSE and a previously established epidermal melanoma model, a melanoma full-thickness skin equivalent (mFTSE) was established. For this purpose, the melanoma cell lines SK-MEL-28 and BLM were implemented in the epidermal part of FTSEs. SK-MEL-28 are widely used in melanoma research and bear a BRAF mutation [142]. The BLM cell line is highly invasive and metastatic and characterized by a NRAS mutation [143, 144].

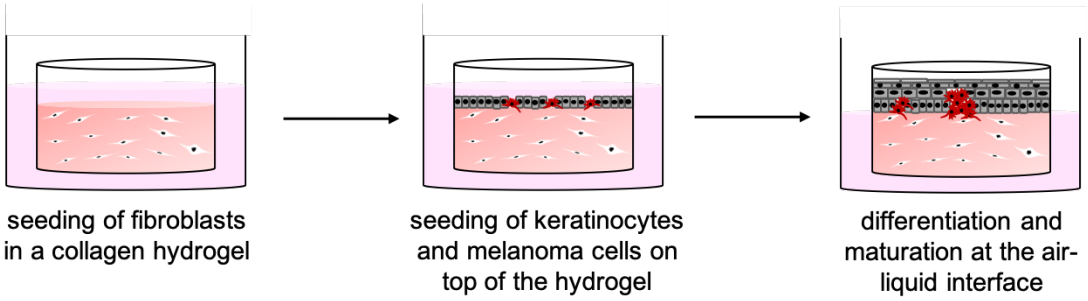

Figure 4.29: Schematic drawing of the generation of a FTSE with melanoma. Fibroblasts are seeded in a collagen hydrogel cast in an insert. After plastic compression of the hydrogel, melanoma cells are seeded together with keratonocytes on top of the gel. During culture at the air-liquid interface, the keratinocytes differentiate to form a stratified epidermis with tumor nests in the basal layer.

The generation of mFTSEs is depicted in figure 4.29 and similar to the generation of FTSEs as described in section 3.5. The only difference is the addition of melanoma cells to the keratinocytes in a ratio of 1:50. To construct a mFTSE comparable to the

in vivo situation, the formation of a well stratified epidermis is decisive. Therefore, the ratio of melanoma cells to keratinocytes is pivotal, as only an optimal ratio leads to the development of tumor nests within the epidermis. Melanoma cells are mixed with the keratinocytes before seeding them on top of the prepared dermal part of the mFTSE. During culture at the air-liquid interface, tumor nests grow originating from the basal layer of the epidermis.

To visualize the tissue morphology and architecture, cross-sections of the mFTSEs were stained with hematoxylin and eosin and compared to control FTSEs without melanoma cells (see figure 4.30). Control FTSEs showed a uniform dermal part seeded with fibroblast and a well stratified epidermis. Integration of melanoma cell line SK-MEL-28 caused the growth of tumor nests at the dermoepidermal junction. These sites were characterized by a loosened tissue and partial rupture between the epidermis and the dermis. This cleft can also occasionally be seen in control FTSE but without these protrusions of unorganized tissue into the dermis. In contrast, in mFTSEs with BLM no tumor nests were observable. To exclude the possibility of a suboptimal ratio of melanoma cells to keratinocytes, several ratios were tested. Even in the highest ratio of 1:25, no visible tumor growth occurred.

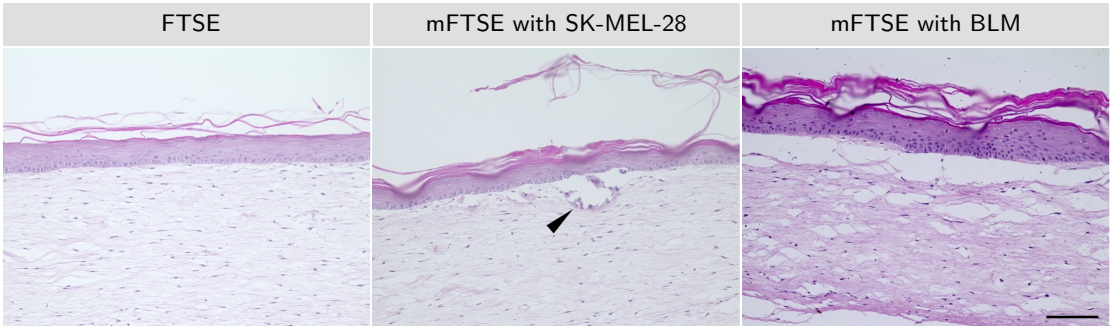

Figure 4.30: HE staining of melanoma FTSEs. The control FTSE shows the dermal part seeded with hdF and a well-stratified epidermis. Integration of SK-MEL-28 in the epidermis led to tumor nests in the epidermal basal layer protruding in the dermis (arrowhead), whereas in case of BLM, a rupture between the epidermis and the dermis occured but no tumor nest formation. Scale bar = 100 µm.

To unambigiouosly identify the generated tumors, cross-sections of the mFTSEs were stained immunohistochemically for melanoma markers. These markers are conventionally used in anatomic pathology as diagnostic tool to distinguish melanoma from other skin diseases [145]. Melan-A is a protein expressed on the surface of melanocytes and is specific for the melanocyte lineage. Thus, it can be found in normal skin and the retina. HMB45, which stands for human melanoma black, is an antibody against the melanocyte protein

PMEL. It is often used in combination with other markers such as Melan-A and S100 to identify melanoma malignancy as it is not very sensitive against adult melanocytes. Figure 4.31 reveals the different expression patterns in FTSEs and mFTSEs. While HMB45 is absent in control FTSEs and Melan-A is expressed just in a few cells within the *stratum basale*, there are massive tumor nests positively stained for both markers in mFTSEs with SK-MEL-28. Whereas in mFTSEs with BLM, staining for both markers was distributed similar to the control FTSE.

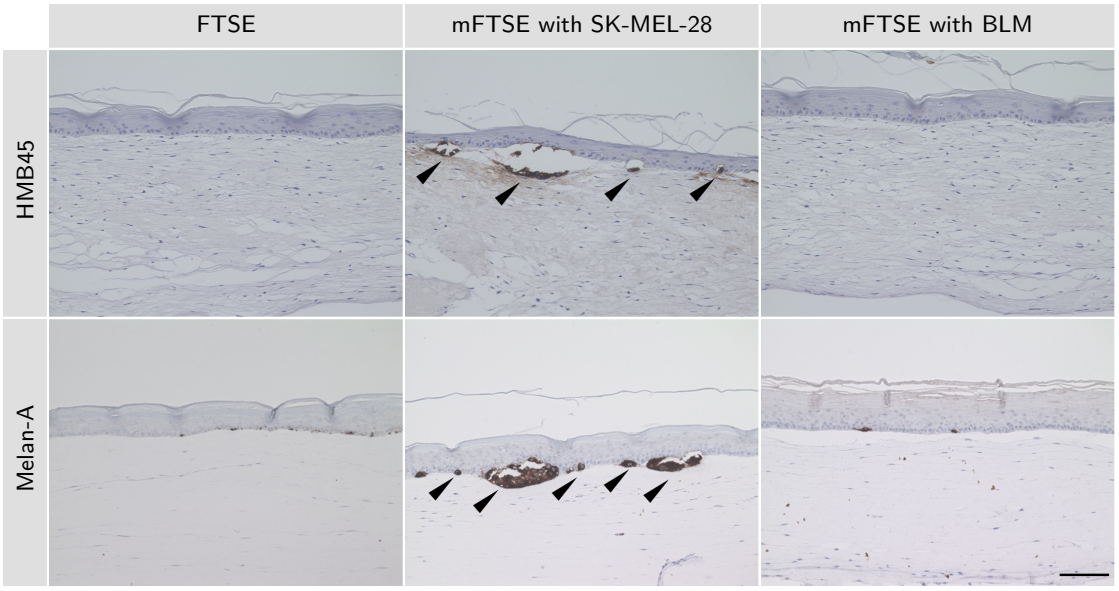

Figure 4.31: Immunohistochemical staining of melanoma FTSEs for melanoma markers. The control FTSE shows no staining for HMB45 and just a few little positive spots in the epidermal basal layer for Melan-A. MFTSEs with SK-MEL-28 exhibit tumor nests of different sizes positively stained for both melanoma markers (arrowheads) while mFTSEs with BLM showed no postitive staining. Scale bar = 100 µm.

For further characterization and visualization of the established mFTSEs, immunofluorescence stainings were conducted (see figures 4.32 and 4.33). With stainings for cytokeratin 10 (figure 4.32 first row, red) and 14 (green), it was confirmed that the physiological architecture seen in control FTSEs is maintained in the mFTSEs but disrupted at sites of tumor growth. The staining for vimentin (figure 4.32 second row, green) showed evenly distributed fibroblasts throughout the dermal part of the FTSE as well as the mFTSEs. Melanoma nests were visualized with the melanoma markers HMB45, Melan-A and S100 (figure 4.32 third to fifth row, green), which were absent in control FTSEs except for some positively stained cells in the *stratum basale*. MFTSEs with SK-MEL-28 had large tumor nests positively stained for all three tumor markers,

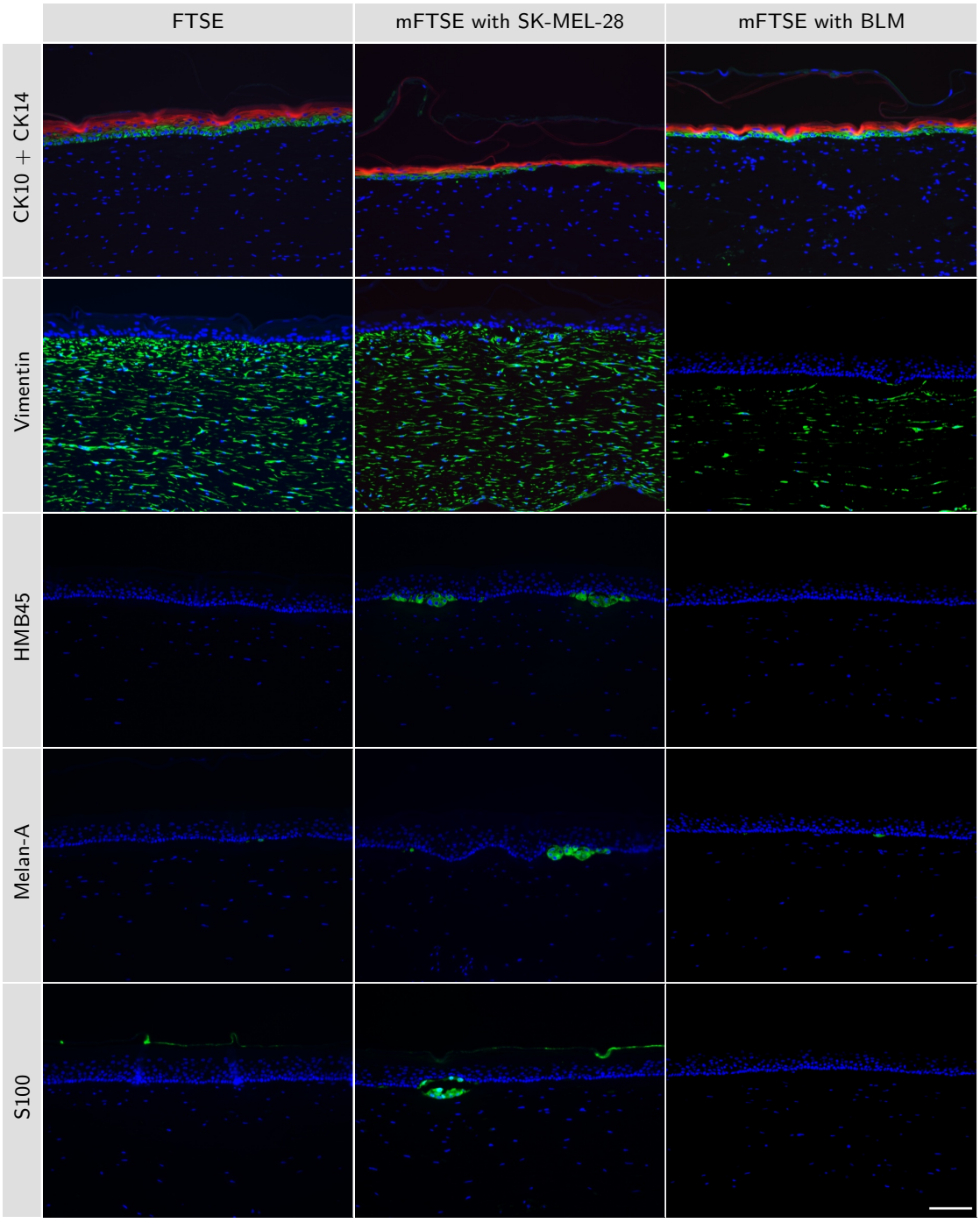

Figure 4.32: Immunofluorescence staining of melanoma FTSEs. Cytokeratin 10 (CK10, red) and 14 (CK14, green) show the proper formation of epidermal layers in the FTSE as well as in mFTSEs. Vimentin (green) is distributed evenly in the dermis of both model types. Melanoma markers HMB45, Melan-A and S100 (green) are absent in the control FTSE and in the mFTSE with BLM, whereas there are positively stained tumor nests in the mFTSE with SK-MEL-28. Cell nuclei were stained with DAPI (blue). Scale bar = 100 µm.

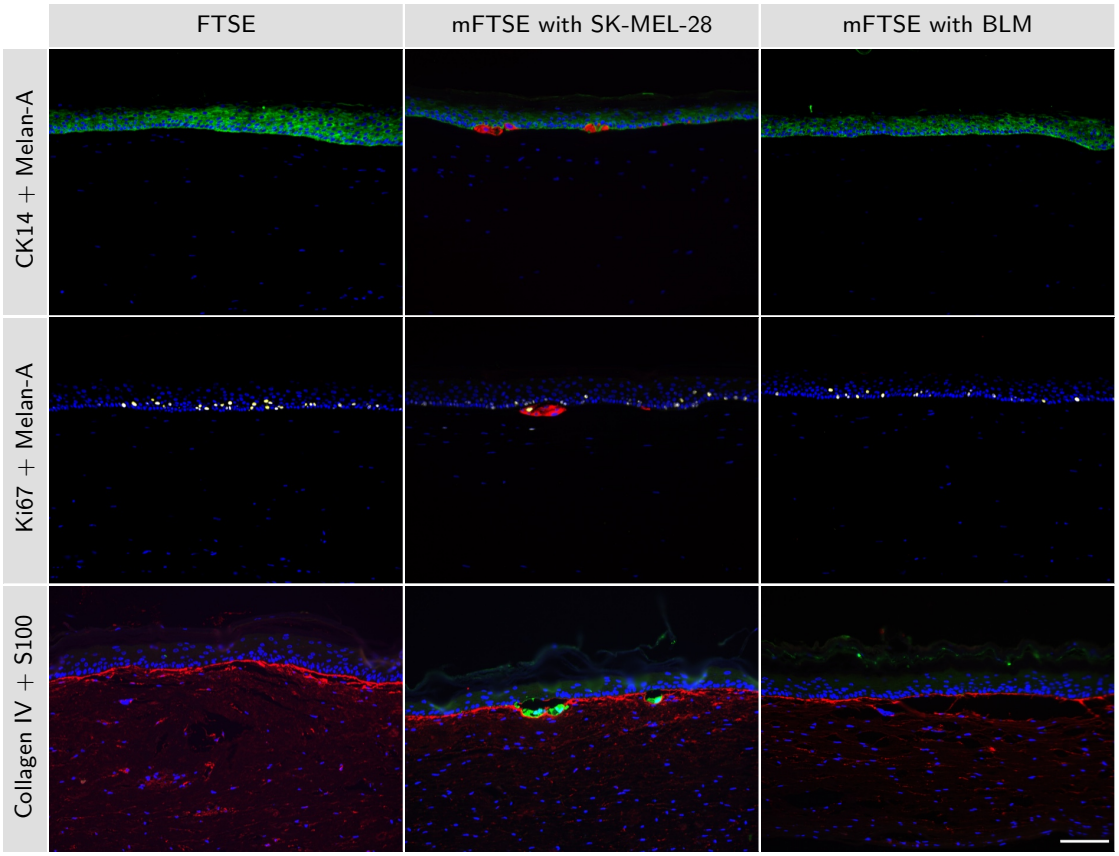

Figure 4.33: Immunofluorescence double-staining of melanoma FTSEs. Double-staining for cytokeratin 14 (CK14, green) and the melanoma marker Melan-A (red) shows the presence of tumor nests within the basal layer of the epidermis only in mFTSEs with SK-MEL-28. Ki67 (yellow) is a proliferation marker positive in single cells in the *stratum basale* in every model, whereas only in mFTSEs with SK-MEL-28 it is slightly co-localised with Melan-A (red). The staining of collagen type IV (red) shows the presence of a basement membrane between epidermis and dermis and also around tumor nests stained positively for S100 in mFTSEs with SK-MEL-28. Cell nuclei were stained with DAPI (blue). Scale bar = 100 µm.

whereas in mFTSEs with BLM there was no positive signal comparable to the results of the immunohistochemical staining.

Double-staining for the epidermal marker CK14 (figure 4.33 first row, green) and the melanoma marker Melan-A (red) showed the localization of the tumor nests within the basal layers of the epidermis in mFTSEs with SK-MEL-28. Positive staining for the proliferation marker Ki67 (figure 4.33 second row, yellow) could be seen in single cells of the basal layer of the epidermis, evenly distributed throughout the model, in all three model types with a slight co-localisation with positive staining for Melan-A (red) in mFTSEs with SK-MEL-28. Collagen type IV (figure 4.33 third row, red), as part of the basement membrane, was predominantly present at the dermo-epidermal junction. In mFTSEs with SK-MEL-28, collagen type IV was also expressed at tumor sites.

4.4.2 Combination of vascularized FTSEs with melanoma FTSEs

To study interactions between hdmEC as part of the vascular system and melanoma cells and provide a model system for melanomagenesis and metastasis, the vascularized FTSEs and the melanoma FTSEs described above were combined. Thus, the vascularized melanoma FTSE (vmFTSE) was comprised of four different cell types: hdF and hdmEC were seeded in the dermal part and heK and melanoma cells built up the epidermal part of the model. As the melanoma cell line BLM could not be detected in the mFTSE, only SK-MEL-28 were employed for these models.

Immunohistochemical stainings for endothelial cell marker CD31 and melanoma cell marker HMB45 proved the presence of both cell types in the vmFTSE (figure 4.34, last column). Endothelial cells in the vmFTSE formed lumen-like structures as seen before in the vFTSE. Thus, the formation of these structures was not impeded by the addition of melanoma cells to the models. The same applies for the growth of tumor nests at the dermo-epidermal junction: In the mFTSE as well as in the vmFTSE, melanoma positively stained for HMB45 arose.

Immunofluorescence double-staining for endothelial marker CD31 and melanoma marker S100 allowed a more detailed analysis. Figure 4.35 reveals frequent tumor nests at the dermo-epidermal junction, protruding in the dermis and also the formation of endothelial lumen-like structures throughout the dermis, but no co-localisation of both markers. This is in line with the findings, that the tumor nests did not break through the basement membrane and invade the dermis. Immunofluorescence signals from the *stratum corneum* are due to unspecific binding of the secondary antibody.

As an alternative approach and in order to bring the cells in more spatial proximity to

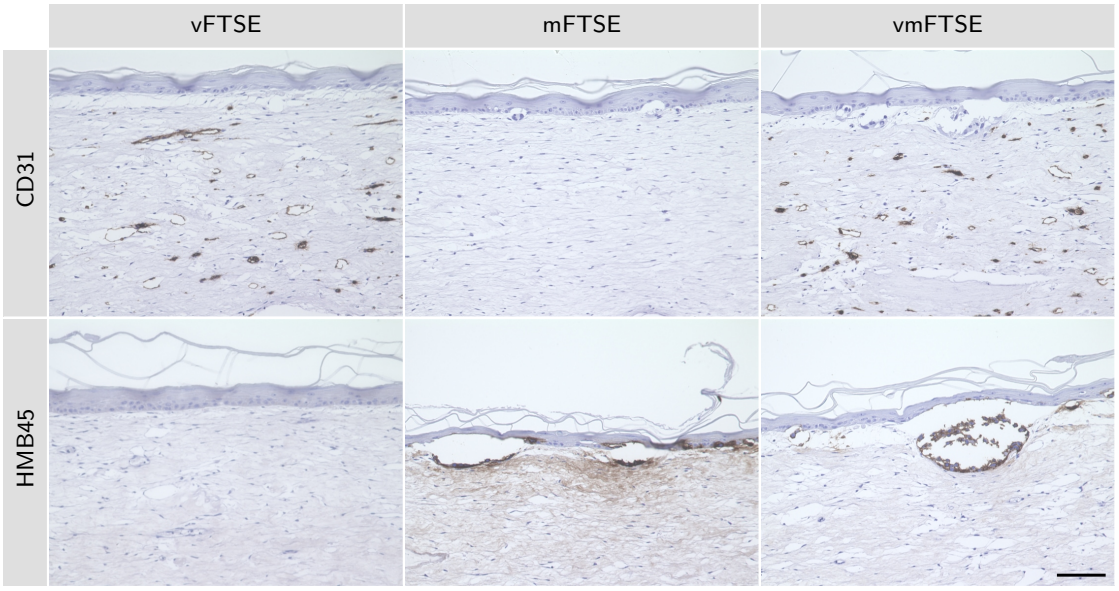

Figure 4.34: Immunohistochemical staining of vascularized melanoma FTSEs. Lumen-like structures positive for CD31 are present in the vascularized FTSE (vFTSE) as well as in the vascularized melanoma FTSE (vmFTSE). Melanoma stained by HMB45 grew in melanoma the FTSE (mFTSE) and in the vmFTSE. Scale bar = 100 µm.

promote co-localisation, SK-MEL-28-spheroids were seeded in the dermal part of vFTSEs. For this purpose, spheroids of about 500 SK-MEL-28 cells were formed according to the generation of endothelial cell spheroids (see section 3.4), but with the deviation of 4 days of culture instead of 1 to allow better formation of a tumor mass. 44 spheroids were seeded together with 45 000 hdF and 294 000 hdmEC per model in the dermal part of FTSEs. In these models, tumor nests grew in the dermis, opposed to the mFTSEs in which melanoma grew at the dermo-epidermal junction. Figure 4.36 provides an overview of the model with a large melanoma spheroid (green) at the top side of the dermis. A more detailed view is depicted in figure 4.37: Endothelial structures (red) appear in spatial proximity to the melanoma spheroids (green) but not within the tumor mass or directed to it. Additionally, tumor nests occur bigger and more widespread.

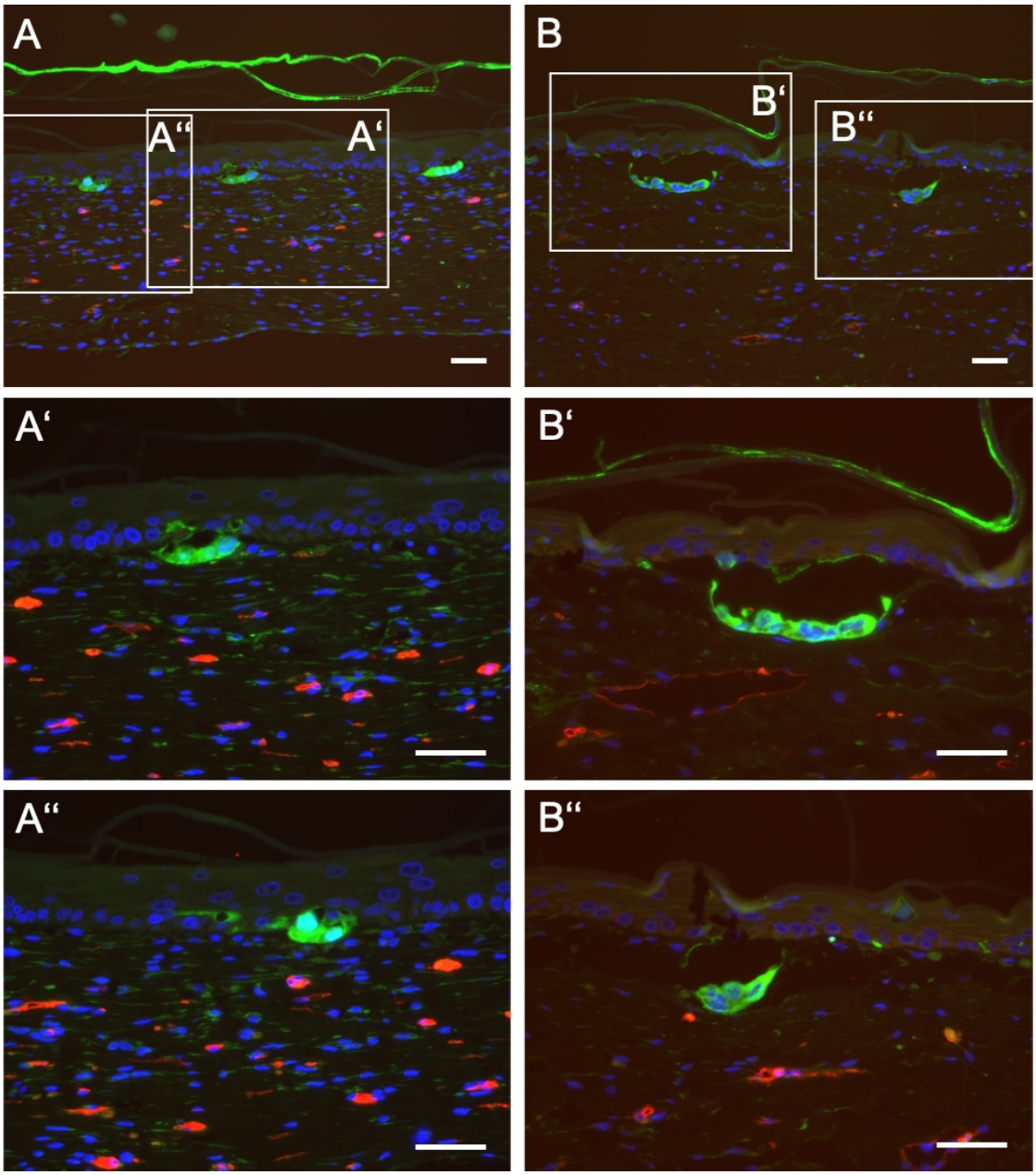

Figure 4.35: Immunofluorescence double-staining of vascularized melanoma FTSEs. Images A and B depict two representative pictures of a vascularized melanoma FTSEs. Endothelial structures are stained with the endothelial marker CD31 (red) and tumor nests are stained with the melanoma marker S100 (green). In the respective magnifications no co-localisation of CD31 and S100 occured (A', A", B', B"). Cell nuclei were stained with DAPI (blue). Scale bars = 50 µm.

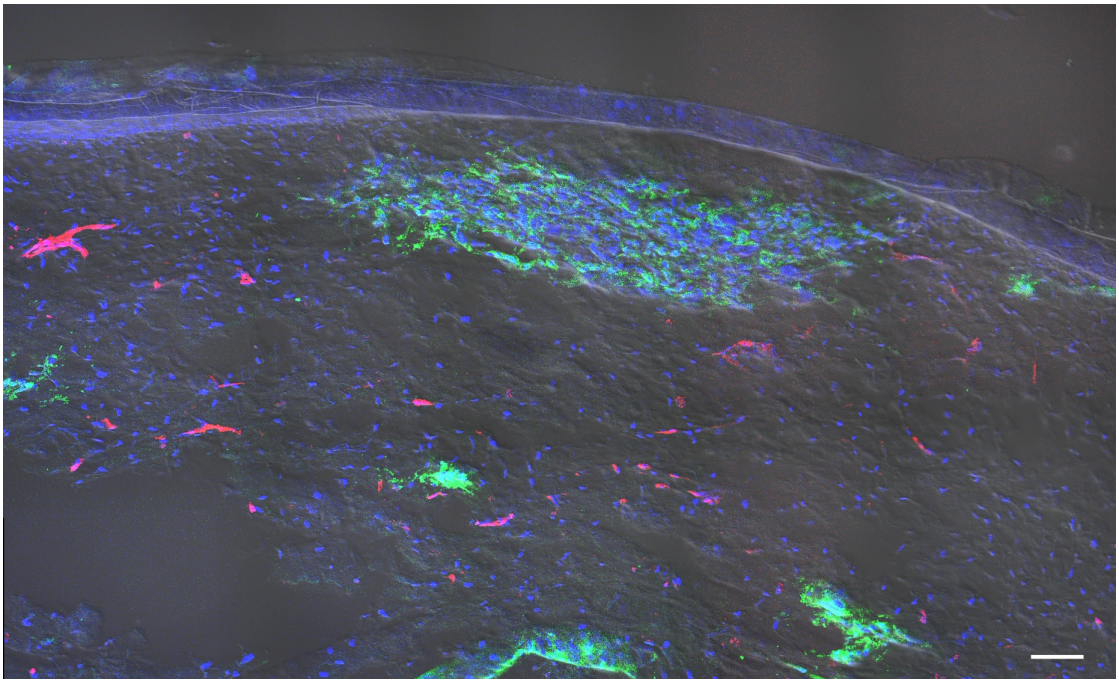

Figure 4.36: Overview of a melanoma spheroid in the dermis of a vFTSE. Confocal microscopic picture of immunofluorescence staining for endothelial marker CD31 (red) and melanoma marker S100 (green) in an overlay with the brightfield image. Cell nuclei were stained with DAPI (blue). Scale bar = 100 µm.

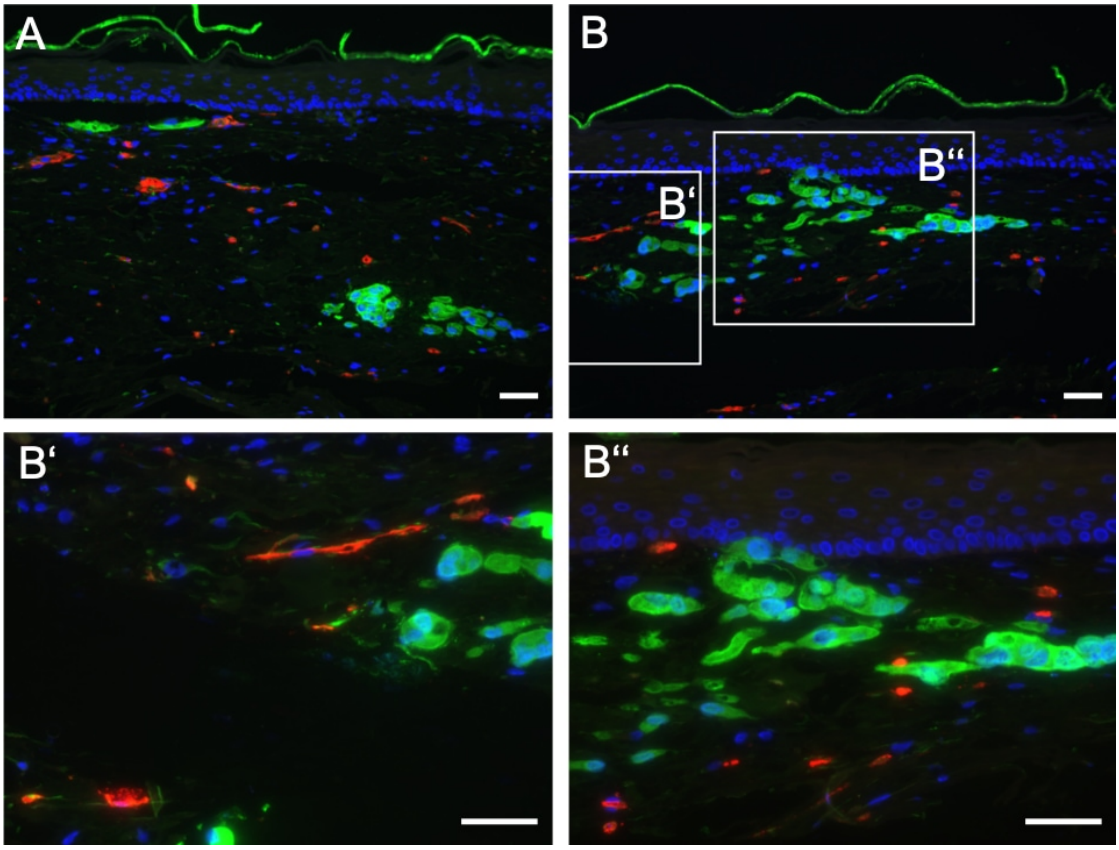

Figure 4.37: Vascularized FTSE with melanoma spheroids in the dermis. Immunofluorescence staining for endothelial marker CD31 (red) and melanoma marker S100B (green) of a vascularized FTSE with SK-MEL-28-spheroids in the dermis. Images A and B depict two representative pictures, while B' and B" represent magnifications of B. Cell nuclei were stained with DAPI (blue). Scale bars = 50 µm.

5 Discussion

In vitro skin equivalents are widely used in various research areas. They are applied in basic research to investigate fundamental processes in the skin and to mimic pathologies to understand the underlying mechanisms or to establish new therapies [17]. Furthermore, they are used as toxicological test systems for risk assessment of chemicals [15, 59]. In this way, they help to implement the 3R principle by reducing and replacing animal experiments [7]. Besides ethical concerns, there are economic and scientific arguments in favour of using *in vitro* models instead of animals. Apart from high costs for maintenance of laboratory animals and conducting the experiments, a major objection is the limited transferability of results obtained in animal experiments due to tremendous species-differences and the specific experimental set-up [146, 147]. Animal experiments are often required in advanced phases of pharmaceutical studies because it is argued that whole organisms are needed to depict every aspect of possible effects of the substance. But results gained from animal models are not always reliable since animals and humans differ considerably in terms of anatomy, physiology and metabolism [148]. Many human diseases do not occur in animals, which is why the specific symptoms of a disease are induced artificially with exogenous factors such as radiation or genetic knockout [148]. Although this is a valuable approach for some investigations in some model organisms, these exogenous factors are not the cause for the disease in humans. Thus, important aspects of the origin of the disorder can not be taken into account.

For example, mice, being the species most commonly used for biomedical research [149,150], rarely develop melanoma spontaneously. Thus, they are genetically manipulated, knocking out certain human cancer-related genes [5]. But this neglects the fact, that many diseases are multi-factorial and not only based on one artificial cause [146]. Moreover, the physiology of rodent skin differs tremendously from human skin, the much stronger hairiness just being the most obvious deviation [50]. Also melanocytes, important for the investigation of melanoma development, have a different distribution pattern: In mouse skin, they are located in the hair follicles, whereas in human skin, melanocytes are scattered in the *stratum basale* in close contact to adjacent keratinocytes [118].

Moreover, pharmaceutical compounds tested in animal models might work differently

in humans due to physiological and metabolic differences [146, 151]. Drugs evaluated positively in treating a particular disease in an animal model might not at all have the desired effect in humans [147, 152]. Even worse, severe side effects can occur that were not apparent in the animal model [153–155]. The poor predictability of animal models was stated in a systematic review in 2007 by Perel et al., who compared animal experimentation results with clinical trial findings and found that the human and animal results were in accordance only half of the time [156]. This fact is also underlined by the low success rate of compounds for cancer therapy in clinical trials: Less than 5 % make it to the market, rendering conventional oncology drug development dramatically inefficient [147, 157].

Furthermore, although being contradictory to the intention to provide a more natural environment, the multicellularity of animal models also impairs the scientific readout by impeding a detailed mechanistic interpretation of experimental findings, as a particular observation can hardly be traced back to a single cause [118, 158]. In contrast, *in vitro* models are generated from a defined set of human cells and aim to provide ideal test systems as close as possible to the human physiology. Of course, they are not able to represent a whole organism and thus only capture a limited aspect of the tissue microenvironment, but this disadvantage is at the same time an advantage as the reduced complexity allows the control of most experimental variables [159]. However, even if they might not be applicable for every pathology, tissue engineered *in vitro* models are a sophisticated solution to overcome inter-species differences. 3D *in vitro* models are meant to bridge the gap between 2D cell cultures, not depicting the tissue microenvironment, and far more complex but not always comparable animal models [5]. In this way, they contribute to the application of the 3R principle.

The skin was one of the first organs being explored in the very beginnings of tissue engineering [9]. To date, many skin equivalents are commercially available for clinical use as well as for research applications [9, 11, 15, 16]. However, a major pitfall for all tissue engineered constructs is the lack of a vasculature. Currently, there are no perfusable vascularized skin models available, which would enable improved *in vitro* perfusion studies, toxicity testing or investigation of diseases involving the vasculature. In the field of melanoma research, vascularized skin models are indispensable for investigating tumor progression and metastasis since these processes rely on the vascular system. Therefore, this thesis aimed at the establishment of a vascularized full-thickness skin model, that can be used as test system for melanoma development.

5.1 Challenges to incorporate hdmEC in collagen hydrogels

Vascularization is a crucial prerequisite in tissue engineering. By the generation of a preformed microvascular network, the nutrient and oxygen supply of the tissue construct shall be ensured [80, 82]. But the formation of capillary vessels in tissue engineered constructs faces many challenges regarding the choice of the specific cell type, co-cultures, scaffold materials and culture conditions [58]. Many aspects have to be considered and tested. Although there have been several attempts to establish vascularized skin equivalents, there is no exclusive solution to this scientific challenge.

In many studies, vascularization approaches for tissue engineered skin constructs include the seeding of endothelial cells into the dermal compartment of the model. Taking advantage of the spontaneous self-assembly of endothelial cells to form lumen-like structures within a matrix, random capillary-like networks were achieved [58,77,89,90]. In the here used FTSE, the dermal part is comprised of collagen type I isolated from rat tail and primary hdF. In the first part of this thesis, the suitability of the used collagen type I hydrogel for the endothelial cells to grow and sprout in should be investigated. To test the sprouting ability of the hdmEC in the collagen hydrogel, sprouting assays were performed. Sprouting assays are widely used as 3D *in vitro* model for angiogenesis [131, 132]. In this assay, preformed endothelial cell spheroids are seeded in a 3D matrix. During incubation, finger-like sprouts arise from the surface of the spheroid growing into the surrounding matrix. The number and length of these sprouts is measured to determine the angiogenic potential of added substances or the effect of the surrounding matrix. The sprouting assays with increasing collagen concentrations revealed that the sprouting lengths of endothelial cell spheroids were higher in all conditions compared to the initial concentration. The highest sprouting length of 2 169 µm was achieved in a high-density hydrogel with a collagen concentration of 19 mg/ml. These results show that not only are the primary hdmEC able to sprout in the used collagen matrix, but increasing collagen concentrations and even high collagen concentrations in a plastically compressed hydrogel do not have negative effects on the sprouting behaviour of the hdmEC. On the contrary, increasing collagen concentrations seemed to have a beneficial effect on the sprouting ability of the hdmEC as the cumulative sprouting length was enhanced in higher concentrations. Previous studies showed that the matrix density and its mechanical properties have direct effects on the endothelial cell sprouting ability and that an increased matrix stiffness results in an increased length and number of endothelial sprouts, highlighting the importance of the ECM on cellular behaviour [160, 161]. In contrast, other angiogenesis models showed a decrease in sprouting length with increasing

collagen concentrations [162, 163]. However, these studies were performed using collagen concentrations ranging from 0.3 to 4 mg/ml, which is the case for most sprouting assays in the literature [131–133, 160–163]. The here used collagen concentrations are much higher in order to test the sprouting ability of the hdmEC as preliminary work for incorporating them in the dermal part of FTSEs. As the cells showed a good sprouting ability and viability even in high-density collagen gels, their suitability for vascularization approaches of FTSEs was assumed.

In vivo, the ECM of the dermis is not only composed of collagen type I, but also of other collagens, elastic fibres, glycoproteins, glycosaminoglycans and proteoglycans [22–24, 134]. Besides providing a structural framework, the ECM also plays an important role in receptor-mediated signaling throughout several developmental processes [164]. Hence, the idea is obvious to not only build up the dermal part of the FTSE from collagen type I, but to add further components of the ECM to ensure a higher similarity to the situation *in vivo*. Supplementation with additional ECM components is not a new approach [165]. In fact, the collagen hydrogel used in this thesis is not only comprised of pure collagen type I but already contains chondroitin sulfate, a glycosaminoglycan as an ingredient of the GNL. For possible further improvement of the hydrogel, decorin was chosen as additional ECM component. Decorin is one of the many ECM proteins secreted by fibroblasts [9] and belongs to the group of small leucine-rich proteoglycans. Proteoglycans are important components of the human dermis, contributing to the mechanical strength of the skin [166, 167]. According to a proteomic analysis performed by Mikesh et al. in 2013, decorin is one of the top 50 most abundant proteins of human skin [134]. Decorin consists of a central region of ten leucine-rich repeats and a side chain of chondroitin or dermatan sulfate [135, 167]. The central leucine-rich repeats are thought to be the binding site for multiple proteins, such as several collagen types, transforming growth factor β (TGF-β) and others. Decorin plays a pivotal role in tissue development and assembly and is vital for maintaining skin integrity at the molecular level [135]. It has an important function in collagen fibrillogenesis, what was first elucidated in mice with a disrupted decorin gene. These mice showed alterations in the collagen fibres, observed as abnormal collagen fibrils and an overall collagen weakness [135, 167]. Thus, it was hypothesized, that decorin not only affects fibril formation but also fibril stability. The exact mechanism is not completely understood, but decorin is meant to be a vital mediator of fibrillogenesis [135, 168, 169]. A possible scenario is that decorin binds to collagen fibrils and slows down their assembly. This delay enables time for optimal interactions to occur and results in structurally optimized fibres [135]. The impact on

fibrillogenesis influences the length and diameter of the fibres and therefore the pore sizes of matrices. This could have an effect on cell behaviour, as the polymerization conditions have considerable influence on the scaffold structure and porosity after *in vitro* reconstitution [165].

To test if the here used collagen type I hydrogel could be improved by supplementation with decorin regarding the stability and suitability of the hydrogel to better mimic the dermal part of the skin, low- and high-density collagen hydrogels with and without added decorin were compared. The low-density collagen gels showed shrinkage to 26.8 % (without decorin) and 30.8 % (with decorin) of the initial weight of the hydrogels (see figure 4.4 B). This is in line with a study from Ruehle et al. who found that the addition of decorin to a collagen hydrogel reduces its contraction [169]. However, they used a lower collagen concentration and a higher decorin concentration. Although the differences were significant at all time points during culture time, the trend was similar in both conditions. It seems the collagen hydrogels without decorin contracted faster as the weight of these gels was already reduced at day 7, while the weight of the collagen hydrogels with decorin was still at a comparable level to the initial value. Nevertheless, during culture time the weights of both conditions approximated. At day 21, the difference between gels with and without decorin was the least. The contraction of cell-laden collagen hydrogels during culture is a well-known phenomenon [170–173]. Fibroblasts constantly degrade and reassemble collagen fibres and other ECM components, thereby remodelling the matrix. In some studies, this circumstance is taken into account with specialised experimental set-ups [81, 82, 101]. Others tried to overcome this problem via crosslinking the collagen matrix to reduce contraction [52]. Another solution is plastic compression: The increased collagen concentration and the reduced water content improve the mechanical properties and lead to less contraction of the collagen hydrogel as shown by Reuter et al. [174]. Likewise, in high-density collagen gels, shrinkage could be prevented to a great extend. Here, the hydrogels with decorin lost only 10 % of their initial weight during culture time. This is in line with the results from Reuter et al., who showed a weight loss of 6.7 % for high-density collagen hydrogels [174]. Interestingly, the control hydrogels without decorin gained weight to a final value of 130 %. This is explainable by a slight swelling of the hydrogels during culture time due to medium absorption. However, the presentation of the data is deceptive. While the presentation in relation to the initial weight facilitates legibility and comparison, looking at the raw data it becomes evident, that the weight of the hydrogels with and without decorin is actually quite similar at days 7, 14 and 21. Only at the initial time point directly after plastic compression the conditions differ with a mean weight of 0.14 g for the hydrogels without decorin and 0.20 g for the ones

with decorin. However, since the initial value is set to 100 %, this circumstance is not taken into account in this presentation method. As explained above, the presumed mode of action of decorin in fibrillogenesis is the deceleration of collagen fibril assembly. The resulting fibres are meant to be structurally more regular [135]. This could lead to a better water retention capacity and therefore to more stable hydrogels. In both collagen concentrations, the hydrogels with decorin showed a higher consistence in their weight over the time course.

The immunohistochemical stainings revealed no differences in morphology of the collagen gels by adding decorin. A similar positive staining for decorin was seen in every condition, comparable to the staining of decorin in native skin (see figure 4.5). The intense positive staining for decorin complies with the findings of Li et al., who showed the localization of decorin in human dermis with an equally intense immunostaining [166]. Since the improper functionality of the used antibody was ruled out, it seems that decorin is abundant in the hydrogels independent from adding it to the collagen. Decorin *in vivo* is bound to collagen type I fibrils [166] and is not only present in the ECM of the dermis but is for example also found in tendons [135]. Due to the collagen isolation process from tendons from rat tails it is possible, that there is still decorin remaining in the collagen. This could be tested by western blot or mass spectrometry. But according to the manufacturer, the anti-decorin antibody is only reactive with human and mouse decorin, but not rat. While the possibility of cross-reactions should not be left out, the positive staining could also result from the presence of human decorin. As decorin is secreted by fibroblasts [9, 166], it is conceivable that they produced it during culture time. In further experiments also other concentrations of decorin should be tested. In this rather low concentration, no differences were observable between the collagen hydrogels with and without decorin. This could change with higher concentrations. Previous studies used decorin concentrations of up to 50 µg/ml but in lower concentrated collagen gels [135, 169]. Thus, the best combination of concentrations should be tested. Furthermore, additional to immunostainings, high-resolution electron microscopy could provide insight into the ultrastructure of the collagen. Decorin affects collagen fibrillogenesis and the resulting ultrastructure of polymerized collagen gels [168, 169]. Thus, further studies should focus on differences in the ultrastructure of the collagen fibrils in gels with and without decorin. To continuously improve the dermal part of FTSE to gain a higher similarity to the dermal ECM, more components of the ECM need to be tested as potential candidates to be added to the collagen hydrogel. Such a systematic approach could improve the mechanical and biological properties of the models and provide a higher similarity to the dermal ECM, but would go beyond the scope of this thesis. Taken together, the results

achieved so far could not show an improvement of the used collagen matrix, therefore decorin was not implemented in further experiments.

With the goal to incorporate endothelial cells in the dermal part of FTSEs, the question of a proper seeding strategy arose. Previous studies showed the feasibility of seeding single endothelial cells in a matrix to generate lumen-like structures [58, 77, 89, 90]. As shown in section 4.1.1, in sprouting assays endothelial cell spheroids are the source for angiogenic sprouts and are used as versatile analysis tool. Apart from that, they are also used as vascularization units in angiogenesis research and regenerative medicine [175]. Thus, it is conceivable, that seeding endothelial cells as spheroids rather than single cells could enhance the formation of connected lumen-like structures. Multi-cellular spheroids have several benefits: The cells are already arranged in spatial proximity and exhibit cell-cell-contacts [175]. This circumstance could facilitate the connection of sprouting endothelial cells to form interconnected capillary structures. Because spheroids are cultured for 1-3 days prior to seeding them in a hydrogel, the endothelial cells are not enzymatically detached from the cell culture surface directly before usage. Thus, surface markers and adhesion proteins are not truncated. This could be beneficial when seeding them in a 3D matrix. Furthermore, the culture of endothelial cells in a spheroid conformation alters their gene expression profile [176]. Due to the size of the spheroid, there is a cell heterogeneity. The cells in the core are exposed to hypoxia due to a diffusion gradient of oxygen. This leads to an increased activity of hypoxia-inducible factor 1 (HIF-1) and subsequently to the production of angiogenic growth factors [175]. Thus, it was hypothesized that endothelial cell spheroids would be superior to single cells to form connected structures in the collagen hydrogel. Therefore, single endothelial cells and preformed endothelial cell spheroids were seeded in a high-density collagen hydrogel and cultured for 3 weeks. The distribution of the cells within the hydrogel was analyzed via immunofluorescence whole-mount staining. Both conditions showed equally distributed cells within the gel (see figure 4.6), suggesting that the spheroids dispersed during culture time and the single cells spread throughout the gel. This explanation is supported by observations of sprouting assays conducted longer than the here described culture time of 24 hours. After 72 hours, single endothelial cells seemed to loose their connection to the elongated sprouts outgrowing the spheroid into the surrounding collagen gel. After 6 days, endothelial cells spread throughout the collagen matrix, partially dissolving the original spheroid. Previous studies showed the development of capillary-like structures from spheroids over a time course of 20 days [158, 177]. In these studies, *ex vivo* generated HUVEC spheroids were employed to form microvessels in a fibronectin matrix *in vivo*.

Lumen-like structures were generated after 20 days of *in vivo* culture in mice, which were covered by ingrowing murine mural cells. Mural cells include pericytes and vascular smooth muscle cells, wrapping around vessels and stabilizing maturing microvessels [30]. As the experiments presented in this thesis were conducted using only endothelial cells, the missing mural cells could be the reason for the non-appearance of any vessel-like structures after 3 weeks of culture. In a previous study, the successful bioengineering of lymphatic capillaries in collagen hydrogel was shown only in the presence of fibroblasts but not without [89]. The authors hypothesize that fibroblasts support the formation of microvessels by their matrix remodelling abilities and by the production of nonsoluble factors. According to these findings, in a next step, the influence of hdF seeded together with hdmEC in the collagen hydrogel was investigated. After 21 days of culture, CD31-positive, lumen-like structures were visible only in the co-culture hydrogels. In the collagen hydrogels with hdmEC only, no lumen-like structures were observable and the hydrogel appeared ruptured. This instability could be attributable to the lack of fibroblasts. Fibroblasts remodel the collagen fibres and thereby alter the mechanical properties of the matrix, rendering it more stable by cross-linking the collagen network. This leads to a higher structural organization of the fibres, helping to connect cells within the matrix [178]. Apart from that "mechanical" help to link and organise the endothelial cells embedded in the collagen hydrogel, fibroblasts play a crucial role in cellular communication [179]. Fibroblasts secrete angiogenic factors such as VEGF, IL-8 and bFGF, thereby strongly influencing the cellular behaviour of endothelial cells [179,180]. In this way, they facilitate endothelial cell migration and capillary formation.

To sum up, angiogenic sprouting of endothelial cell spheroids is feasible in the here used high-density collagen type I hydrogel. The addition of the proteoglycan decorin showed no improvements of the collagen matrix, therefore this approach was discarded. In a first approach, endothelial cell spheroids showed no success in generating lumen-like structures, however the co-culture with fibroblasts seems promising.

5.2 Generation of vascularized full-thickness skin equivalents

Based on the results described above, the incorporation of hdmEC in the FTSE should be established. First, a suitable cell density had to be determined. The established FTSE contains $4 * 10^5$ hdF/ml in the dermal equivalent. This was maintained while the optimal amount of hdmEC had to be elucidated. Starting with $4 * 10^5$ hdmEC/ml, the endothelial cell density was stepwise increased to a maximum endothelial cell density of $6.4 * 10^6$ hdmEC/ml. A significant rise of CD31-positive, lumen-like structures within the dermis

of vFTSEs was revealed for models of $2.6 * 10^6$ hdmEC/ml and more (see figure 4.10 A on page 61). Higher hdmEC densities did not further improve the generation of endothelial structures as the measured values for the models seeded with hdmEC concentrations between $2.6 * 10^6$ and $6.4 * 10^6$ hdmEC/ml showed no significant differences.

Previous vascularization approaches for skin equivalents mainly employed HUVEC [58, 77, 82, 90] or hdmEC [78, 89] seeded in the same density as hdF but in very different cell concentrations varying from $6 * 10^4$ to $2.86 * 10^6$ endothelial cells/ml. Another approach used 10 times more hdmEC ($7.5 * 10^5$ endothelial cells/ml) than hdF to generate vascularized human skin equivalents, albeit in a much lower collagen gel density [173]. Besides these differences, they all used different dermal scaffolds, rendering direct comparisons difficult. In the in this thesis performed experiments, hdmEC seeded in the same density as hdF, which was $4 * 10^5$ endothelial cells/ml, already succeeded in generating small lumen-like endothelial structures within the dermal part of FTSEs. However, these structures were rather sparsely distributed, justifying the need for a higher endothelial cell density. In a recently published systematic approach, the seeding of different endothelial cell densities ($0.5 - 2 * 10^6$ endothelial cells/ml) in varying collagen gel densities (2-6 mg/ml) was tested [181]. The results showed a robust network formation with increasing cell and collagen densities. The authors stated that a match of cell and collagen densities is important for a proper network formation as they could observe that high densities of collagen required high cell numbers to succeed in network formation. This corresponds to the results gained in this thesis: Here, a high-density collagen hydrogel is employed and it could be shown that it is feasible to generate an adequate amount of endothelial structures within the vFTSE by seeding at least $2.6 * 10^6$ hdmEC/ml.

Another factor that had to be considered for the establishment of vFTSEs was the cell culture medium. The medium in which cells are cultured *in vitro* has crucial influence on the survival, growth or differentiation of the cells not only in 2D but also in 3D. In fact, especially in 3D the cellular needs can vary and the requirements for the medium might be different. It provides nutrients, salts, amino acids, vitamins and growth factors and promotes proliferation and maintenance of various kinds of cells. Thus, every cell type needs a distinct medium with its special set of supplements. This is why there is a plethora of different cell culture media on the market, ranging from simple formulations used for many cell lines to sophisticated, very specialised media [182].

The vFTSE consists of three different cell types, which are cultured in 2D in their very own medium. HdF were cultured in the common and for several cell types used DMEM, while hdmEC and heK need a more elaborated medium, specifically for their

needs. The best choice of medium has to be tested individually and might differ from lab to lab. In this work, hdmEC were cultured in VascuLife, optimized for the proliferation of endothelial cells, whereas heK were cultured in EpiLife, prepared for the culture of epidermal cells. Combining these different cell types in one model, challenges the experimenter to choose a medium or an optimal composition of several media to meet the needs of all cells within the model. Furthermore, it has to be considered that the cells influence each other with their metabolism or by secreting growth factors, what can be advantageous or disadvantageous. For the generation and culture of FTSEs, the E10 culture medium has already been established. Next to supplements specially for the differentiation of the heK in 3D culture, it contains 10 % FibroLife to account for the hdF. With the incorporation of hdmEC in the vFTSE, the question arose which medium would be ideal and whether a combination could be advantageous. To address this question, vFTSE with $4 * 10^5$ or $6.4 * 10^6$ hdmEC/ml were cultured in E10 only or in a mixture of E10 and VascuLife. VascuLife only was not an option, since the keratinocytes could not grow in this endothelial cell culture medium. While there was no improvement of the generation of endothelial structures by the addition of VascuLife, it had a negative impact on the epidermis. It seems the heK are more sensitive to a media composition change than the hdmEC and the decisive factor here, which is why the medium should not be changed by addition of VascuLife. In fact, the E10 medium does not seem to be detrimental for the hdmEC. After the generation of the dermal equivalent, the collagen hydrogels with incorporated hdF and hdmEC are cultured for one week in VascuLife. Before seeding the heK, the medium is changed to E10. Looking at the composition of E10, it is noticeable that E10 already contains some components that are also part of VascuLife such as ascorbic acid, IGF, EGF and hydrocortisone hemisuccinate, although in slightly different concentrations. The FibroLife in the E10 medium contributes basic FGF, glutamine and FCS, albeit in small proportions as its share in E10 is 10 %. Thus, E10 already contains some of VascuLife's supplements, what could be the reason for the good performance of the hdmEC in vFTSEs cultured in E10 only. However, the most important supplement of VascuLife is missing in E10: VEGF. VEGF is considered a crucial factor for angiogenesis and maturation and stabilisation of growing microvessels though alone probably not sufficient [70]. In 1992, Brown et al. observed *in vivo* the expression of VEGF mRNA in keratinocytes during wound healing [183]. Ever since, the source of cutaneous VEGF was extensively studied. Today it is known, that VEGF is expressed in heK cultured in 2D as well as in the epidermis *in vivo* and that keratinocytic VEGF is an essential mitogen for hdmEC, especially up-regulated in diseases associated with angiogenesis and inflammation [184–186]. Furthermore, VEGF as well as other

angiogenic factors are secreted by fibroblasts [179, 180]. Thus, it can be assumed that the other cells present in the model secrete VEGF and that the co-culture in the models is beneficial for the generation of endothelial structures within the dermal part.

Another approach to further ameliorate the generation of lumen-like structures in the vFTSEs was to consider the spatial organization of the seeded endothelial cells by seeding them as spheroids in lieu of single cells. As described above, the first approaches of seeding endothelial cell spheroids in a plain collagen gel did not show any promising results. But with the now gained knowledge about the capability of the hdmEC to form lumen-like structures in the dermal part of FTSEs, the angiogenic sprouting seen in the sprouting assays should be applied to the generation of vFTSEs.

In recent years, spheroids have been used to generate microtissues with capillary-like networks. These vascularized constructs can be created in form of co-culture spheroids containing endothelial and tissue-specific cells [175]. In order to generate vascular structures in larger tissues, bioprinting techniques have been described which use spheroids as building blocks to generate elongated vascular segments [187–189]. In other studies, spheroids were successfully employed to generate human microvessels in a mouse model [158, 177] and the authors suggest the exploitation of their technique for tissue engineering purposes. However, in these studies HUVEC in a fibrin/matrigel matrix were employed and transplanted into mice, interacting with the host cells. This depicts different conditions and is not applicable for collagen-based *in vitro* models.

In the here described model, endothelial cells seeded as spheroids in the dermal part of FTSEs were capable to form lumen-like structures as seen in figure 4.12 on page 63. However, there was no difference or advantage compared to the model seeded with the same cell count but in form of single cells. In both conditions, occasionally distributed, small lumen-like, CD31-positive structures were observable.

It is striking, that the endothelial structures present in the models seeded with spheroids are much smaller than the actual spheroids as seen in the sprouting assays. Preformed spheroids exhibit a diameter of 150 to 200 µm, whereas the small, lumen-like structures in the models are rarely larger than 100 µm, mostly below 50 µm. It was hypothesized, that the preformed aggregation of endothelial cells in the spheroid would serve as a focal starting point for angiogenesis. Instead, it seems the spheroids dispersed and did not facilitate the formation of lumen-like structures as they were not larger or more organised than the lumen-like structures in the control models seeded with single cells. This is in line with the already mentioned observation of the supposed dissolution of the spheroids within the collagen matrix during long-term culture.

The sparse occurrence of the structures is not surprising, but corresponds to the previous results regarding the optimal seeding density of hdmEC described in section 4.2.1. According to these findings, a cell density of $2.6 * 10^6$ hdmEC/ml or more is required to achieve large and widespread endothelial structures distributed across the whole model. The cell concentration used here was with $3.4 * 10^5$ hdmEC/ml much lower and predetermined by the count of the spheroids seeded per model. Thus, this approach would need to be pursued with a higher number of spheroids per model to obtain reliable results. However, lab experience teaches one that preparing the spheroid count needed would go beyond any feasible practice in terms of manpower, time and materials. To solve this issue, automated high-throughput production of spheroids would be necessary. Therefore, the successful seeding of single endothelial cells is the preferred strategy here to generate vFTSEs.

In the literature, vascularization approaches are conducted using mostly HUVEC [58,64,65,77,82,136] or hdmEC [89,94,190,191]. Both cell types do have their advantages but also disadvantages.

HdmEC are isolated from the microvessels in human skin. Originating from capillaries, they approximate the physiological features of *in vivo* skin as closely as possible to generate capillaries in skin equivalents *in vitro*. An easily available source for juvenile skin are foreskin biopsies obtained at circumcisions, whereas adult skin can be obtained from plastic surgery. But due to the isolation process, there is the risk of contamination with other cell types, predominantly fibroblasts [192]. Furthermore, as primary cells, they show a high donor-dependent variability.

HUVEC are primary, non-immortalized human endothelial cells, that are isolated from the vein of the post-natal resected umbilical cord. They are often used due to their low cost, simple isolation techniques and good proliferation in cell culture. Moreover, they can be employed up to higher passage numbers than other primary cells [193]. HUVEC are often used as model system to investigate endothelial cell function, angiogenesis and vascular pathologies [193, 194].

Endothelial cells line the lumen of all vessels, ranging from large arteries or veins to small capillaries. These different blood vessel types are associated with specific biochemical and physiological properties *in vivo*. Thus, it is important to consider from which vessel type the endothelial cells originate from for fabricating vasculature *in vitro* [164]. As opposed to hdmEC originating from microvessels, HUVEC are cells of a vein, displaying a much larger vessel. Due to their fetal origin, their behaviour might differ from that of dermal endothelial cells [191]. HUVEC maintain a lot of features of

native endothelial cells including the expression of endothelial cell-specific markers, such as CD31 and von Willebrand factor [194]. However, there are also differences in marker expression between hdmEC and HUVEC, for example the expression of CD36, a cell surface receptor for collagen, among other things [192], or the expression of cell adhesion molecules and major histocompatibility complex (MHC) antigens [195]. Moreover, a potential limitation for the use of HUVEC in clinical applications is their non-dermal and non-autologous nature [191].

For these reasons, for the vascularization approaches in this thesis, hdmEC were employed. However, to ensure compatibility with other studies, the incorporation of HUVEC into the vFTSEs was tested regarding their potential to generate lumen-like structures. Therefore, vFTSEs with either hdmEC or HUVEC were produced and compared histologically. Both endothelial cell types succeeded in formation of lumen-like structures in the vFTSEs. As there were no differences evident regarding the overall architecture of the model or the generation of endothelial structures, it can be assumed that the here presented model with hdmEC is comparable to models generated with HUVEC. Indeed, due to the non-microvascular origin of HUVEC explained above, the usage of primary hdmEC is beneficial for the recapitulating of the dermal vasculature.

The results so far showed that it is feasible to generate lumen-like structures in the dermal part of FTSEs by seeding at least $2.6 * 10^6$ hdmEC/ml as single cells and that the models can be cultured in E10 medium. Now, the established vFTSEs were characterized in more detail: The vFTSEs had a typical morphology as shown by histological HE staining. Immunohistological characterization of the vFTSEs revealed the proper generation of the epidermal layer, shown by staining for CK10 and CK14, and the distribution of vimentin-positive fibroblasts within the dermal layer similar to FTSEs (see figure 4.15 on page 66). Thus, the overall architecture and the natural epidermal differentiation of the FTSEs was not impaired by the incorporation of hdmEC. The marker localisation in the FTSEs and vFTSEs correlates with native skin. CK14 is a marker for basal keratinocytes, while CK10 is an early differentiation keratinocyte marker, thus staining the suprabasal layers of the epidermis [25].

The basement membrane at the dermo-epidermal junction is a factor to determine the quality of the skin equivalent. It anchors the epidermis on the dermis and controls the exchange of substances and cells between the two skin layers [20,22,26]. Furthermore, it is an important barrier for the vertical growth of malignant melanoma in early progression states [196]. Type IV collagen is a main component of basement membranes [20, 23, 26] and its presence at the dermo-epidermal junction is indicative for the quality of the model

as this is considered a mature skin hallmark [67]. For the characterization of vFTSEs, collagen type IV was visualized as integral component of the basement membrane. The immunohistological staining proved the presence of collagen type IV at the dermo-epidermal junction of FTSEs as well as of vFTSEs. In the literature, it is known that keratinocytes produce components of the basement membrane and that also fibroblasts in the dermis contribute to the formation of the basement membrane [26, 197].

The successful generation of lumen-like structures in the vFTSEs is visualized impressively by staining for CD31 and collagen type IV within the dermal layer. CD31, also known as platelet endothelial cell adhesion molecule (PECAM-1), contributes to intercellular junctions and is likely involved in angiogenesis [198]. Present at the surface of endothelial cells, it is a commonly used endothelial cell marker. Staining for CD31 showed numerous lumen-like structures within the dermal part of vFTSEs, proving them to be of endothelial origin. Apart from epithelia, basement membranes also underly endothelia to delineate them from the surrounding tissue [26, 199]. Immunostaining of the main component of the basement membrane, collagen type IV, showed a proper deposition of the vascular basement membrane around the endothelial, lumen-like structures, which is a prerequisite for capillary formation and the stabilization of the growing microvessel [88]. Previous studies described the synthesis of collagen type IV by hdmEC cultured in 2D [200] as well as surrounding generated microvessels [58, 82, 173].

Taken together, the characterization of vFTSEs showed comparable results to other published skin equivalents [58, 82, 94, 174]. Thus, it is possible to integrate hdmEC in the FTSE to form lumen-like structures and the establishment of a vFTSE was successful. However, as capillaries *in vivo* are not only comprised of endothelial cells but also contain pericytes, further improvement of the model should include the incorporation of pericytes for better functionality and resemblance of the situation *in vivo*.

5.3 A bioreactor system to generate perfused collagen hydrogels

Vascularization approaches based on the self-assembly capacity of endothelial cells to form random capillary-like networks have one pitfall in common: They cannot be perfused because they are not accessible to be connected to an external pump. Consequently, supplying nutrients or sampling media via a medium flow is not possible, limiting the application scenarios for such models. Perfusion is not only crucial for the development of larger tissue equivalents, but also for the proper maturation of the endothelial cells and for certain scientific questions such as transendothelial perfusion studies or basic research on diseases comprising the vasculature. Thus, to enable perfusion, on the one

hand, a tubular structure is needed that can be connected to a fluidic system, and, on the other hand, the exterior requirements providing medium flow have to be met. Therefore, many approaches employing bioreactor technology showed the applicability of perfusion bioreactors in the culture of vascularized tissue engineered constructs [81, 93, 95, 201]. With these dynamic culture conditions, a steady medium flow is guaranteed ensuring nutrient supply and limiting periodic fluctuations in medium composition [97, 100]. *In vivo*, the vascular system is organized hierarchically with larger vessels branching into smaller ones and finally into the capillary network, that is responsible for the exchange of gas, nutrients and waste products, supplying the surrounding tissue [23,27,28]. Mimicking this anatomical organization, the approach pursued here aimed at the generation of a central perfused channel, resembling a larger vessel, that can be used to supply a capillary-like network in the surrounding collagen hydrogel.

In vivo, every blood vessel is lined by a monolayer of endothelial cells. In the same way, vessels produced *in vitro* should be composed and are therefore seeded with endothelial cells. Accordingly, in the approach presented here, the generated channel should be seeded with hdmEC. Therefore, first of all, it was assessed if the hdmEC could adhere properly to the used collagen matrix and if endothelial cell adhesion could be improved by coating the surface. Many protocols recommend the coating of the cell culture surface for endothelial cell culture. Fibronectin and collagen type IV are often used as they are components of the ECM and play a central role in cell adhesion [137, 139, 202]. The adhesion of endothelial cells to different concentrations of fibronectin, collagen types I and IV and the combination of fibronectin and collagen type IV in coated wells was tested using two different methods. It could be shown, that most of the cells adhered to the surface 2 hours after seeding. Both methods showed slight differences between the adhesion on the different coatings. However, none of them were statistically significant.

As already the coating with collagen type I showed good adhesion rates, it was assumed that a further coating of the collagen type I surface of the channel with other proteins is not necessary. With these findings, the next step was concentrated on the generation of the central channel.

For the generation of a perfused collagen hydrogel, different setups were tested. The basic principle for all was, that collagen is cast in a mold containing a central wire or cannula as placeholder. Once the collagen hydrogel was solidified, the wire or cannula was removed, leaving a central channel through the hydrogel for perfusion. To rebuild a central vessel, the channel was seeded with endothelial cells.

The first attempts aimed at small and simple setups, enabling cost- and time-efficient

easily parallelizable approaches. With both, the silicone tube setup and the channel chamber setup, channels could be generated within the collagen hydrogel that were seeded with endothelial cells. However, both setups failed in dynamic flow culture. Moreover, a major disadvantage was that the collagen could not be plastically compressed for better mechanical properties.

This requirement was finally met with the design of two bioreactors by Miriam Komma and Marius Gensler as part of her Master's thesis [140]. Both bioreactors served the same purpose, but differed in their complexity with the bioreactor design C being a further development of the bioreactor design B. They provided a sophisticated setup for the plastic compression and subsequent dynamic culture of a perfused collagen hydrogel. With both bioreactors it was possible to create a central channel within the collagen hydrogel. The viability of the cells within the compressed collagen hydrogel was verified via MTT assay, confirming the metabolic activity of the cells. This is in line with the results of Krziminski et al., showing that cell survival rates of hdF after compression in a similar setup is about 76 % [93]. Hence, dynamic culture with medium perfusion through the channel was sufficient to supply the cells incorporated within the collagen hydrogel. The channels were successfully seeded with hdmEC and cultured under dynamic flow conditions for up to 14 days, both in low-density and high-density collagen gels.

Hence, the possibility to generate a perfused collagen hydrogel with an endothelial cell-lined central channel in a custom-made 3D printed bioreactor could be shown. Both bioreactor designs were suitable and had individual advantages and disadvantages. The bioreactor design B was easier in handling as less parts had to be prepared. Another advantage is that less parts reduce the risk of leakage problems. The lid made of silicone was easy to attach and its translucency allowed to some extent the inspection of the hydrogel surface without opening the system. But also this lid was prone to leakage. In this case, the lid of the bioreactor design C was advantageous because it was fixed with screws. The interior of the bioreactor design C was more complex with barb-like structures at the in- and outlet of the bioreactor to prevent detaching of the channel from them and thereby disrupting the medium flow.

Comparing the endothelial cell lining of the channel lumen with the two previous setups, it is noticeable that far more hdmEC adhered to the surface and formed a monolayer within the channel. There are several possible explanations for this fact: First, it is possible, that more hdmEC initially adhered to the collagen surface because due to the dynamic flow culture the collagen hydrogel was soaked with VascuLife. Second, it is known that fluidic shear stress is beneficial for the endothelial cells [30, 92]. Third, the hydrogels were cultured in the bioreactors for 2 weeks, whereas in the previous setups,

they were cultured statically over night. Thus the endothelial cells had far more time to proliferate. Immunofluorescence staining revealed the lining of the channel lumen with hdmEC and vimentin-positive cells surrounding the channel, comparable to the blood vessels in human skin (see figure 4.26 on page 80). Furthermore, small, lumen-like endothelial structures could be seen within the collagen hydrogel nearby the channel. Since hdmEC were only seeded in the channel but not within the hydrogel, they must have migrated from the channel surface in the surrounding collagen matrix.

The diameter of the generated channel is predetermined by the cannula used as negative mold to form the channel. The here used 18G cannula has an outer diameter of 1.3 mm. Due to the forces acting on the collagen, the created channel has a diameter of approximately 500 to 800 µm. With this size, the central channel has the dimensions of small arteries [23]. That is actually the case for most perfusable vascularized tissue constructs [81, 82, 93, 103]. To recreate that kind of vessels, the incorporation of other cell types, especially smooth muscle cells, is necessary and is consequently a next step. Also one should think about another endothelial cell source. Different kinds of endothelial cells originating from different vessel types are associated with varying physiological properties, which should be considered when rebuilding vasculature *in vitro* [164]. HdmEC are of microvascular origin, therefore predestined for the generation of capillary-like structures. For a larger vessel in contrast the usage of for example HUVEC could be a good choice as they originate from a vein. It is also conceivable to decrease the size of the channel a bit. The usage of the peripheral venous catheters and the connection of the bioreactor to the fluidic system via their Luer-connectors easily allows a change of the cannula size in the setup. However, it would have to be tested if a smaller channel could be perfused and would not collapse during culture time. The approach from Mori et al. for example used nylon wires for creating slightly smaller channels, that were also seeded only with endothelial cells [81]. Furthermore, they could show that the perfusion of the generated channel is necessary for its stability and that it will collapse without perfusion.

For the overall goal of a vascularized, perfused skin equivalent, this channel should serve as a central vessel to provide medium flow to the capillary network. It was hypothesized that capillary-like structures within the collagen hydrogel would connect to the central vessel to generate a perfusable network. The capillary-like structures should be generated just as for the vFTSE. Recently, Salameh et al. pursued a similar approach and could show that HUVEC seeded in the dermal part of FTSEs formed branching networks that anastomosed to sprouts coming from endothelial cells lining perfused preformed channels [82]. However, these findings do not translate directly to the here used approach

as they used a low-density collagen hydrogel and HUVEC seeded in a plane between two layers of collagen hydrogel but not permeating the whole hydrogel.

To combine those two techniques of generating lumen-like structures and the endothelialized central channel, perfused collagen hydrogels were generated using both bioreactor designs. Additionally, hdmEC were seeded within the collagen hydrogel together with the hdF. In a first approach, hdmEC were present within the collagen hydrogel as confirmed by immunohistological staining for CD31. Lumen-like structures, however, were not observable. This is likely due to the non-optimal endothelial cell concentration within the collagen hydrogel. In section 4.2.1 it was shown, that at least $2.6 * 10^6$ hdmEC/ml are needed for the formation of widely distributed lumen-like structures. The here used cell concentration was $5.7 * 10^5$ hdmEC/ml and thus too low. Furthermore, the missing epidermis as well as the size and the concentration of the collagen gel were different compared to the vFTSEs and could have an impact. Another problem that arose here was that for the hydrogel cultured in bioreactor design B, no channel could be found on images of histological cross-sections. Explanations for that could be that the channel closed during culture time due to insufficient perfusion and the remodelling of the collagen by the fibroblasts [81] or that the channel was present in the hydrogel but not within the section plane of the specimen as it was sometimes difficult to find out the correct orientation of the fixated hydrogel. For the hydrogel cultured in bioreactor design C the channel was present but lacked an endothelial cell lining. Instead, endothelial cells lined small cavities nearby the channel. These are drawbacks that occurred for some of the hydrogels and cannot be avoided when working with biological material. This approach was only carried out once like this, thus more repetitions would contribute to clarify the findings.

To further improve the resemblance between the perfused collagen hydrogels and the vFTSEs, a higher collagen concentration and a higher cell density were needed. Therefore, the bioreactor design B and the compression stamp were modified to enable a higher compression factor. Using this it was possible to produce a perfused central channel within a collagen hydrogel with a collagen concentration of 36 mg/ml and final cell concentrations of $4 * 10^5$ hdF/ml and $6.5 * 10^6$ hdmEC/ml, corresponding to the characteristics of the vFTSE. After two weeks of culture, cross-sections of the hydrogel revealed the presence of a thin channel within a highly layered collagen hydrogel. Unfortunately, no cells were observable lining the channel surface. As mentioned before, this was a problem in the culture of the perfused collagen hydrogels that occurred in some instances and could not be solved yet. By further pursuing this approach it will be possible to generate and culture a perfused high-density collagen hydrogel with similar characteristics to the vFTSEs.

5.4 Melanoma models as application for vascularized skin equivalents

The vascularization approaches for FTSEs were pursued with the aim to provide a test system for melanoma progression. Although early diagnosis due to better screenings and the awareness of risk factors help to improve patient survival rates, malignant melanoma remains an aggressive and dangerous skin malignancy with rising incidence over the last decades [203]. With the increasing incidence, also the death rate from malignant melanoma is rising, emphasizing the need for the development of new treatment strategies [106]. For this purpose, manifold approaches were made to study melanomagenesis and performing drug efficacy testing [117, 204]. Many investigations were done using 2D cell culture of melanoma cells. While this is a fast and simple approach to assess the proliferative, migrational or metabolic properties of melanoma cells or to perform toxicity testings, these cells grow under completely artificial conditions, not representative for the situation *in vivo* and limiting their predictiveness [5]. The microenvironment, in which cells and tissues occur in an organism, fundamentally influences cellular development and fate [116]. Instead of growing in a monolayer of homogenous cells in 2D cell culture with perfectly balanced culture conditions, cells in their natural environment grow in a 3D context in a complex interplay of different cell types and exogeneous determinants with constantly changing environmental conditions. The tumor microenvironment has been shown to significantly influence tumor behavior [116, 205, 206]. In skin for example, keratinocytes regulate the proliferation and localization of melanocytes. During the transformation of melanocytes to melanoma cells, tumor cells escape the tight control of keratinocytes by downregulating adhesion molecules [207, 208]. Furthermore, in 2D cell culture vertical invasion processes, being a crucial feature of melanoma, cannot be investigated [123]. Therefore, studies intending to assess melanomagenesis, metastasis or anti-melanoma therapies, cannot rely on 2D cell culture. Here, animal models are meant to provide a physiologically more relevant context. Primarily murine models have been established in various versions to display tumor growth, development and dissemination *in vivo* [209]. Often used are human xenografts, in which human melanoma cell lines are subcutaneously engrafted into immunocompromised mice, syngeneic transplantation models, allowing for the interaction of melanoma cells with the immune system, and genetically engineered mouse models [5]. These models provide a natural environment for the tumor to grow in, are easy to manipulate and widely available [209]. However, for the reasons stated above, alternatives to animal experimentation are desirable. In recent years, many approaches were made to mimic melanoma *in vitro*, ranging from tumor

spheroids [210] to the incorporation of melanoma cells into epidermal and full-thickness skin models [50, 63, 64, 121–123].

In this thesis, melanoma cells were successfully incorporated into the FTSE. By seeding the melanoma cells together with the keratinocytes on top of the dermal equivalent, melanoma nests could be generated in the epidermis, recapitulating the tumor microenvironment. Here, the ratio of melanoma cells to keratinocytes is important and has to be tested individually for every melanoma cell line and for different model types. Too few melanoma cells would not lead to tumor growth, whereas too much melanoma cells would overgrow the keratinocytes and impede epidermal differentiation. The successful formation of melanoma nests within the epidermis was observed in HE-stainings of cross-sections of the models. Integration of melanoma cell line SK-MEL-28 resulted in large tumor nests at the dermo-epidermal junction, observable as unorganized and ruptured tissue protruding into the dermis (see figure 4.30 on page 85). Apart from tumor sites, the epidermis was well stratified, showing that the formation of the epidermis in the models was not impaired by the melanoma cells. The tumor nests were further identified by immunofluorescence stainings for melanoma markers HMB-45, Melan-A and S100 (see figure 4.32 on page 87), matching results of previous studies [50, 63, 64, 122, 123].

Co-staining for collagen type IV and S100 (see figure 4.33 on page 88) showed that the melanoma cells were not able to break down the basement membrane and invade into the dermis, although some authors describe SK-MEL-28 as a metastatic cell line [50, 122, 123]. In the literature, SK-MEL-28 melanoma cells have already been incorporated in several 3D skin equivalents. The results regarding the invasiveness of SK-MEL-28 into the dermal part are however controversial: In a study from Gibot et al., SK-MEL-28 cells showed no invasion into the dermis [64]. The same applies for the melanoma model of Bourland et al. [63]. Other studies showed the spreading of SK-MEL-28 cells into the dermis with partial disruption of the basement membrane [50, 122, 123]. However, these events did not occur until after a longer culture time of 4 weeks [50, 122] or with the employment of much more melanoma cells in relation to keratinocytes [123]. Thus, it could be that the invasiveness would benefit from a prolonged culture time or a higher share of melanoma cells in the model. Furthermore, all these studies used a different kind of dermal matrix. As the substrate stiffness is critical for tumor cell behaviour [210], this fact renders comparisons difficult. The here used collagen hydrogels had a far higher collagen concentration compared to other models. Due to the plastic compression, the collagen network is denser and mechanically more stable [174]. This could have an impact on the behaviour and the migratory properties of the melanoma cells.

The melanoma cell line SK-MEL-28 was chosen because it is widely used in melanoma

research and well characterized. It was isolated from the cutaneous melanoma from an 51 years old male patient by Takahashi and colleagues in 1976 [211, 212]. SK-MEL-28 cells harbour a $BRAF^{V600E}$ mutation along with other genetic alterations [142].

The BLM cell line is a subline of the human amelanotic melanoma cell line BRO and was isolated from a lung metastasis produced after subcutaneous inoculation of nude mice with BRO cells [213, 214]. BLM cells are characterized by a NRAS mutation [143, 144] and an aggressive and invasive nature as it develops spontaneous metastases after subcutaneous inoculation of nude mice very frequently [213, 214].

Many observations claim that melanoma cells *in vitro* exhibit tumor stage-specific behavior. That means cells isolated from a melanoma in the radial-growth phase will grow within the epidermis but not break through the basement membrane. Whereas cells isolated from a more progressed state such as the vertical-growth phase or even a distant metastasis, will exhibit a more aggressive behaviour and invade the dermis [5, 118, 215]. Based on this and with the knowledge of the aggressive behaviour of BLM cells *in vivo*, it was hypothesized that they could invade the dermis in the mFTSE, which is why they were chosen for these experiments.

Although BLM inoculated into mice caused tumor growth *in vivo* [213, 214, 216], integration of melanoma cell line BLM did not result in the formation of observable tumor nests. It was not possible to stain the melanoma cells with the used melanoma markers. Here, other markers could be tested, for example EGFR, showing elevated expression in BLM cells [217, 218]. However, it is not clear, if a suitable marker would help to visualize BLM cells within the models, because they were not even visible in the HE staining, in contrast to the SK-MEL-28 cells, which formed recognisable tumour nests.

To succeed in generating mFTSEs with BLM, another seeding strategy might be appropriate. In the here generated models, melanoma cells were seeded together with keratinocytes. In other approaches, melanoma cells are seeded on top of the dermal equivalent prior to seeding the keratinocytes [39, 50, 122]. This might help the melanoma cells to adhere and form first small aggregations. Others used preformed melanoma spheroids instead of single cells to form melanomas in skin models [39, 63]. Furthermore, the optimal seeding density for melanoma cells should be reevaluated. For the experiments performed in this thesis, SK-MEL-28 were seeded in a ratio of melanoma cells to keratinocytes of 1:50. This resulted in visible tumor nests within a well stratified epidermis. As no tumor formation was seen for BLM, in these models the ratio was changed to 1:25. Even with this increased seeding ratio, tumor formation was not successful. In *in vivo* studies, $0.5 - 2 * 10^6$ BLM cells in 100 µl are injected at one spot [213, 214, 216], whereas in the *in vitro* models, 20 000 BLM cells are suspended

together with the keratinocytes in 250 µl and seeded onto the model. It might be that for BLM cells, a higher number of cells is required to form tumor nests. In other studies, ratios of up to 1:5 were used [118, 215]. This could be a conceivable approach for the integration of BLM into the mFTSEs.

Taken together, a melanoma skin model could be established based on the FTSEs by incorporating the melanoma cell line SK-MEL-28. The here presented tumor model is suitable to recapitulate the melanoma microenvironment as tumor nests formed within a stratified epidermis. By providing the basement membrane and the dermis, the model holds the potential to mimic invasive behaviour of the tumor and to be used as a test system for melanoma development and anti-melanoma therapies. However, the model has its limitations: As it cannot be cultured for long term, the observation and testing period is limited. Thus, most studies testing anti-melanoma therapies start with an early treatment thereby rather interfering with tumor nest formation than inducing regression of existing tumor nests [219]. Furthermore, in part due to the limited culture time, the tumor nests are rather small, resembling an early melanoma progression state, while most melanomas are bigger, when they are diagnosed [220]. Potential anti-melanoma therapeutics that could be tested using melanoma skin models such as for example vemurafenib are rather used to treat metastases than the primary tumor as primary tumors are mostly excised [221]. Thus, the here presented model could be more valuable to study melanoma development than as a test system for anti-melanoma therapies. Nevertheless, the model has several advantages: The usage of primary derived skin cells bears the possibility for personalised medicine. With the incorporation of patient-derived tumor cells instead of a melanoma cell line, patient-specific models could be generated to help to study the characteristics of the individual tumor. The generation of the model is relatively straightforward, albeit experience and special equipment is necessary. Due to the reduced complexity, it is easier to attribute certain phenomena to one cause [118]. Thus, the established model can contribute to study melanoma development and concomitantly to the reduction of animal experimentation.

However, the establishment of the melanoma FTSE was just an interim goal. A crucial step in melanomagenesis is metastasis formation. Having gained the capability to cross the basement membrane and invade into the dermis, the tumor cells are able to enter the blood and lymph vascular system and spread to distant body sites. Once this step is reached, survival chances of patients massively decrease [222]. Thus, studies unravelling the underlying mechanisms that lead to metastasis formation tremendously contribute to a deeper understanding of this disease and will help to develop anti-melanoma therapies.

But the tumor not only needs the vascular system for dissemination, but also for its own nutrition. As the growing tumor requires oxygen and nutrients to survive, it will initiate the formation of new blood vessels, a process known as tumor angiogenesis [73, 124, 223]. Observing that rapidly growing tumors are heavily vascularized while dormant ones are not, Judah Folkman postulated already in 1971 the concept that initiation of angiogenesis was required for tumor progression [124]. Based on these findings, further studies revealed the influence of pro-angiogenic factors such as VEGF on the induction of tumor angiogenesis, leading to anti-angiogenic therapy approaches [73]. The normal vasculature is quiescent, and endothelial cells are not proliferative. This state is balanced by an interplay of pro- and antiangiogenic factors. A dominating pro-angiogenic signaling however leads to the induction of blood vessel formation, a process that in tumors is called the "angiogenic switch" [224]. By secreting pro-angiogenic factors or stimulating associated cells to do so, the tumor attracts endothelial cells to proliferate and form new vessels [124, 125]. The emerging tumor vasculature is abnormal, chaotic and leaky, but will supply the tumor cells and is required for progression [30].

Thus, there are manifold interactions between tumor cells and the vasculature, leading to tumor progression and metastasis. Consequently, to study melanomagenesis and exploit possible treatments, model systems without vasculature do not reflect the tumor environment properly. To date, most studies regarding tumor angiogenesis and melanoma metastasis have been performed in animals. They provide a whole vascular system, but for the above mentioned reasons, alternative models are needed. The approaches to form capillary networks in 3D skin equivalents in recent years provide a valuable tool that, in combination with melanoma models, could help elucidate determinants responsible for melanoma progression and deepen the understanding of cellular crosstalk between the melanoma and the vasculature.

For this reason, the established vFTSE should be used as a test system for melanoma development and progression. Therefore, the vFTSE had to be combined with the mFTSE. The resulting vmFTSE was thus composed of four cell types: HdF and hdmEC incorporated into the high-density collagen hydrogel built up the dermal part of the model, while heK and melanoma cells were seeded on top to generate the epidermis with tumor nests. Immunohistological stainings revealed the successful formation of the skin equivalents with large tumor nests at the dermo-epidermal junction and lumen-like structures of endothelial origin within the dermis (see figure 4.34 on page 90). Neither was the formation of the lumen-like structures impeded by the incorporation of the melanoma cells, nor impaired the addition of hdmEC the growth of tumor nests at the dermo-epidermal junction. Immunofluorescence double-stainings for the endothelial

marker CD31 and the melanoma marker S100 visualized the spatial proximity of tumor nests protruding in the dermis and the endothelial structures, but no co-localisation was found. It was hypothesized that the capillary-like structures would enhance the dermal invasion of the tumor cells or that the tumor cells would attract the endothelial cells, but this was not observed. Gibot et al., who developed a microvascularized melanoma skin model based on the cell sheet technique, also observed neither infiltration of the dermis by SK-MEL-28 cells, nor influence on the vascular network by the tumor cells [64]. They claim this is due to the derivation of SK-MEL-28 from a primary tumor site, since the incorporation of metastatic melanoma cell lines led to different results. Bourland et al. established a 3D melanoma model with blood and lymphatic capillaries [63]. Although they showed the growth of tumor clusters into the dermis in spatial proximity to lymphatic capillaries, there was no co-localisation.

As the origin of the SK-MEL-28 cell line from a primary tumor or a skin metastasis and therefore their belonging to a cancer stage is not clear in the literature, the potential of the model to study endothelial-melanoma cell interactions should be tested with other metastatic melanoma cell lines, such as Malme 3 M or RPMI 7951.

In an attempt to bring the melanoma cells in more spatial proximity to the endothelial structures to facilitate interaction, the seeding strategy for the melanoma cells was changed. Melanoma spheroids were seeded directly in the dermis together with hdF and hdmEC, instead of seeding them as single cells in the epidermis. With spheroids, a critical tumor mass can be generated in a short time and the tumor spheroids accurately recapitulate the heterogeneity of tumor cell growth and drug resistance seen *in vivo* [118]. Vörsmann et al. incorporated melanoma spheroids in the dermal part of their skin equivalents for the advantages of including a defined number and size of tumor nests in the model, reflecting a more complex intratumoral diversity, and having tumor nests immediately incorporated into the model to start treatment experiments [39]. Interestingly, they showed that the melanoma spheroids in the dermis resemble melanoma metastases.

Immunofluorescence stainings of the vmFTSE revealed the presence of large tumor spheroids within the dermis. Compared to the tumor nests formed at the dermo-epidermal junction from single cells, they were much bigger. Staining for CD31 revealed the formation of lumen-like structures by the hdmEC in the dermis. They were observable in proximity to the tumor spheroids but also dispersed throughout the dermis, so that a directed formation or attraction could not be verified. Moreover, some of the tumor spheroids seemed to be loosely packed and breaking apart, also some rather small tumor nests were observable. That could indicate that the preformed spheroids, which were

preformed in 4 days, are not mature enough and that they could benefit from a longer culture time prior to seeding them into the model. In the study from Vörsmann et al. melanoma spheroids were cultured for 15 days prior to usage, resulting in larger and more compact tumor spheroids within the dermis [39]. Furthermore, they claim that the large size of their spheroids is needed to establish different sub-populations within the spheroid due to a lack of nutrient and oxygen in the core. However, such a hypoxic core could trigger the secretion of pro-angiogenic factors, attracting capillaries to grow in, just like in a tumor *in vivo*. That leads to the conclusion, that the here introduced model could be further refined by prolonging the culture time for preforming the melanoma spheroids to gain larger and more stable tumors.

6 Conclusion and Outlook

In this thesis, three independent models were established: The vFTSE, the mFTSE and the perfused collagen hydrogel. While they could be applied on their own, for instance in basic research to study the interactions of the different cell types in the model, they are intended to be combined to expand their application possibilities. By combination of the vFTSE with the technique of the perfused collagen hydrogel, perfusable vascularized skin models will be generated. Besides improving the nutrient supply and the resemblance of *in vivo* skin due to the implementation of further anatomical structures, these models enable the evaluation of skin permeability as well as the evaluation of systemic delivery of compounds [82]. The easily accessible perfusion system allows the analysis of substances diffused into the medium flow or, in contrast, the application of systemically delivered substances via the medium flow. Here, the additional barrier of endothelial cells lining the vessels contribute to a better simulation of the situation *in vivo*, being advantageous compared to conventional penetration studies.

For the overall goal to create a test system for melanoma metastasis, this model is intended to be combined with the in this thesis established melanoma skin equivalent. The anatomical structures present in the model like the dermis, the dermo-epidermal junction and the vasculature, provide a suitable microenvironment for the melanoma to develop and depict the prerequisites for metastasis formation. These vascularized melanoma skin models will enable the investigation of melanoma progression as well as the interactions between melanoma cells and vasculature. As test system for anti-melanoma therapies, it can contribute to the reduction of animal experiments and enhance the success rate of preclinical testing in oncology. Furthermore, due to the usage of primary derived cells, personalized melanoma models to assess treatment strategies are conceivable [39]. But this is also where the limitations of the model become apparent. The culture time of the skin equivalents is limited and so far, the generated tumors depict a more early phase of melanoma development, wherefore using these models it is more likely to be a study of development than a therapy testing.

Besides malignant melanoma, there are many other diseases interacting with or influenced by the vasculature. Hence, the vFTSE could be used to mimic diseased states of

skin disorders such as wounds, inflammation, psoriasis, or other cancers. Furthermore, vascularization is a prerequisite to add further anatomical structures to the skin equivalent like hair follicles or sweat glands. *In vivo*, skin appendages are supplied via a rich network of vessels [22], that is missing in most of the available skin equivalents. A perfused vascularized skin equivalent could help to ensure the supply of the appendages and to better mimic the anatomy of human skin. But also the implementation of other cell types such as macrophages or T cells is conceivable [58]. The combination of a perfusable model with immune cells could be useful in infection research or auto-immune reactions.

The results gained in this thesis regarding the generation of a perfused collagen hydrogel can be applied to other emerging techniques generating hollow structures for perfusion, such as bioprinting. With this technique it would be possible to fabricate vessels with a smaller diameter as well as with more complex geometries [95].

All in all, with the established models further steps towards the overall goal of a perfusable, vascularized melanoma skin model have been taken. Although this ambitious aim could not be achieved within the time of this thesis, the established models show a great potential for further development. They are applicable in different research fields with almost unlimited adaption possibilities in diverse directions. Combined with modern and sophisticated techniques such as bioprinting or iPSC technology, they will contribute to improve tissue engineered skin for better preclinical test systems and to reduce animal experimentation.

Bibliography

[1] Langer, R. and Vacanti, J. P. "Tissue Engineering". In: *Science*, 260 (1993), pp. 920–926.

[2] Fuchs, J. R., Nasseri, B. A., and Vacanti, J. P. "Tissue engineering: A 21st century solution to surgical reconstruction". In: *Annals of Thoracic Surgery*, 72 (2001), pp. 577–591.

[3] O'Brien, F. J. "Biomaterials & scaffolds for tissue engineering". In: *Materials Today*, 14 (2011), pp. 88–95.

[4] Schimek, K., Hsu, H. H., Boehme, M., Kornet, J. J., Marx, U., Lauster, R., Pörtner, R., and Lindner, G. "Bioengineering of a full-thickness skin equivalent in a 96-well insert format for substance permeation studies and organ-on-a-chip applications". In: *Bioengineering*, 5 (2018), pp. 1–19.

[5] Beaumont, K., Mohana-Kumaran, N., and Haass, N. "Modeling Melanoma In Vitro and In Vivo". In: *Healthcare*, 2 (2013), pp. 27–46.

[6] Kirk, R. G. "Recovering The Principles of Humane Experimental Technique: The 3Rs and the Human Essence of Animal Research". In: *Science Technology and Human Values*, 43 (2018), pp. 622–648.

[7] Russell, W. M. S. and Burch, R. L. *The Principles Of Humane Experimental Technique*. Methuen, London (1959).

[8] Europäische Kommission. "RICHTLINIE 2010/63/EU DES EUROPÄISCHEN PARLAMENTS UND DES RATES vom 22. September 2010 zum Schutz der für wissenschaftliche Zwecke verwendeten Tiere" (2010).

[9] Mansbridge, J. "Tissue-engineered skin products". In: *Principles of Tissue Engineering*, pp. 1483–1497. INC (2020).

[10] Vig, K., Chaudhari, A., Tripathi, S., Dixit, S., Sahu, R., Pillai, S., Dennis, V. A., and Singh, S. R. "Advances in skin regeneration using tissue engineering". In: *International Journal of Molecular Sciences*, 18 (2017).

[11] Kaur, A., Midha, S., Giri, S., and Mohanty, S. "Functional skin grafts: Where biomaterials meet stem cells". In: *Stem Cells International*, 2019 (2019).

[12] Nyame, T. T., Chiang, H. A., and Orgill, D. P. "Clinical applications of skin substitutes". In: *Surgical Clinics of North America*, 94 (2014), pp. 839–850.

[13] Kamel, R. A., Ong, J. F., Eriksson, E., Junker, J. P. E., and Caterson, E. J. "Tissue engineering of skin". In: *Journal of the American College of Surgeons*, 217 (2013), pp. 533–555.

[14] Daugherty, S. and Spear, M. "Skin and skin substitutes-an overview". In: *Plastic Surgical Nursing*, 35 (2015), pp. 92–97.

[15] Groeber, F., Holeiter, M., Hampel, M., Hinderer, S., and Schenke-Layland, K. "Skin tissue engineering - In vivo and in vitro applications". In: *Advanced Drug Delivery Reviews*, 63 (2011), pp. 352–366.

[16] Wever, B. D. E., Petersohn, D., and Mewes, K. R. "Overview of human three-dimensional (3D) skin models used for dermal toxicity assessment". In: *HPC Today*, 8 (2013), pp. 18–23.

[17] Abaci, H. E., Guo, Z., Doucet, Y., Jacków, J., and Christiano, A. "Next generation human skin constructs as advanced tools for drug development". In: *Experimental Biology and Medicine*, 242 (2017), pp. 1657–1668.

[18] Abd, E., Yousef, S. A., Pastore, M. N., Telaprolu, K., Mohammed, Y. H., Namjoshi, S., Grice, J. E., and Roberts, M. S. "Skin models for the testing of transdermal drugs". In: *Clinical Pharmacology: Advances and Applications*, 8 (2016), pp. 163–176.

[19] Mancini, A. J. "Skin". In: *Pediatrics*, 113 (2004).

[20] Kolarsick, P. A. J. B., Kolarsick, M. A. M. A.-C., and Goodwin, C. A.-B. F. "Anatomy and Physiology of the Skin". In: *Journal of the Dermatology Nurses' Association*, 3 (2011), pp. 203–213.

[21] Brandner, J. M., Zorn-Kruppa, M., Yoshida, T., Moll, I., Beck, L. A., and De Benedetto, A. "Epidermal tight junctions in health and disease". In: *Tissue Barriers*, 3 (2015).

[22] Kanitakis, J. "Anatomy, histology and immunohistochemistry of normal human skin". In: *European Journal of Dermatology*, 12 (2002), pp. 390–399.

[23] Schiebler, T. H. and Korf, H.-W. *Anatomie*. Steinkopff Verlag, 10. auflag edition (2007).

[24] Haake, A., Scott, G. A., and Holbrook, K. A. "Structure and function of the skin: overview of the epidermis and dermis". In: Freinkel, R. K. and Woodley, D. T., editors, *The Biology of the Skin*, chapter 2, pp. 19–45. The Parthenon Publishing Group Inc. (2001).

[25] Elaine Fuchs. "Epidermal Differentiation: The Bare Essentials The Program of Terminal Differentiation". In: *The Journal of Cell Biology*, 111 (1990), pp. 2807–2814.

[26] Breitkreutz, D., Mirancea, N., and Nischt, R. "Basement membranes in skin: Unique matrix structures with diverse functions?" In: *Histochemistry and Cell Biology*, 132 (2009), pp. 1–10.

[27] Fleischer, S., Tavakol, D. N., and Vunjak-Novakovic, G. "From Arteries to Capillaries: Approaches to Engineering Human Vasculature". In: *Advanced Functional Materials*, 30 (2020).

[28] Datta, P., Ayan, B., and Ozbolat, I. T. "Bioprinting for vascular and vascularized tissue biofabrication". In: *Acta Biomaterialia*, 51 (2017), pp. 1–20.

[29] Pugsley, M. and Tabrizchi, R. "The vascular system An overview of structure and function M.K." In: *Journal of Pharmacological and Toxicological Methods*, 44 (2000), pp. 333–340.

[30] Jain, R. K. "Molecular regulation of vessel maturation". In: *Nature Medicine*, 9 (2003), pp. 685–693.

[31] Braverman, I. M. "Ultrastructure and organization of the cutaneous microvasculature in normal and pathologic states". In: *Journal of Investigative Dermatology*, 93 (1989), pp. S2–S9.

[32] Singh, S. and Swerlick, R. A. "Structure and function of the cutaneous vasculature". In: Freinkel, R. K. and Woodley, D., editors, *The Biology of the Skin*, chapter 10, pp. 177–190. The Parthenon Publishing Group Inc. (2001).

[33] Braverman, I. M. "The cutaneous microcirculation". In: *Journal of Investigative Dermatology Symposium Proceedings*, 5 (2000), pp. 3–9.

[34] Gledhill, K., Guo, Z., Umegaki-Arao, N., Higgins, C. A., Itoh, M., and Christiano, A. M. "Melanin transfer in human 3D skin equivalents generated exclusively from induced pluripotent stem cells". In: *PLoS ONE*, 10 (2015), pp. 1–16.

[35] Schmid, F., Groeber-Becker, F., Schwab, S., Thude, S., Goebeler, M., Walles, H., and Hansmann, J. "A standardized method based on pigmented epidermal models evaluates sensitivity against UV-irradiation". In: *Altex*, 35 (2018), pp. 390–396.

[36] Facy, V., Flouret, V., Régnier, M., and Schmidt, R. "Reactivity of Langerhans cells in human reconstructed epidermis to known allergens and UV radiation". In: *Toxicology in Vitro*, 19 (2005), pp. 787–795.

[37] Desmet, E., Ramadhas, A., Lambert, J., and Van Gele, M. "In vitro psoriasis models with focus on reconstructed skin models as promising tools in psoriasis research". In: *Experimental Biology and Medicine*, 242 (2017), pp. 1158–1169.

[38] Jean, J., Lapointe, M., Soucy, J., and Pouliot, R. "Development of an in vitro psoriatic skin model by tissue engineering". In: *Journal of Dermatological Science*, 53 (2009), pp. 19–25.

[39] Vörsmann, H., Groeber, F., Walles, H., Busch, S., Beissert, S., Walczak, H., and Kulms, D. "Development of a human three-dimensional organotypic skin-melanoma spheroid model for in vitro drug testing." In: *Cell Death and Disease*, 4 (2013), p. e719.

[40] Kiesewetter, L., Littau, L., Walles, H., Boccaccini, A. R., and Groeber-Becker, F. "Reepithelialization in focus: Non-invasive monitoring of epidermal wound healing in vitro". In: *Biosensors and Bioelectronics*, 142 (2019), pp. 1–9.

[41] Draize, J. H., Woddard, G., and Calvery, H. O. "Methods for the study of irritation and toxicity of substances applied topically to the skin and mucous membranes". In: *Journal of Pharmacology and Experimental Therapeutics*, 82 (1944), pp. 377–390.

[42] The European Parliament and the Council of the European Union. "Regulation (EC) No 1223/2009 of the European Parliament and of the Council of 30 November 2009 on cosmetic products." (2009).

[43] Welss, T., Basketter, D. A., and Schröder, K. R. "In vitro skin irritation: Facts and future. State of the art review of mechanisms and models". In: *Toxicology in Vitro*, 18 (2004), pp. 231–243.

[44] OECD. *Test No. 431: In vitro skin corrosion: reconstructed human epidermis (RHE) test method*. OECD Guidelines for the Testing of Chemicals, Section 4. OECD (2019).

[45] OECD. *Test No. 439: In Vitro Skin Irritation: Reconstructed Human Epidermis Test Method*. OECD Guidelines for the Testing of Chemicals, Section 4. OECD (2020).

[46] Ng, K. W. and Hutmacher, D. W. "Reduced contraction of skin equivalent engineered using cell sheets cultured in 3D matrices". In: *Biomaterials*, 27 (2006), pp. 4591–4598.

[47] Lee, J. J., Lee, S. G., Park, J. C., Yang, Y. I., and Kim, J. K. "Investigation on biodegradable PLGA scaffold with various pore size structure for skin tissue engineering". In: *Current Applied Physics*, 7 (2007), pp. 37–40.

[48] Kee Woei Ng, Hutmacher, D. W., Schantz, J. T., Chin Seng Ng, Too, H. P., Thiam Chye Lim, Toan Thang Phan, and Swee Hin Teoh. "Evaluation of ultra-thin poly(ϵ-caprolactone) films for tissue-engineered skin". In: *Tissue Engineering*, 7 (2001), pp. 441–455.

[49] Bokhari, M., Carnachan, R. J., Cameron, N. R., and Przyborski, S. A. "Novel cell culture device enabling three-dimensional cell growth and improved cell function". In: *Biochemical and Biophysical Research Communications*, 354 (2007), pp. 1095–1100.

[50] Hill, D. S., Robinson, N. D., Caley, M. P., Chen, M., O'Toole, E. A., Armstrong, J. L., Przyborski, S., and Lovat, P. E. "A novel fully humanized 3D skin equivalent to model early melanoma invasion". In: *Molecular Cancer Therapeutics*, 14 (2015), pp. 2665–2673.

[51] Reuter, C., Walles, H., and Groeber, F. "Preparation of a Three-Dimensional Full Thickness Skin Equivalent". In: Koledova, Z., editor, *3D Cell Culture, Methods and Protocols*, pp. 191–198. Humana Press, New York, NY, New York (2017).

[52] Lotz, C., Schmid, F. F., Oechsle, E., Monaghan, M. G., Walles, H., and Groeber-Becker, F. "Cross-linked Collagen Hydrogel Matrix Resisting Contraction to Facilitate Full-Thickness Skin Equivalents". In: *ACS Applied Materials and Interfaces*, 9 (2017), pp. 20417–20425.

[53] Rossi, A., Appelt-Menzel, A., Kurdyn, S., Walles, H., and Groeber, F. "Generation of a Three-dimensional Full Thickness Skin Equivalent and Automated Wounding". In: *Journal of Visualized Experiments*, (2015).

[54] Sun, L. P., Wang, S., Zhang, Z. W., Wang, X. Y., and Zhang, Q. Q. "Biological evaluation of collagen-chitosan scaffolds for dermis tissue engineering". In: *Biomedical Materials*, 4 (2009), pp. 0–6.

[55] Savoji, H., Godau, B., Hassani, M. S., and Akbari, M. "Skin Tissue Substitutes and Biomaterial Risk Assessment and Testing". In: *Frontiers in Bioengineering and Biotechnology*, 6 (2018), pp. 1–18.

[56] Liu, H., Mao, J., Yao, K., Yang, G., Cui, L., and Cao, Y. "A study on a chitosan-gelatin-hyaluronic acid scaffold as artificial skin in vitro and its tissue engineering applications". In: *Journal of Biomaterials Science, Polymer Edition*, 15 (2004), pp. 25–40.

[57] Mazlyzam, A. L., Aminuddin, B. S., Fuzina, N. H., Norhayati, M. M., Fauziah, O., Isa, M. R., Saim, L., and Ruszymah, B. H. "Reconstruction of living bilayer human skin equivalent utilizing human fibrin as a scaffold". In: *Burns*, 33 (2007), pp. 355–363.

[58] Kreimendahl, F., Marquardt, Y., Apel, C., Bartneck, M., Zwadlo-Klarwasser, G., Hepp, J., Jockenhoevel, S., and Baron, J. M. "Macrophages significantly enhance wound healing in a vascularized skin model". In: *Journal of Biomedical Materials Research - Part A*, 107 (2019), pp. 1340–1350.

[59] Zhang, Z. and Michniak-Kohn, B. B. "Tissue engineered human skin equivalents". In: *Pharmaceutics*, 4 (2012), pp. 26–41.

[60] Medalie, D. A., Eming, S. A., Tompkins, R. G., Yarmush, M. L., Krueger, G. G., and Morgan, J. R. "Evaluation of human skin reconstituted from composite grafts of cultured keratinocytes and human acellular dermis transplanted to athymic mice". In: *Journal of Investigative Dermatology*, 107 (1996), pp. 121–127.

[61] Zhong, S. P., Zhang, Y. Z., and Lim, C. T. "Tissue scaffolds for skin wound healing and dermal reconstruction". In: *Wiley Interdisciplinary Reviews: Nanomedicine and Nanobiotechnology*, 2 (2010), pp. 510–525.

[62] Lindberg, K. and Badylak, S. F. "Porcine small intestinal submucosa (SIS): A bioscaffold supporting in vitro primary human epidermal cell differentiation and synthesis of basement membrane proteins". In: *Burns*, 27 (2001), pp. 254–266.

[63] Bourland, J., Fradette, J., and Auger, F. A. "Tissue-engineered 3D melanoma model with blood and lymphatic capillaries for drug development". In: *Scientific Reports*, 8 (2018), pp. 1–13.

[64] Gibot, L., Galbraith, T., Huot, J., and Auger, F. "Development of a tridimensional microvascularized human skin substitute to study melanoma biology." In: *Clinical and experimental metastasis*, (2012).

[65] Matsusaki, M., Fujimoto, K., Shirakata, Y., Hirakawa, S., Hashimoto, K., and Akashi, M. "Development of full-thickness human skin equivalents with blood and lymph-like capillary networks by cell coating technology". In: *Journal of Biomedical Materials Research Part A*, 103 (2015), pp. 3386–3396.

[66] Kim, B. S., Lee, J.-S., Gao, G., Cho, D.-W., Cubo, N., Garcia, M., and Del Cañizo, J. F. "Direct 3D cell-printing of human skin with functional transwell system 3D bioprinting of functional human skin: production and in vivo analysis". In: *Biofabrication*, 9 (2017), pp. 1–12.

[67] Perez-Valle, A., Amo, C. D., and Andia, I. "Overview of current advances in extrusion bioprinting for skin applications". In: *International Journal of Molecular Sciences*, 21 (2020), pp. 1–28.

[68] Cubo, N., Garcia, M., Del Cañizo, J. F., Velasco, D., and Jorcano, J. L. "3D bioprinting of functional human skin: Production and in vivo analysis". In: *Biofabrication*, 9 (2017).

[69] Rouwkema, J. and Khademhosseini, A. "Vascularization and Angiogenesis in Tissue Engineering: Beyond Creating Static Networks." In: *Trends in biotechnology*, 34 (2016), pp. 733–45.

[70] Jain, R. K., Au, P., Tam, J., Duda, D. G., and Fukumura, D. "Engineering vascularized tissue". In: *Nature Biotechnology*, 23 (2005), pp. 821–823.

[71] Patel-Hett, S. and D'Amore, P. A. "Signal transduction in vasculogenesis and developmental angiogenesis". In: *International Journal of Developmental Biology*, 55 (2011), pp. 353–369.

[72] Balaji, S., King, A., Crombleholme, T. M., and Keswani, S. G. "The Role of Endothelial Progenitor Cells in Postnatal Vasculogenesis: Implications for Therapeutic Neovascularization and Wound Healing". In: *Advances in Wound Care*, 2 (2013), pp. 283–295.

[73] Lugano, R., Ramachandran, M., and Dimberg, A. "Tumor angiogenesis: causes, consequences, challenges and opportunities". In: *Cellular and Molecular Life Sciences*, 77 (2020), pp. 1745–1770.

[74] Yetkin-Arik, B., Vogels, I. M., Neyazi, N., van Duinen, V., Houtkooper, R. H., van Noorden, C. J., Klaassen, I., and Schlingemann, R. O. "Endothelial tip cells in vitro are less glycolytic and have a more flexible response to metabolic stress than non-tip cells". In: *Scientific Reports*, 9 (2019), pp. 1–17.

[75] Patan, S., Alvarez, M. J., Schittny, J. C., and Burri, P. H. "Intussusceptive Micro vascular Growth: A Common Alternative to Capillary Sprouting". In: *Archives of Histology and Cytology*, 55 (1992), pp. 65–75.

[76] Simons, M. "Angiogenesis: Where do we stand now?" In: *Circulation*, 111 (2005), pp. 1556–1566.

[77] Tremblay, P. L., Hudon, V., Berthod, F., Germain, L., and Auger, F. A. "Inosculation of tissue-engineered capillaries with the host's vasculature in a reconstructed skin transplanted on mice". In: *American Journal of Transplantation*, 5 (2005), pp. 1002–1010.

[78] Sahota, P. S., Burn, J. L., Heaton, M., Freedlander, E., Suvarna, S. K., Brown, N. J., and Mac Neil, S. "Development of a reconstructed human skin model for angiogenesis". In: *Wound Repair and Regeneration*, 11 (2003), pp. 275–284.

[79] Young, D. M., Greulich, M. S., and Weier, H. G. "Species-Specific In Situ Hybridization With Fluorochrome-Labeled DNA Probes to Study Vascularization of Human Skin Grafts on Athymic Mice". In: *The Journal of Burn Care and Rehabilitation*, 17 (1996), pp. 305–310.

[80] Laschke, M. W. and Menger, M. D. "Prevascularization in tissue engineering: Current concepts and future directions". In: *Biotechnology Advances*, 34 (2016), pp. 112–121.

[81] Mori, N., Morimoto, Y., and Takeuchi, S. "Skin integrated with perfusable vascular channels on a chip". In: *Biomaterials*, 116 (2017), pp. 48–56.

[82] Salameh, S., Tissot, N., Cache, K., Lima, J., Suzuki, I., Marinho, P. A., Rielland, M., Soeur, J., Takeuchi, S., Germain, S., and Breton, L. "A perfusable vascularized full-thickness skin model for potential topical and systemic applications". In: *Biofabrication*, 13 (2021).

[83] Shoda, T., Futamura, K., Orihara, K., Emi-Sugie, M., Saito, H., Matsumoto, K., and Matsuda, A. "Recent advances in understanding the roles of vascular endothelial cells in allergic inflammation". In: *Allergology International*, 65 (2016), pp. 21–29.

[84] Sanchez, B., Li, L., Dulong, J., Aimond, G., Lamartine, J., Liu, G., and Sigaudo-Roussel, D. "Impact of human dermal microvascular endothelial cells on primary dermal fibroblasts in response to inflammatory stress". In: *Frontiers in Cell and Developmental Biology*, 7 (2019), pp. 1–10.

[85] Liu, X., Michael, S., Bharti, K., Ferrer, M., and Song, M. J. "A Biofabricated Vascularized Skin Model of Atopic Dermatitis for Preclinical Studies". In: *Biofabrication*, 12 (2020).

[86] Unger, R. E., Sartoris, A., Peters, K., Motta, A., Migliaresi, C., Kunkel, M., Bulnheim, U., Rychly, J., and Kirkpatrick, C. J. "Tissue-like self-assembly in cocultures of endothelial cells and osteoblasts and the formation of microcapillary-like structures on three-dimensional porous biomaterials". In: *Biomaterials*, 28 (2007), pp. 3965–3976.

[87] Lesman, A., Koffler, J., Atlas, R., Blinder, Y. J., Kam, Z., and Levenberg, S. "Engineering vessel-like networks within multicellular fibrin-based constructs". In: *Biomaterials*, 32 (2011), pp. 7856–7869.

[88] Montaño, I., Schiestl, C., Schneider, J., Pontiggia, L., Luginbühl, J., Biedermann, T., Böttcher-Haberzeth, S., Braziulis, E., Meuli, M., and Reichmann, E. "Formation of human capillaries in vitro: the engineering of prevascularized matrices." In: *Tissue engineering. Part A*, 16 (2010), pp. 269–282.

[89] Marino, D., Luginbuhl, J., Scola, S., Meuli, M., and Reichmann, E. "Bioengineering Dermo-Epidermal Skin Grafts with Blood and Lymphatic Capillaries". In: *Science Translational Medicine*, 6 (2014), pp. 221ra14–221ra14.

[90] Black, A. F., Berthod, F., L'Heureux, N., Germain, L., and Auger, F. A. "In vitro reconstruction of a human capillary-like network in a tissue-engineered skin equivalent". In: *The FASEB Journal*, 12 (1998), pp. 1331–1340.

[91] Kim, J. J., Hou, L., and Huang, N. F. "Vascularization of three-dimensional engineered tissues for regenerative medicine applications." In: *Acta biomaterialia*, 41 (2016), pp. 17–26.

[92] Li, Y. S. J., Haga, J. H., and Chien, S. "Molecular basis of the effects of shear stress on vascular endothelial cells". In: *Journal of Biomechanics*, 38 (2005), pp. 1949–1971.

[93] Krziminski, C., Kammann, S., Hansmann, J., Edenhofer, F., Dandekar, G., Walles, H., and Leistner, M. "Development of a bioreactor system for pre-endothelialized cardiac patch generation with enhanced viscoelastic properties by combined collagen I compression and stromal cell culture". In: *Journal of Tissue Engineering and Regenerative Medicine*, (2020), pp. 1–14.

[94] Groeber, F., Engelhardt, L., Lange, J., Kurdyn, S., Schmid, F. F., Rücker, C., Mielke, S., Walles, H., and Hansmann, J. "A first vascularized skin equivalent as an alternative to animal experimentation". In: *Altex*, 33 (2016), pp. 415–422.

[95] Miller, J. S., Stevens, K. R., Yang, M. T., Baker, B. M., Nguyen, D.-H. T., Cohen, D. M., Toro, E., Chen, A. A., Galie, P. A., Yu, X., Chaturvedi, R., Bhatia, S. N., and Chen, C. S. "Rapid casting of patterned vascular networks for perfusable engineered three-dimensional tissues". In: *Nature Materials*, 11 (2012), pp. 768–774.

[96] Selden, C. and Fuller, B. "Role of bioreactor technology in tissue engineering for clinical use and therapeutic target design". In: *Bioengineering*, 5 (2018), pp. 1–10.

[97] Hansmann, J., Groeber, F., Kahlig, A., Kleinhans, C., and Walles, H. "Bioreactors in tissue engineering-principles, applications and commercial constraints". In: *Biotechnology Journal*, 8 (2013), pp. 298–307.

[98] Zhao, J., Griffin, M., Cai, J., Li, S., Bulter, P. E., and Kalaskar, D. M. "Bioreactors for tissue engineering: An update". In: *Biochemical Engineering Journal*, 109 (2016), pp. 268–281.

[99] Gensler, M., Leikeim, A., Möllmann, M., Komma, M., Heid, S., Müller, C., Boccaccini, A. R., Salehi, S., Groeber-Becker, F., and Hansmann, J. "3D printing of bioreactors in tissue engineering : A generalised approach". In: *PLoS ONE*, 15 (2020), pp. 1–25.

[100] Groeber, F., Kahlig, A., Loff, S., Walles, H., and Hansmann, J. "A bioreactor system for interfacial culture and physiological perfusion of vascularized tissue equivalents". In: *Biotechnology Journal*, 8 (2013), pp. 308–316.

[101] Mori, N., Morimoto, Y., and Takeuchi, S. "Perfusable and stretchable 3D culture system for skin-equivalent". In: *Biofabrication*, 11 (2019).

[102] Abaci, H. E., Guo, Z., Coffman, A., Gillette, B., Lee, W. H., Sia, S. K., and Christiano, A. M. "Human Skin Constructs with Spatially Controlled Vasculature Using Primary and iPSC-Derived Endothelial Cells". In: *Advanced Healthcare Materials*, 5 (2016), pp. 1800–1807.

[103] Kim, B. S., Gao, G., Kim, J. Y., and Cho, D. W. "3D Cell Printing of Perfusable Vascularized Human Skin Equivalent Composed of Epidermis, Dermis, and Hypodermis for Better Structural Recapitulation of Native Skin". In: *Advanced Healthcare Materials*, 8 (2019), pp. 1–11.

[104] Garbe, C., Peris, K., Hauschild, A., Saiag, P., Middleton, M., Spatz, A., Grob, J. J., Malvehy, J., Newton-Bishop, J., Stratigos, A., Pehamberger, H., and Eggermont, A. "Diagnosis and treatment of melanoma: European consensus-based interdisciplinary guideline". In: *European Journal of Cancer*, 46 (2010), pp. 270–283.

[105] Miller, A. J. and Mihm, M. C. "Melanoma". In: *New England Journal of Medicine*, 355 (2006), pp. 51–65.

[106] Kaatsch, D. P., Spix, D. C., Katalinic, P. D. A., Hentschel, D. S., Luttmann, D. S., Waldeyer-Sauerland, D. M., Waldmann, D. A., Christ, M., Folkerts, D. J., Hansmann, D. J., Klein, D. S., Kranzhöfer, D. K., Kunz, D. B., Manegold, D. K., Penzkofer, D. A., Treml, D. K., Vollmer, D. G., Weg-Remers, D. S., Barnes, D. B., Buttmann-Schweiger, N., Dahm, D. S., Fiebig, J., Franke, M., Gurung-Schönfeld, I., Haberland, D. J., Kraywinkel, D. K., and Wienecke, D. A. "Krebs in Deutschland für 2015/2016". Technical report, Robert Koch-Institut, Berlin (2019).

[107] Winder, M. and Virós, A. "Mechanisms of Drug Resistance in Melanoma". In: Mandalà, M. and Romano, E., editors, *Mechanisms of Drug Resistance in Cancer Therapy. Handbook of Experimental Pharmacology, vol 249*, pp. 251–263. Springer International Publishing (2017).

[108] Damsky, W. E., Rosenbaum, L. E., and Bosenberg, M. "Decoding melanoma metastasis". In: *Cancers*, 3 (2011), pp. 126–163.

[109] Schadendorf, D., Fisher, D. E., Garbe, C., Gershenwald, J. E., Grob, J. J., Halpern, A., Herlyn, M., Marchetti, M. A., McArthur, G., Ribas, A., Roesch, A., and Hauschild, A. "Melanoma". In: *Nature Reviews Disease Primers*, 1 (2015), pp. 1–20.

[110] Clark, W. H., Elder, D. E., Guerry, D., Epstein, M. N., Greene, M. H., and Van Horn, M. "A study of tumor progression: The precursor lesions of superficial spreading and nodular melanoma". In: *Human Pathology*, 15 (1984), pp. 1147–1165.

[111] Dhillon, A. S., Hagan, S., Rath, O., and Kolch, W. "MAP kinase signalling pathways in cancer". In: *Oncogene*, 26 (2007), pp. 3279–3290.

[112] Hayward, N. K., Wilmott, J. S., Waddell, N., Johansson, P. A., Field, M. A., Nones, K., Patch, A. M., Kakavand, H., Alexandrov, L. B., Burke, H., Jakrot, V., Kazakoff, S., Holmes, O., Leonard, C., Sabarinathan, R., Mularoni, L., Wood, S., Xu, Q., Waddell, N., Tembe, V., Pupo, G. M., De Paoli-Iseppi, R., Vilain, R. E., Shang, P., Lau, L. M., Dagg, R. A., Schramm, S. J., Pritchard, A., Dutton-Regester, K., Newell, F., Fitzgerald, A., Shang, C. A., Grimmond, S. M., Pickett, H. A., Yang, J. Y., Stretch, J. R., Behren, A., Kefford, R. F., Hersey, P., Long, G. V., Cebon, J., Shackleton, M., Spillane, A. J., Saw, R. P., López-Bigas, N., Pearson, J. V., Thompson, J. F., Scolyer, R. A., and Mann, G. J. "Whole-genome landscapes of major melanoma subtypes". In: *Nature*, 545 (2017), pp. 175–180.

[113] Heppt, M. V., Siepmann, T., Engel, J., Schubert-Fritschle, G., Eckel, R., Mirlach, L., Kirchner, T., Jung, A., Gesierich, A., Ruzicka, T., Flaig, M. J., and Berking, C. "Prognostic significance of BRAF and NRAS mutations in melanoma: a German study from routine care". In: *BMC cancer*, 17 (2017), p. 536.

[114] Goel, V. K., Lazar, A. J., Warneke, C. L., Redston, M. S., and Haluska, F. G. "Examination of mutations in BRAF, NRAS, and PTEN in primary cutaneous melanoma". In: *Journal of Investigative Dermatology*, 126 (2006), pp. 154–160.

[115] Colombino, M., Capone, M., Lissia, A., Cossu, A., Rubino, C., De Giorgi, V., Massi, D., Fonsatti, E., Staibano, S., Nappi, O., Pagani, E., Casula, M., Manca, A., Sini, M. C., Franco, R., Botti, G., Caracò, C., Mozzillo, N., Ascierto, P. A., and Palmieri, G. "BRAF/NRAS mutation frequencies among primary tumors and metastases in patients with melanoma". In: *Journal of Clinical Oncology*, 30 (2012), pp. 2522–2529.

[116] Pampaloni, F., Reynaud, E. G., and Stelzer, E. H. K. "The third dimension bridges the gap between cell culture and live tissue". In: *Nature Reviews Molecular Cell Biology*, 8 (2007), pp. 839–845.

[117] Marconi, A., Quadri, M., Saltari, A., and Pincelli, C. "Progress in melanoma modelling in vitro". In: *Experimental Dermatology*, 27 (2018), pp. 578–586.

[118] Smalley, K. S., Lioni, M., Noma, K., Haass, N. K., and Herlyn, M. "In vitro three-dimensional tumor microenvironment models for anticancer drug discovery". In: *Expert Opinion on Drug Discovery*, 3 (2008), pp. 1–10.

[119] Sutherland, R. M., McCredie, J. A., and Inch, W. R. "Growth of multicell spheroids in tissue culture as a model of nodular carcinomas." In: *Journal of the National Cancer Institute*, 46 (1971), pp. 113–120.

[120] Zanoni, M., Piccinini, F., Arienti, C., Zamagni, A., Santi, S., Polico, R., Bevilacqua, A., and Tesei, A. "3D tumor spheroid models for in vitro therapeutic screening: A systematic approach to enhance the biological relevance of data obtained". In: *Scientific Reports*, 6 (2016), pp. 1–11.

[121] Commandeur, S., Sparks, S. J., Chan, H. L., Gao, L., Out, J. J., Gruis, N. A., Van Doorn, R., and El Ghalbzouri, A. "In-vitro melanoma models: Invasive growth is determined by dermal matrix and basement membrane". In: *Melanoma Research*, 24 (2014), pp. 305–314.

[122] Michielon, E., López González, M., Burm, J. L. A., Waaijman, T., Jordanova, E. S., de Gruijl, T. D., and Gibbs, S. "Micro-environmental cross-talk in an organotypic human melanoma-in-skin model directs M2-like monocyte differentiation via IL-10". In: *Cancer Immunology, Immunotherapy*, (2020).

[123] Haridas, P., McGovern, J. A., McElwain, S. D., and Simpson, M. J. "Quantitative comparison of the spreading and invasion of radial growth phase and metastatic melanoma cells in a three-dimensional human skin equivalent model". In: *PeerJ*, 2017 (2017).

[124] Folkman, J. "Tumor Angiogenesis: Therapeutic Implications". In: *New England Journal of Medicine*, 285 (1971), pp. 1182–1186.

[125] Nishida, N., Yano, H., Nishida, T., Kamura, T., and Kojiro, M. "Angiogenesis in cancer". In: *Vascular Health and Risk Management*, 2 (2006), pp. 213–219.

[126] Brown, J. M. "Vasculogenesis: A crucial player in the resistance of solid tumours to radiotherapy". In: *British Journal of Radiology*, 87 (2014).

[127] Bergers, G. and Benjamin, L. E. "Tumorigenesis and the angiogenic switch". In: *Nature Reviews Cancer*, 3 (2003), pp. 401–410.

[128] Jones, K. H. and Senft, J. A. "An improved method to determine cell viability by simultaneous staining with fluorescein diacetate-propidium iodide". In: *Journal of Histochemistry and Cytochemistry*, 33 (1985), pp. 77–79.

[129] Ross, D. D., Joneckis, C. C., Ordonez, J. V., Sisk, A. M., Wu, R. K., Hamburger, A. W., and Nora, R. E. "Estimation of Cell Survival by Flow Cytometric Quantification of Fluorescein Diacetate/Propidium Iodide Viable Cell Number 1". In: *Cancer Research*, 49 (1989), pp. 3776–3782.

[130] Korff, T. and Augustin, H. G. "Tensional forces in fibrillar extracellular matrices control directional capillary sprouting". In: *Journal of Cell Science*, 112 (1999), pp. 3249–3258.

[131] Heiss, M., Hellström, M., Kalén, M., May, T., Weber, H., Hecker, M., Augustin, H. G., and Korff, T. "Endothelial cell spheroids as a versatile tool to study angiogenesis in vitro". In: *FASEB Journal*, 29 (2015), pp. 3076–3084.

[132] Tuz Zahra, F., Choleva, E., Sanaullah Sajib, M., Papadimitriou, E., and M. Mikelis, C. "In vitro spheroid sprouting assay of angiogenesis". In: *Methods in Molecular Biology*, 1952 (2019), pp. 211–218.

[133] Tetzlaff, F. and Fischer, A. "Human Endothelial Cell Spheroid-based Sprouting Angiogenesis Assay in Collagen". In: *Bio-Protocol*, 8 (2018), pp. 1–10.

[134] Mikesh, L. M., Aramadhaka, L. R., Moskaluk, C., Zigrino, P., Mauch, C., and Fox, J. W. "Proteomic anatomy of human skin". In: *Journal of Proteomics*, 84 (2013), pp. 190–200.

[135] Reed, C. C. and Iozzo, R. V. "The role of decorin in collagen fibrillogenesis and skin homeostasis". In: *Glycoconjugate Journal*, 19 (2003), pp. 249–255.

[136] Miyazaki, H., Tsunoi, Y., Akagi, T., Sato, S., Akashi, M., and Saitoh, D. "A novel strategy to engineer pre-vascularized 3-dimensional skin substitutes to achieve efficient, functional engraftment". In: *Scientific Reports*, 9 (2019), pp. 1–3.

[137] Ruoslahti, E. "Fibronectin and Its Receptors". In: *Annu. Rev. Biochem.*, (1988), pp. 375–413.

[138] Humphries, M. J., Obara, M., Olden, K., and Yamada, K. M. "Role of fibronectin in adhesion, migration, and metastasis". In: *Cancer Investigation*, 7 (1989), pp. 373–393.

[139] Paulson, M. "Basement membrane proteins: Structure, assembly, and cellular interactions". In: *Critical Reviews in Biochemistry and Molecular Biology*, 27 (1992), pp. 93–127.

[140] Komma, M. *Erprobung zweier 3D-Druckverfahren bezüglich ihrer Eignung für medizinische Anwendungen*. Master thesis, Julius-Maximilians-Universität Würzburg (2019).

[141] Kliche, J. *Investigation of Tumour-Host Interactions in an Organotypic Model of the Malignant Melanoma*. Master thesis, Julius-Maximilians-Universität Würzburg (2019).

[142] Daveri, E., Valacchi, G., Romagnoli, R., Maellaro, E., and Maioli, E. "Antiproliferative Effect of Rottlerin on Sk-Mel-28 Melanoma Cells". In: *Evidence-based Complementary and Alternative Medicine*, 2015 (2015).

[143] Vogel, C. J., Smit, M. A., Maddalo, G., Possik, P. A., Sparidans, R. W., van der Burg, S. H., Verdegaal, E. M., Heck, A. J., Samatar, A. A., Beijnen, J. H., Altelaar, A. F., and Peeper, D. S. "Cooperative induction of apoptosis in NRAS mutant melanoma by inhibition of MEK and ROCK". In: *Pigment Cell and Melanoma Research*, 28 (2015), pp. 307–317.

[144] Müller, J., Krijgsman, O., Tsoi, J., Robert, L., Hugo, W., Song, C., Kong, X., Possik, P. A., Cornelissen-Steijger, P. D., Foppen, M. H., Kemper, K., Goding, C. R., McDermott, U., Blank, C., Haanen, J., Graeber, T. G., Ribas, A., Lo, R. S., and Peeper, D. S. "Low MITF/AXL ratio predicts early resistance to multiple targeted drugs in melanoma". In: *Nature Communications*, 5 (2014).

[145] Kobayashi, J., Fujimoto, D., Murakami, M., Hirono, Y., and Goi, T. "A report of amelanotic malignant melanoma of the esophagus diagnosed appropriately with novel markers: A case report". In: *Oncology Letters*, 15 (2018), pp. 9087–9092.

[146] Hartung, T. "Food for thought ... on animal tests". In: *Altex*, (2008), pp. 3–9.

[147] Mak, I. W., Evaniew, N., and Ghert, M. "Lost in translation: Animal models and clinical trials in cancer treatment". In: *American Journal of Translational Research*, 6 (2014), pp. 114–118.

[148] Akhtar, A. "The Flaws and Human Harms of Animal Experimentation". In: *Cambridge Quarterly of Healthcare Ethics*, 24 (2015), pp. 407–419.

[149] Hickman, D., Johnson, J., Vemulapalli, T., Crisler, J., and Shepherd, R. "Commonly Used Animal Models". In: *Principles of Animal Research for Graduate and Undergraduate Students.*, chapter 7, pp. 117–175 (2017).

[150] The Senate Commission on Animal Protection and Experimentation. "Animal Experimentation in Biomedical Research". Technical report, Deutsche Forschungsgemeinschaft, Bonn (2016).

[151] Bailey, J. and Balls, M. "Recent efforts to elucidate the scientific validity of animal-based drug tests by the pharmaceutical industry, pro-testing lobby groups, and animal welfare organisations". In: *BMC Medical Ethics*, 20 (2019), pp. 1–7.

[152] Bracken, M. B. "Why animal studies are often poor predictors of human reactions to exposure". In: *Journal of the Royal Society of Medicine*, 102 (2009), pp. 120–122.

[153] Bhogal, N. and Combes, R. "TGN1412: Time to Change the Paradigm for the Testing of New Pharmaceuticals". In: *Alternatives to Laboratory Animals*, (2006), pp. 225–239.

[154] McKenzie, R., Fried, M. W., Sallie, R., Conjeevaram, H., Bisceglie, A. M. D., Yoon Park, R., Barbara Savarese, R., Kleiner, D., Tsokos, M., Luciano, C., Pruett, T., Stotka, J. L., Straus, S. E., and Hoofnagle, J. H. "Hepatic Failure and Lactic Acidosis Due to Fialuridine (FIAU), an Investigational Nucleoside Analogue for Chronic Hepatitis B". In: *New England Journal of Medicine*, 333 (1995), pp. 1099–1105.

[155] Chaikin, P. "The Bial 10-2474 Phase 1 Study—A Drug Development Perspective and Recommendations for Future First-in-Human Trials". In: *Journal of Clinical Pharmacology*, 57 (2017), pp. 690–703.

[156] Perel, P., Roberts, I., Sena, E., Wheble, P., Briscoe, C., Sandercock, P., Macleod, M., Mignini, L. E., Jayaram, P., and Khan, K. S. "Comparison of treatment effects between animal experiments and clinical trials: Systematic review". In: *British Medical Journal*, 334 (2007), pp. 197–200.

[157] Bhattacharjee, Y. "Pharma firms push for sharing of cancer trial data". In: *Science*, 338 (2012), p. 29.

[158] Alajati, A., Laib, A. M., Weber, H., Boos, A. M., Bartol, A., Ikenberg, K., Korff, T., Zentgraf, H., Obodozie, C., Graeser, R., Christian, S., Finkenzeller, G., Stark, G. B., Héroult, M., and Augustin, H. G. "Spheroid-based engineering of a human vasculature in mice". In: *Nature Methods*, 5 (2008), pp. 439–445.

[159] Katt, M. E., Placone, A. L., Wong, A. D., Xu, Z. S., and Searson, P. C. "In vitro tumor models: Advantages, disadvantages, variables, and selecting the right platform". In: *Frontiers in Bioengineering and Biotechnology*, 4 (2016).

[160] Shamloo, A. and Heilshorn, S. C. "Matrix density mediates polarization and lumen formation of endothelial sprouts in VEGF gradients". In: *Lab on a Chip*, 10 (2010), pp. 3061–3068.

[161] Mason, B. N., Starchenko, A., Williams, R. M., Bonassar, L. J., and Reinhart-King, C. A. "Tuning three-dimensional collagen matrix stiffness independently of collagen concentration modulates endothelial cell behavior". In: *Acta Biomaterialia*, 9 (2013), pp. 4635–4644.

[162] Vernon, R. B. and Sage, E. H. "A novel, quantitative model for study of endothelial cell migration and sprout formation within three-dimensional collagen matrices". In: *Microvascular Research*, 57 (1999), pp. 118–133.

[163] Edgar, L. T., Underwood, C. J., Guilkey, J. E., Hoying, J. B., and Weiss, J. A. "Extracellular matrix density regulates the rate of neovessel growth and branching in sprouting angiogenesis". In: *PLoS ONE*, 9 (2014), pp. 1–10.

[164] Kim, J. J., Hou, L., and Huang, N. F. "Vascularization of three-dimensional engineered tissues for regenerative medicine applications". In: *Acta Biomaterialia*, 41 (2016), pp. 17–26.

[165] Wolf, K., Alexander, S., Schacht, V., Coussens, L. M., von Andrian, U. H., van Rheenen, J., Deryugina, E., and Friedl, P. "Collagen-based cell migration models in vitro and in vivo". In: *Seminars in Cell and Developmental Biology*, 20 (2009), pp. 931–941.

[166] Li, Y., Liu, Y., Xia, W., Lei, D., Voorhees, J. J., and Fisher, G. J. "Age-dependent alterations of decorin glycosaminoglycans in human skin". In: *Scientific Reports*, 3 (2013), pp. 1–8.

[167] Nikolovska, K., Renke, J. K., Jungmann, O., Grobe, K., Iozzo, R. V., Zamfir, A. D., and Seidler, D. G. "A decorin-deficient matrix affects skin chondroitin/dermatan sulfate levels and keratinocyte function". In: *Matrix Biology*, 35 (2014), pp. 91–102.

[168] Reese, S. P., Underwood, C. J., and Weiss, J. A. "Effects of decorin proteoglycan on fibrillogenesis, ultrastructure, and mechanics of type I collagen gels". In: *Matrix Biology*, 32 (2013), pp. 414–423.

[169] Ruehle, M. A., Krishnan, L., LaBelle, S. A., Willett, N. J., Weiss, J. A., and Guldberg, R. E. "Decorin-containing collagen hydrogels as dimensionally stable scaffolds to study the effects of compressive mechanical loading on angiogenesis". In: *MRS Communications*, 7 (2017), pp. 466–471.

[170] Gillery, P., Maquart, F. X., and Borel, J. P. "Fibronectin dependence of the contraction of collagen lattices by human skin fibroblasts". In: *Experimental Cell Research*, 167 (1986), pp. 29–37.

[171] Ngo, P., Ramalingam, P., Phillips, J. A., and Furuta, G. T. "Collagen gel contraction assay." In: *Methods in molecular biology (Clifton, N.J.)*, 341 (2006), pp. 103–109.

[172] Bell, E., Ivarsson, B., and Merrill, C. "Production of a tissue-like structure by contraction of collagen lattices by human fibroblasts of different proliferative potential in vitro". In: *Proceedings of the National Academy of Sciences of the United States of America*, 76 (1979), pp. 1274–1278.

[173] Sanchez, M. M. and Morgan, J. T. "Generation of self-assembled vascularized human skin equivalents". In: *Journal of Visualized Experiments*, 2021 (2021), pp. 1–31.

[174] Reuter, C., Imdahl, F., Hauf, L., Vafadarnejad, E., Fey, P., Finger, T., Walles, H., Saliba, A.-E., and Groeber-Becker, F. "Vector-borne Trypanosoma brucei parasites develop in artificial human skin and persist as skin tissue forms". In: *bioRxiv*, (2021), pp. 1–53.

[175] Laschke, M. W. and Menger, M. D. "Spheroids as vascularization units: From angiogenesis research to tissue engineering applications". In: *Biotechnology Advances*, 35 (2017), pp. 782–791.

[176] Zuo, X., Zhang, H., Zhou, T., Duan, Y., Shou, H., Yu, S., and Gao, C. "Spheroids of Endothelial Cells and Vascular Smooth Muscle Cells Promote Cell Migration in Hyaluronic Acid and Fibrinogen Composite Hydrogels". In: *Research*, 2020 (2020), pp. 1–15.

[177] Laib, A. M., Bartol, A., Alajati, A., Korff, T., Weber, H., and Augustin, H. G. "Spheroid-based human endothelial cell microvessel formation in vivo". In: *Nature Protocols*, 4 (2009), pp. 1202–1215.

[178] Babaei, B., Davarian, A., Lee, S.-L., Pryse, K. M., McConnaughey, W. B., Elson, E. L., and Genin, G. M. "Remodeling by fibroblasts alters the rate-dependent mechanical properties of collagen". In: *Acta Biomaterialia*, June (2016), pp. 28–37.

[179] Heller, M., Bauer, H. K., Schwab, R., Blatt, S., Peters, K., Nezi-Cahn, S., Unger, R. E., Hasenburg, A., and Brenner, W. "The impact of intercellular communication for the generation of complex multicellular prevascularized tissue equivalents". In: *Journal of Biomedical Materials Research - Part A*, 108 (2020), pp. 734–748.

[180] Velazquez, O. C., Snyder, R., Liu, Z. J., Fairman, R. M., and Herlyn, M. "Fibroblast-dependent differentiation of human microvascular endothelial cells into capillary-like 3-dimensional networks." In: *The FASEB journal*, 16 (2002), pp. 1316–1318.

[181] Morgan, J. T., Shirazi, J., Comber, E. M., Eschenburg, C., and Gleghorn, J. P. "Fabrication of centimeter-scale and geometrically arbitrary vascular networks using in vitro self-assembly". In: *Biomaterials*, Jan (2019), pp. 37–47.

[182] Schmitz, S. *Der Experimentator: Zellkultur*. Spektrum Akademischer Verlag, Heidelberg, 3. edition (2011).

[183] Brown, L. F., Yeo, K. T., Berse, B., Yeo, T. K., Senger, D. R., Dvorak, H. F., and Van De Water, L. "Expression of vascular permeability factor (vascular endothelial growth factor) by epidermal keratinocytes during wound Healing". In: *Journal of Experimental Medicine*, 176 (1992), pp. 1375–1379.

[184] Viac, J., Palacio, S., Schmitt, D., and Claudy, A. "Expression of vascular endothelial growth factor in normal epidermis, epithelial tumors and cultured keratinocytes". In: *Arch Dermatol Res*, 289 (1997), pp. 158–163.

[185] Weninger, W., Uthman, A., Pammer, J., Pichler, A., Ballaun, C., Lang, I. M., Plettenberg, A., Bankl, H. C., Stürzl, M., and Tschachler, E. "Vascular endothelial growth factor production in normal epidermis and in benign and malignant epithelial skin tumors". In: *Laboratory Investigation*, 75 (1996), pp. 647–657.

[186] Bae, O. N., Noh, M., Chun, Y. J., and Jeong, T. C. "Keratinocytic vascular endothelial growth factor as a novel biomarker for pathological skin condition". In: *Biomolecules and Therapeutics*, 23 (2015), pp. 12–18.

[187] Fleming, P. A., Argraves, W. S., Gentile, C., Neagu, A., Forgacs, G., and Drake, C. J. "Fusion of uniluminal vascular spheroids: A model for assembly of blood vessels". In: *Developmental Dynamics*, 239 (2010), pp. 398–406.

[188] Mironov, V., Visconti, R. P., Kasyanov, V., Forgacs, G., Drake, C. J., and Markwald, R. R. "Organ printing: Tissue spheroids as building blocks". In: *Biomaterials*, 30 (2009), pp. 2164–2174.

[189] Norotte, C., Marga, F. S., Niklason, L. E., and Forgacs, G. "Scaffold-free vascular tissue engineering using bioprinting". In: *Biomaterials*, 30 (2009), pp. 5910–5917.

[190] Knezevic, L., Schaupper, M., Mühleder, S., Schimek, K., Hasenberg, T., Marx, U., Priglinger, E., Redl, H., and Holnthoner, W. "Engineering Blood and Lymphatic Microvascular Networks in Fibrin Matrices". In: *Frontiers in Bioengineering and Biotechnology*, 5 (2017), pp. 1–12.

[191] Supp, D. M., Wilson-Landy, K., and Boyce, S. T. "Human dermal microvascular endothelial cells form vascular analogs in cultured skin substitutes after grafting to athymic mice". In: *FASEB Journal*, 16 (2002), pp. 797–804.

[192] Gupta, K., Ramakrishnan, S., Browne, P. V., Solovey, A., and Hebbel, R. P. "A novel technique for culture of human dermal microvascular endothelial cells under either serum-free or serum-supplemented conditions: Isolation by panning and stimulation with vascular endothelial growth factor". In: *Experimental Cell Research*, 230 (1997), pp. 244–251.

[193] Jiménez, N., Krouwer, V. J., and Post, J. A. "A new, rapid and reproducible method to obtain high quality endothelium in vitro". In: *Cytotechnology*, 65 (2013), pp. 1–14.

[194] Park, H. J., Zhang, Y., Georgescu, S. P., Johnson, K. L., Kong, D., and Galper, J. B. "Human umbilical vein endothelial cells and human dermal microvascular endothelial cells offer new insights into the relationship between lipid metabolism and angiogenesis". In: *Stem Cell Reviews*, 2 (2006), pp. 93–102.

[195] Swerlick, R. A., Garcia-Gonzalez, E., Kubota, Y., Xu, Y., and Lawley, T. J. "Studies of the Modulation of MHC Antigen and Cell Adhesion Molecule Expression on Human Dermal Microvascular Endothelial Cells". In: *The Journal of Investigative Dermatology*, 97 (1991), pp. 190–196.

[196] Bandarchi, B., Ma, L., Navab, R., Seth, A., and Rasty, G. "From melanocyte to metastatic malignant melanoma". In: *Dermatology Research and Practice*, 2010 (2010).

[197] Lee, D. Y. and Cho, K. H. "The effects of epidermal keratinocytes and dermal fibroblasts on the formation of cutaneous basement membrane in three-dimensional culture systems". In: *Archives of Dermatological Research*, 296 (2005), pp. 296–302.

[198] Lertkiatmongkol, P., Liao, D., Heng Mei, Y. H., and Newman, P. J. "Endothelial functions of PECAM-1 (CD31)". In: *Curr Opin Hematol.*, 23 (2016), pp. 253–259.

[199] Jayadev, R. and Sherwood, D. R. "Basement membranes". In: *Current Biology*, 27 (2017), pp. R207–R211.

[200] Kramer, R. H., Fuh, G. M., and Karasek, M. A. "Type IV Collagen Synthesis by Cultured Human Microvascular Endothelial Cells and Its Deposition into the Subendothelial Basement Membrane". In: *Biochemistry*, 24 (1985), pp. 7423–7430.

[201] Kress, S., Baur, J., Otto, C., Burkard, N., Braspenning, J., Walles, H., Nickel, J., and Metzger, M. "Evaluation of a Miniaturized Biologically Vascularized Scaffold in vitro and in vivo". In: *Scientific Reports*, 8 (2018), pp. 1–13.

[202] Relou, I. A., Damen, C. A., Van Der Schaft, D. W., Groenewegen, G., and Griffioen, A. W. "Effect of culture conditions on endothelial cell growth and responsiveness". In: *Tissue and Cell*, 30 (1998), pp. 525–530.

[203] Rigel, D. S. and Carucci, J. A. "Malignant Melanoma: Prevention, Early Detection, and Treatment in the 21st Century". In: *CA: A Cancer Journal for Clinicians*, 50 (2000), pp. 215–236.

[204] Rebecca, V. W., Somasundaram, R., and Herlyn, M. "Pre-clinical modeling of cutaneous melanoma". In: *Nature Communications*, 11 (2020), pp. 1–9.

[205] Brandner, J. M. and Haass, N. K. "Melanoma's connections to the tumour microenvironment". In: *Pathology*, 45 (2013), pp. 443–452.

[206] Hölken, J. M. and Teusch, N. E. "Recent developments of 3D models of the tumor microenvironment for cutaneous melanoma: Bridging the gap between the bench and the bedside?" In: *Journal of Translational Science*, 7 (2020), pp. 1–7.

[207] Gurzu, S., Beleaua, M. A., and Jung, I. "The role of tumor microenvironment in development and progression of malignant melanomas – A systematic review". In: *Romanian Journal of Morphology and Embryology*, 59 (2018), pp. 23–28.

[208] Villanueva, J. and Herlyn, M. "Melanoma and the Tumor Microenvironment". In: *Curr Oncol Rep.*, (2008), pp. 439–446.

[209] Kuzu, F., Nguyen, F. D., Noory, M. A., and Sharma, A. "Current State of Animal (Mouse) Modeling in Melanoma Research Supplementary Issue: Animal Models of Cancer Biology". In: *CanCer Growth and Metastasis*, 8 (2015), pp. 81–94.

[210] Klicks, J., Maßlo, C., Kluth, A., Rudolf, R., and Hafner, M. "A novel spheroid-based co-culture model mimics loss of keratinocyte differentiation, melanoma cell invasion, and drug-induced selection of ABCB5-expressing cells". In: *BMC Cancer*, 19 (2019), pp. 1–14.

[211] Shiku, H., Takahashi, T., Oettgen, H. F., and Old, L. J. "Cell surface antigens of human malignant melanoma. II. Serological typing with immune adherence assays and definition of two new surface antigens." In: *Journal of Experimental Medicine*, 144 (1976), pp. 873–881.

[212] Carey, T. E., Takahashi, T., Resnick, L. A., Oettgen, H. F., and Old, L. J. "Cell surface antigens of human malignant melanoma: Mixed hemadsorption assays for humoral immunity to cultured autologous melanoma cells". In: *Proceedings of the National Academy of Sciences of the United States of America*, 73 (1976), pp. 3278–3282.

[213] Quax, P. H., Van Muijen, G. N., Weening-Verhoeff, E. J., Lund, L. R., Dano, K., Ruiter, D. J., and Verheijen, J. H. "Metastatic behavior of human melanoma cell lines in nude mice correlates with urokinase-type plasminogen activator, its type-1 inhibitor, and urokinase-mediated matrix degradation". In: *Journal of Cell Biology*, 115 (1991), pp. 191–199.

[214] Van Muijen, G. N., Cornelissen, L. M., Jansen, C. F., Figdor, C. G., Johnson, J. P., Bröcker, E. B., and Ruiter, D. J. "Antigen expression of metastasizing and non-metastasizing human melanoma cells xenografted into nude mice". In: *Clinical & Experimental Metastasis*, 9 (1991), pp. 259–272.

[215] Meier, F., Nesbit, M., Hsu, M. Y., Martin, B., Van Belle, P., Elder, D. E., Schaumburg-Lever, G., Garbe, C., Walz, T. M., Donatien, P., Crombleholme, T. M., and Herlyn, M. "Human melanoma progression in skin reconstructs: biological significance of bFGF." In: *The American journal of pathology*, 156 (2000), pp. 193–200.

[216] Adam, C., Fusi, L., Weiss, N., Goller, S. G., Meder, K., Frings, V. G., Kneitz, H., Goebeler, M., Houben, R., Schrama, D., and Schmidt, M. "Efficient Suppression of NRAS-Driven Melanoma by Co-Inhibition of ERK1/2 and ERK5 MAPK Pathways". In: *Journal of Investigative Dermatology*, 140 (2020), pp. 2455–2465.e10.

[217] Boone, B., Jacobs, K., Ferdinande, L., Taildeman, J., Lambert, J., Peeters, M., Bracke, M., Pauwels, P., and Brochez, L. "EGFR in melanoma: Clinical significance and potential therapeutic target". In: *Journal of Cutaneous Pathology*, 38 (2011), pp. 492–502.

[218] de Wit, P. E., Moretti, S., Koenders, P. G., Weterman, M. A., van Muijen, G. N., Gianotti, B., and Ruiter, D. J. "Increasing epidermal growth factor receptor expression in human melanocytic tumor progression". In: *Journal of Investigative Dermatology*, 99 (1992), pp. 168–173.

[219] Kulms, D. and Meier, F. "In vitro models of melanoma". In: Marques, A. P., Pirraco, R. P., Cerqueira, M. T., and Reis, R. L., editors, *Skin Tissue Models*, chapter 3, pp. 57–75. Academic Press (2018).

[220] Paul, S. P. "Micromelanomas: A Review of Melanomas < 2 mm and a Case Report". In: *Case Reports in Oncological Medicine*, 2014 (2014), pp. 1–4.

[221] Domingues, B., Lopes, J., Soares, P., and Populo, H. "Melanoma treatment in review". In: *ImmunoTargets and Therapy*, Volume 7 (2018), pp. 35–49.

[222] Sandru, A., Voinea, S., Panaitescu, E., and Blidaru, A. "Survival rates of patients with metastatic malignant melanoma". In: *Journal of medicine and life*, 7 (2014), pp. 572–576.

[223] Folkman, J. and Dyckman, J. "Tumor Angiogenesis". In: *CA: A Cancer Journal for Clinicians*, 22 (1972), pp. 226–229.

[224] Hanahan, D. and Folkman, J. "Patterns and emerging mechanisms of the angiogenic switch during tumorigenesis". In: *Cell*, 86 (1996), pp. 353–364.

Affidavit

I hereby confirm that my thesis entitled *Vascularization Strategies for Full-Thickness Skin Equivalents to Model Melanoma Progression* is the result of my own work. I did not receive any help or support from commercial consultants. All sources and / or materials applied are listed and specified in the thesis.

Furthermore, I confirm that this thesis has not yet been submitted as part of another examination process neither in identical nor in similar form.

Place, Date	Signature

Eidesstattliche Erklärung

Hiermit erkläre ich an Eides statt, die Dissertation *Vaskularisierungsstrategien für Vollhautäquivalente zur Modellierung der Melanom-Progression* eigenständig, d.h. insbesondere selbständig und ohne Hilfe eines kommerziellen Promotionsberaters, angefertigt und keine anderen als die von mir angegebenen Quellen und Hilfsmittel verwendet zu haben.

Ich erkläre außerdem, dass die Dissertation weder in gleicher noch in ähnlicher Form bereits in einem anderen Prüfungsverfahren vorgelegen hat.

Ort, Datum	Unterschrift

Publications and Conference Contributions

Publications

Marius Gensler*, **Anna Leikeim***, Marc Möllmann, Miriam Komma, Susanne Heid, Claudia Müller, Aldo R. Boccaccini, Sahar Salehi, Florian Groeber-Becker, Jan Hansmann, "3D printing of bioreactors in tissue engineering: A generalised approach". In: PlosOne 15(11) (2020), doi: 10.1371/journal.pone.0242615.

* contributed equally

Anna Leikeim*, Maximiliane Wußmann*, Freia F. Schmidt*, Kendra Tiltmann, Corinna Junger, Franziska Benz, Nuno Neton, Michael Monaghan, Bastian Schilling, Florian Groeber-Becker, "A preclinical Model of cutaneous Melanoma based on Reconstructed Human Epidermis". Planned submission at Scientific Reports, in preparation.

* contributed equally

Conference Contributions

2021 **3D Cell Culture**, *DECHEMA*, Freiburg, Germany (online), Oral presentation and Poster: Development of melanoma skin equivalents for studying metastasis and anti-melanoma therapies.

2020 **EUREKA 2020**, *Graduate School of Life Sciences*, Würzburg, Germany (online), Poster: Development of melanoma skin equivalents for studying metastasis and anti-melanoma therapies.

2019 **49th ESDR Annual Meeting**, *European Society for Dermatological Research*, Bordeaux, France, Poster: Development of melanoma skin equivalents for studying metastasis and anti-melanoma therapies.

2019 **3D Tissue Infection Symposium**, *Graduiertenkolleg 2157 der Universität Würzburg*, Würzburg, Germany, Poster: Vascularization Strategies for Full-Thickness Skin Equivalents.

Acknowledgements

First, I want to thank Prof. Dr. Heike Walles for giving me the opportunity to write my doctoral thesis at the Department for Tissue Engineering and Regenerative Medicine of the University Hospital Würzburg, especially in a moment when this didn't seem sure. Thanks for being part of my thesis committee and for taking on the part as first examiner.

I am tremendously grateful to my supervisor Dr. Florian Groeber-Becker, who "adopted" me in the skin group and gave me this interesting topic to work on. Thanks for all your advices, your critical, honest and helpful feedback, for pushing and motivating me and for being able to praise. I learnt a lot during the last four years.

I also want to thank the other members of my thesis committee for their time and interest in my work and for inspiring discussions. Thank you, Prof. Dr. Marc Schmidt, for the supervision of my doctoral thesis as second examiner, for providing the BLM cells and your experience about them. Thank you, Dr. Dieter Groneberg, for helpful discussions and for sharing parts of your enormous knowledge with me. I also thank Prof. Dr. Christian Janzen for fulfilling the function of the chairman.

I really enjoyed working at the institute and want to thank all members of the Department for Tissue Engineering and Regenerative Medicine for providing a friendly atmosphere and always giving helpful advices. Special thanks go to Özlem Elbert and Anna-Kristina Stefl for your organisational skills and for all your help with official and other issues. I loved the scientific discussions as well as many conversations besides science in our wonderful office, that was the meeting place for so many coffee lovers. Thank you Dr. Christian Lotz, Dr. Ramkumar Ramani Mohan, Dr. Anna Schliermann, Dr. Robin Fischer, Christoph Malkmus, Sanjana Mathew, Jihyoung Choi and Lukas Königer for making that time unforgettable. Also I want to acknowledge my colleagues in the skin group. Working with you was always a pleasure and I appreciated the collegial interaction and that we can always count on each other! I am especially grateful to have met here Dr. Lisa Kiesewetter, Christoph Malkmus, Maximilane Wußmann, Verena

Weigel and Kendra Tiltmann, who were not only colleagues providing advice and support, but who became friends.

Another thank you to my former master student Johanna Kliche who did a lot of work regarding the mFTSE and to Marius Gensler and his master student Miriam Komma who designed and produced the bioreactors.

Furthermore, I want to thank all friends, colleagues and family members, who frequently asked me about the status and progress of my thesis. That really helped a lot and had great impact! ;)

I owe gratitude to my family who always believed in me and supported me. Without them, I wouldn't be where and who I am today. Thanks to my home office co-workers Mila and Diego, who were a great support not only in pandemic times! Finally, I thank from the bottom of my heart my partner Andreas for his encouragement and patience during the writing process of this thesis. I could not have done that without you! Thank you for your good coaxing, cheering me up, your technical support and for making waffles whenever I wanted them!